HepaChip-MP: a microfluidic liver model in multiwellplate format for the assessment of metabolism, toxicity and modeling of disease as an example of microfluidic in vitro models to mimic physiological organ behavior

Dissertation

der Mathematisch-Naturwissenschaftlichen Fakultät

der Eberhard Karls Universität Tübingen

zur Erlangung des Grades eines

Doktors der Naturwissenschaften

(Dr. rer. nat.)

vorgelegt von

M.Sc. Marius Busche

aus Hannover

Tübingen

2023

Gedruckt mit Genehmigung der Mathematisch-Naturwissenschaftlichen Fakultät der Eberhard Karls Universität Tübingen.

Tag der mündlichen Qualifikation:	30.04.2024
Dekan:	Prof. Dr. Thilo Stehle
1. Berichterstatter/-in:	Prof. Dr. Katja Schenke-Layland
2. Berichterstatter/-in:	Prof. em. Dr. Rolf Gebhardt
3. Berichterstatter/-in:	Prof. Dr. Peter Loskill

Table of Content

Abstract

Drug-induced injury and especially drug-induced liver injury (DILI) are a big health concern. One reason for this is that preclinical models currently in use fail to predict substance effects in humans reliably. Organ-on-chip models are promising systems to improve these effects. The HepaChip-MP is such an organ-on-chip system modelling the liver sinusoid. The aim of this thesis was to demonstrate usability of this chip system by culturing primary human hepatocytes in it and showing liver-specific cell function as well as detecting substance-induced cell damage.

In this thesis, cell culture processes were established to assemble, culture, and analyze primary human hepatocytes. Handling of the HepaChip-MP with a pipetting robot was optimized to improve repeatability of experiments and ease-of-use for non-expert end-users. After optimizing the process to prepare and fill the cell culture chambers, on average more than 18 of the 24 chambers of the chip could be used per experiment. Also, the process for cell assembly was optimized which led to mostly complete coverage of the cell culture areas with cells at the start of the culture. After optimizing the technical aspects of chip handling, different media compositions were investigated in order to improve long-term stability of cell culture in the HepaChip-MP. A medium was identified which supports dense cell aggregates for at least 12 days in the chip. Assays were established to analyze cell vitality and function. A resazurine assay and an ATP-assay were adapted to the HepaChip-MP and used to detect diclofenac- and acetaminophen-induced cell damage. Function and induction of cytochrome P450 (CYP) enzymes was demonstrated via substance turnover (mass spectrometry analysis conducted by A & M Labor fuer Analytik und Metabolismusforschung Service GmbH Bergheim, Germany). Also, a coculture of human primary hepatocytes and human primary liver endothelial cells was established. The different cell types were stained with cell type specific antibodies which demonstrated the possibility to assemble different cell types in the HepaChip-MP. Oxygen sensors were introduced in the HepaChip-MP in collaboration with colleagues from Graz University of Technology (Graz, Austria) and Pyroscience AT GmbH (Aachen, Germany) allowing online measurement of oxygen consumption. This allows for a detailed analysis of substance-induced effects on cellular respiration.

In conclusion, procedures have been established to analyze cell vitality and function after substance treatment in an innovative parallelized organ-on-chip system of the

liver allowing for automated handling with a pipetting robot. Liver specific cell function was shown and especially, online measurement of oxygen consumption under continuous flow conditions after substance treatment has been established.

Zusammenfassung

Durch Medikamente hervorgerufene Schädigungen und insbesondere medikamenteninduzierte Leberschäden (DILI, *drug-induced liver injury*) stellen ein großes gesundheitliches Problem dar. Ein Grund dafür ist, dass die derzeit verwendeten präklinischen Modelle die Wirkungen von Substanzen auf Menschen nicht zuverlässig vorhersagen können. Organ-on-Chip-Modelle sind vielversprechende Systeme um verbesserte Vorhersagen tätigen zu können. Der HepaChip-MP ist ein solches Organ-on-Chip-System. Er modelliert die kleinste Einheit der Leber, den Lebersinusoid. Ziel dieser Arbeit war es, die Anwendbarkeit dieses Chipsystems zu demonstrieren, indem primäre humane Hepatozyten darin kultiviert und leberspezifische Zellfunktionen untersucht sowie substanzinduzierte Zellschäden nachgewiesen werden.

In dieser Arbeit wurden Zellkulturprozesse etabliert, um primäre humane Hepatozyten zu assemblieren, zu kultivieren und zu analysieren. Die Handhabung des HepaChip-MP mit einem Pipettierroboter wurde optimiert, um die Wiederholbarkeit von Experimenten und die Benutzerfreundlichkeit für nicht erfahrene Endanwender zu verbessern. Nach der Optimierung der Prozesse konnten im Durchschnitt mehr als 18 der 24 Kammern des Chips pro Experiment verwendet werden. Außerdem konnte erreicht werden, dass die Zellen die Zellkulturbereiche bedecken. Nach der Optimierung der technischen Aspekte der Chip-Handhabung wurden verschiedene Medien zur Unterstützung der Langzeitkultur getestet. Es wurde ein Medium gefunden, das die Kultivierung dichter Zellaggregate für mindestens 12 Tage auf dem Chip unterstützt. Es wurden Assays zur Analyse der Zellvitalität und -funktion entwickelt. Ein Resazurin-Assay und ein ATP-Assay wurden an den HepaChip-MP angepasst und anschließend zum Nachweis von Diclofenac- und Acetaminophen-induzierten Zellschäden eingesetzt. Die Funktion und Induktion von Cytochrom P450 (CYP)-Enzymen wurde über den Nachweis der Produkte der Metaboliserung von bestimmten Substraten nachgewiesen (mittels Massenspektrometrie durchgeführt von A & M Labor für Analytik und Metabolismusforschung Service GmbH Bergheim, Deutschland). Außerdem wurde eine Kokultur aus humanen primären Hepatozyten und humanen primären Leberendothelzellen etabliert. Die verschiedenen Zelltypen wurden mit zelltypspezifischen Antikörpern angefärbt. Dadurch konnte gezeigt warden, dass es möglich ist verschiedene Zelltypen im HepaChip-MP zu kultivieren. In

Zusammenarbeit mit Kollegen der Technischen Universität Graz (Graz, Österreich) und der Pyroscience AT GmbH (Aachen, Deutschland) wurden Sauerstoffsensoren in den HepaChip-MP eingebaut, die eine Online-Messung des Sauerstoffverbrauchs ermöglichen. Dies ermöglichte eine detaillierte Analyse der substanzinduzierten Auswirkungen auf die Zellatmung.

Zusammenfassend wurden Verfahren zur Analyse der Zellvitalität und -funktion nach Substanzbehandlung in einem innovativen parallelisierten Organ-on-Chip-System des Lebersinusoids etabliert. Die Handhabung des Chip-Systems ist automatisiert mit einem Pipettierroboter möglich. Es wurde leberspezifische Zellfunktion gezeigt und insbesondere die Online-Messung des Sauerstoffverbrauchs unter kontinuierlichen Flussbedingungen nach Behandlung mit verschiedenen Substanzen etabliert. Dies zeigt das große Potenzial für weitere detailierte Untersuchungen mit der HepaChip-MP.

Abbreviations

2D	2-dimensional
3D	3-dimensional
ADR	Adverse drug reaction
ALF	Acute liver failure
ANOVA	Analysis of variance
Approx.	approximately
ATP	Adenosine triphosphate
BCA assay	Bicinchoninic acid assay
CD31	Cluster of Differentiation 31
CK18	Cytokeratin 18
COP	Cyclin olefin polymer
CYP	Cytochrome P450
DEP	Dielectrophoresis
DILI	Drug-induced liver injury
DIV	Day in vitro
e.g.	Exempli gratia (meaning: for example)
EU	European Union
FBS	Fetal bovine serum
FCCP	Carbonyl cyanide-p-trifluoromethoxyphenylhydrazone
FH	Fulminant Hepatitis
Fig.	Figure
g	Gram
GSH	Glutathion
HepaChip-MP	HepaChip multiwellplate
HEPES	4-(2-Hydroxyethyl)piperazine-1-ethane-sulfonic acid)
HuLEC	Human liver endothelial cells
HSC	Hepatic stellate cells
IC_{50}	Half-maximal Inhibition Concentration (concentration which reduces the effect by 50%)
kHz	Kilohertz

LSEC	Liver sinusoidal endothelial cells
Na-pyruvate	Natrium pyruvate
Na-selen	Natrium selen
ng	nanogram
No.	number
NPC	Non-parenchymal cells
M	Molar
mg	milligram
min	minute
mM	Millimolar
OC	Oxygen consumption
P_i	Phosphate
PDMS	Polymethyl siloxane
PHH	Primary human hepatocytes
pmol	picomol
ROS	Reactive oxygen species
R/A	Rotenone/Antimycin A
R&D	Research and Development
sec	Second(s)
µl	Microliter
µM	Micromolar
μm^3	Micro cubic meter

List of Figures

List of Publications

1. Busche M, et al., HepaChip-MP - a twenty-four chamber microplate for a continuously perfused liver coculture model. Lab Chip. 2020;20:2911-26. doi: 10.1039/d0lc00357c
2. Busche M, et al., Continous, non-invasive monitoring of oxygen consumption in a parallelized microfluidic in vitro system provides novel insight into the response to nutrients and drugs of primary human hepatocytes, EXCLI J, 2022; 21: 144–161. doi: 10.17179/excli2021-4351

Contributions

No.	Accepted for publication	Number of authors	Position of the candidate in the list of authors	Scientific ideas by candidate (%)	Data generation by candidate (%)	Interpretion and analysis by candidate (%)	Paper writing by candidate (%)
1	yes	24	1	20	75	60	65
2	yes	7	1	50	100	75	80

1 Introduction

1.1 Adverse drug reactions and drug-induced liver injury

Lacoste-Roussillon et al. extrapolated that 123,000 adverse drug reactions (ADRs) occur in France per year [1]. This demonstrates that drug-induced injury is big health concern. Drugs with a higher incidence of ADRs are generally withdrawn from the market due to health concerns while drugs with low risk-benefit-ratio stay in the market. But even still used drugs can cause ADRs which can lead to serious health problems. Between 2002 and 2011, 19 drugs have been withdrawn in the EU member states due to safety issues. Nine of them were withdrawn because they induced cardiovascular events or disorders and four were withdrawn due to case reports of liver damage [2]. Hence, cardiovascular and hepatic toxicity are responsible for more than 65% of drug withdrawals. Other implications are neurological and psychiatric disorders [2]. Drugs are metabolized by specific enzymes of the liver. In some cases, these liver enzymes even activate the drugs by metabolizing them to substances which can lead to organ damage. Often, genetic differences in drug-metabolizing liver enzymes lead to differing drug concentrations in individual patients. This can lead to ADRs in especially the cardiovascular system [3]. As the liver plays a critical role in drug metabolism (and even activation), it is in the focus of research on drug-induced organ damage and preclinical drug testing.

As mentioned above, the liver itself suffers from ADRs as well. Next to viral infections, drugs are the most common cause for acute liver failure (ALF) and fulminant hepatitis (FH) [4]. Due to vaccination and improved treatment options, viral infections become less relevant in the etiology of ALF while the incidence of drug-induced liver injury (DILI) increases especially in western countries [4, 5]. Björnsson reviewed several studies from different countries to evaluate the global epidemiology of DILI. He found that up to approx. 24 in 100,000 hospitalized patients suffer from DILI [6]. Considering that drugs are supposed to improve the patient's health, this number is too high. In conclusion, ADRs are a health concern of high relevance and the liver is one of the main organs contributing to as well as suffering from ADR.

Improving preclinical testing strategies may prevent potential harmful drugs to reach the market. Consequently, there is a need for optimization of preclinical testing in pharmaceutical research and development (R&D). This hypothesis is also supported

by economic considerations. Scannel et al. reported that the number of approved drugs per billion US dollars spent on R&D has halved roughly every nine years since 1950 [7]. Drug development gets more expensive because it becomes harder to beat the gold standard and regulators developed higher standards for a drug to reach the market [7]. Often, drugs fail to reach the market due to efficacy or safety issues in clinical trials [8]. Clinical trials belong to the most expensive parts in the drug development pipeline [9]. Hence, by sorting out failing drugs earlier in the pipeline (e.g. during preclinical testing), R&D costs could be decreased substantially. Hence, improving preclinical testing with e.g. innovative cell culture models is a promising approach to both improve drug safety and reduce R&D costs [10]. As discussed above, the liver is one of the organs in the focus of currently ongoing development of new and innovative cell culture models to improve the drug development pipeline.

1.2 Liver physiology

The liver is located in the upper part of the abdominal cavity below the diaphragm. Beneath the liver are the stomach, the right kidney and the intestines. The livers blood supply is secured by the hepatic artery (25-30%) and the portal vein (70-75%) [11]. The blood mixes in the hepatic sinusoids and is collected first in the central vein and later in the liver vein. Finally, it reaches the *vena cava inferior* which flows into the right atrium of the heart. The portal vein contains nutrient-rich blood from the gastrointestinal tract. Hence, all substances taken orally are passing the liver before entering the human circulation. The portal veins blood is low in oxygen. The hepatic artery, however, provides arterial and, thus, oxygen-rich blood. The liver has various functions, which ensure human survival and are described below. [12]

1.2.1 Function of the liver

The liver produces blood proteins like albumin, coagulation proteins and acute phase proteins. It also secretes bile acids, which are important for digestive functions and waste removal. The liver is next to the skeletal muscles the biggest glycogen storage in the human body and communicates with adipose tissue to balance the lipid metabolism. Hence, it plays an important role in human energy metabolism. As an organ involved in lipid metabolism, the liver also stores lipids and fat-soluable vitamins. One of the most prominent function of the liver is the detoxification of xenobiotic

substances. The detoxification reactions in the liver are mainly catalyzed by cytochrome P450 (CYP) enzymes. These enzymes metabolize 70-80% of the drugs in clinical use and therefore, are very important enzymes in relation to clinical pharmacology and the above mentioned ADR [13]. CYP enzymes catalyze the so-called Phase I metabolism, which represents oxidation, reduction and hydrolysis reactions. CYP3A4/5 is responsible for the metabolism of approx. 30%-40% of drugs in clinical use and is by that the most important enzyme in terms of drug metabolism [14]. In Phase II metabolism, small substances like glucuronic acid (glucuronidation) or gluthathion are conjugated to the metabolized substance. This results in a more hydrophilic molecule, which can more easily be excreted by the kidneys. One example for a Phase II enzyme is UGT1A1, which is responsible for bilirubin glucuronidation [15]. Hence, in liver failure, bilirubin is not prepared for excretion anymore and it accumulates in the plasma. This leads to the famous icterus which is known as a common symptom of liver disfunction.

1.2.2 Intrahepatic anatomical structure

The liver is built out of 1-1.5 mio small units called lobules (Figure 1). They are hexagonal-like structures, which have a size of 0.7-2 mm. Each lobule inhabits up to six so-called portal triads, located at the corners of the lobule. Portal triads consist out of the portal vein, hepatic artery and bile duct. The bile duct transports the liver-secreted bile to the gastrointestinal tract. The portal vein contains nutrient-rich blood from the gastrointestinal tract and is low in oxygen. The hepatic artery provides arterial blood, which is rich in oxygen. The blood from the portal vein and the hepatic artery is mixed and flows through so called sinusoids to the center of the lobule. Here, the central vein is located which transports the venous blood to the liver vein and *vena cava inferior*. The sinusoid is lined with different hepatic cell types. [16]

The parenchymal cells of the liver are the hepatocytes. They comprise 60% of the cells in the liver and 80% of total liver mass. Most of the liver functions described above (see 1.2.1) are carried out by the hepatocytes. They are arranged radially in the lobule and build the matrix for the sinusoids. Cell sheets of hepatocytes are one to two cells thick. Hepatocytes are polarized cells and may be polyploid. Between hepatocytes and the blood, liver sinusoidal endothelial cells (LSEC) are located. They build a fenestrated barrier, participate in the regulation of blood flow and have a very high

endocytosis activity. LSECs also have immunologic functions. They play an important role in antigen presentation, leucocyte recruitment and they secrete cytokines after activation [17, 18]. The liver inhabits a variety of cells actively contributing to the immune system including different lymphocytes like T-cells and natural killer cells. In addition, 80% of all macrophages in the human body are located in the liver. Resident macrophages of the liver are called Kupffer cells. Together with the LSECs, the Kupffer cells are the main cells responsible for keeping up liver homeostasis by removing damaged cells and proteins. Hepatic stellate cells (HSC) are also resident cells in the liver and store fat-soluable vitamins, e.g. vitamin A. After injury, HSCs are activated and produce extracellular matrix to support regeneration. All cell types of the liver communicate with each other and influence their respective behavior. [19]

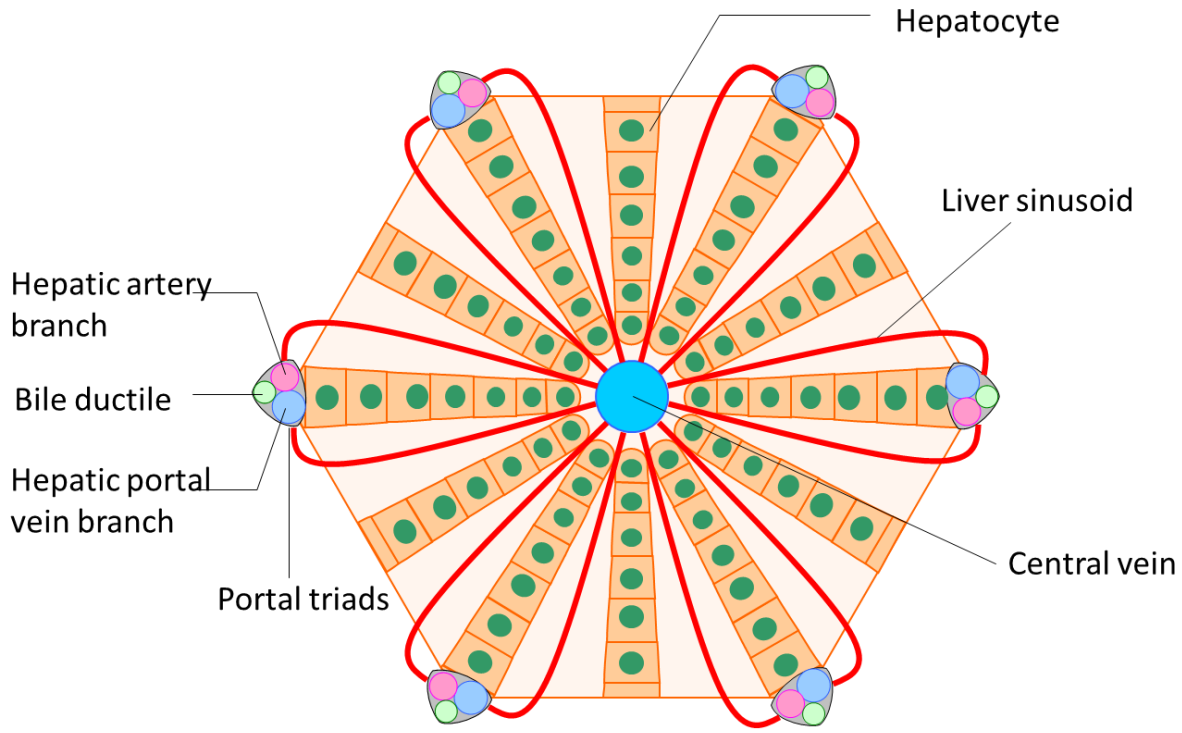

Figure 1: Schematic representation of the hepatic lobule. Each lobule inhabits up to six portal triads. It shows the portal triad with the hepatic artery, portal vein and bile ducts. The parenchymal cells (hepatocytes) are radial arranged. Blood flows from the portal triads through sinusoids to the central vein.

1.3 Cell culture models of the liver

Animal models currently fail to reliably predict human hepatotoxicity of substances [20, 21]. Hence, other model systems for translation to human are needed. One system with high potential are innovative in vitro systems inhabiting human cells. While

establishing an in vitro test system, it is important to consider which question the system should answer. For academic use, this can be any question of interest in basic or application-oriented research and there are countless possibilities for systems fitting to different topics. For model systems used in pharmaceutical industry, there are a few aspects, which are more important and should be reproduced. Baudy et al. discussed these specifications for liver models for safety risk assessments in the pharmaceutical industry in detail [22]. Briefly, these requirements include the production of different substances like albumin and urea, metabolic function of the cells and reproducing known cell responses after challenge with substances. Concerning metabolic function of the cells, especially cytochrome P450 (CYP) activity and induction is an important measure. For substance-challenging of the cells, substances should be used, which cover different mechanisms to cause DILI in human. A list of such substances is provided in [22].

For setting up an in vitro system, the choice of cells to be employed is critical. Since animal models lack correlation to the situation in human, animal cells are not perfectly suited to predict toxicity in human as well. Differentiating of human stem cells is one possible source of hepatocytes. Unfortunately, and despite great efforts in using soluable molecules and different matrices, there is currently no protocol available to produce fully mature hepatocytes [23-25]. Hence, primary human hepatocytes (PHH) and human-derived hepatic cell lines are often used in in vitro systems and will be briefly discussed here. HepG2 and HepaRG cells are the most frequently used cell lines. HepG2 cells are known to have low CYP activity in comparison to HepaRG cells [26]. Also, physiologic CYP induction is better preserved in HepaRG cells than in HepG2 [27]. Nevertheless, PHH show even higher CYP expression, activity and inducibility. In addition, PHH have higher sensitivity to predict hepatotoxicity of substances than HepaRG which in turn have a higher sensitivity than HepG2 cells [27]. Hence, PHH are the gold standard to be utilized to set up a physiologic in vitro model of the liver. Unfortunately, continuous and low-cost supply of PHH cannot always be assured. Consequently, the respective cell source to be used has to be selected in the scope of the question of interest and other experimental factors [24].

Cells can be cultured in different microenvironments ranging from simple 2D monolayers to complex 3D cell structures in microfluidic systems. These diverse

systems are discussed in several reviews [28-33] and are described in the following sections.

1.3.1 Non-perfused models to model liver function

Human liver microsomes are subcellular fractions derived from hepatic cells. They inhabit enzymes of Phase I and Phase II metabolism and are used to analyze the xenobiotic metabolism of substances. Since microsomes are only representing a subcellular fraction, they do not function autonomously and need cofactors. Also, they do not cover the whole range of liver functions. For this, whole cell systems are needed.[33]

Hepatocytes can be cultured in 2D monolayers or in 3D cell aggregates. For 2D monolayers, PHH are cultured on culture plates coated with proteins supporting the adhesion. Mostly, Collagen I is used. In this culture system, PHH are known to quickly dedifferentiate which results in a decrease in hepatocyte-specific function and changes in metabolism. Liver-specific function can be maintained for approximately one week [34]. By using growth factors, chemical substances, genetic modifications or co-culture with non-parenchymal cells, the time window can be enhanced to culture functional hepatocytes for up to 90 days [35-43]. Khetani et al. developed micropatterned cocultures, where 2D islets of PHH are surrounded by fibroblast feeder cells. Amongst other things, the authors demonstrated improved albumin synthesis, urea syntheses, CYP expression as well as CYP activity in comparison to monocultures of PHH [44, 45].

Another approach is to seed the cells on collagen and coat them with another layer of collagen. This system was developed by Dunn et al. and is called collagen-sandwich [46]. Cells cultured in the collagen-sandwich have prolonged secretion of albumin, transferrin, fibrinogen, bile acids and urea [46, 47]. In addition, this system supports polarization of hepatocytes, formation of bile canaliculi, physiologic transporter activity as well as activity of phase I and phase II enzymes [48-52].

The next level of complexity is to culture hepatocytes in 3-dimensional systems like spheroids or in hydrogels. Culturing primary rat hepatocytes in an alginate hydrogel leads to increased albumin and urea production as well as improved xenobiotic metabolism [53, 54]. To produce three-dimensional structures without a hydrogel as a matrix, there are mainly two different possibilities. These are the hanging drop system

and ultra-low attachment (ULA) plates. In general, spheroids of hepatocytes show higher liver-specific function like, but not limited to, CYP activity and albumin production than 2D monolayer cultures [55, 56]. As discussed, PHH are the most suitable cells to produce a liver-mimicking system. Hence, spheroid systems of PHH will be briefly discussed here. For spheroid systems of stem-cell derived, HepG2 and HepaRG cells, the reader is referred to Lauschke et al. [31].

PHH spheroids are often prepared in co-culture with other cell types. Generally, and as described above for 2D cultures, the coculture with other cell types is supportive to keep up hepatocyte-specific cell function. Likewise, No et al. demonstrated that spheroids out of PHH and human adipose-derived stem cells show higher albumin production and CYP activity than monocultured PHH spheroids [57]. Spheroid cultures of PHH and non-parenchymal cells (NPC) as well show stable viability, CYP activity and albumin production over 5 weeks [58, 59]. In addition, Bell et al. demonstrated the toxicity of fialuridine on PHH-NPC spheroids for the first time in vitro [58]. Proctor et al. showed that spheroids out of PHH and NPC show higher sensitivity than monolayers of PHH to detect hepatotoxicants out of 110 substances [60]. Likewise, Vorrink et al. and Li et al. demonstrated superior sensitivity of PHH spheroids without NPCs to PHH in monolayers to detect hepatotoxicity of more than 100 substances [61, 62]. Bell et al. demonstrated higher sensitivity of spheroids than sandwich-cultured monolayers of PHH to five different hepatotoxicants in different laboratories [63].

There are also different approaches emerging to use bioprinting to set up in vitro models of the liver. The authors try to reproduce anatomical dimensions of the liver or enable automated patterned co-culture with feeder cells to establish systems for drug testing [64-67]. For a recent review, the reader is referred to Ma et al. [68].

1.3.2 Microfluidic models

Dash et al. demonstrated that primary rat hepatocytes cultured under dynamic conditions show e.g. higher albumin and urea production as well as higher gene expression and activity of CYP enzymes compared to static conditions [69]. Novik et al. reported similar CYP activity for monocultures of PHH under both, static and flow conditions [70]. However, when cocultured with NPC, flow conditions significantly increased CYP activity [70]. This demonstrates the importance of shear stress and coculture with NPC for liver-specific function of hepatocytes. Consequently, different

perfused organ-on-chip systems have been developed aiming at improved physiology of in vitro liver models. These systems realize perfusion by pumps or gravitational driven flow and inhabit mono- or cocultures of liver cells in either 2- or 3-dimensional cell aggregates.

One approach is to use a membrane to separate two different areas in a microfluidic chip [71, 72]. One side of the membrane inhabits macrophages and endothelial cells. On this side, also the medium is perfused. On the other side of the membrane, hepatocytes and stellate cells are seeded. Rennert et al. confirmed increased albumin and urea production in this system in comparison to static conditions and conventional 2D monocultures [72]. Prodanov et al. demonstrated stable albumin and urea production as well as CYP3A4 activity over 28 days [71]. In a recent publication, Ewart et al. used such a system to demonstrate toxicity out of a blinded set of 27 known hepatotoxicants with a sensitivity of 80% [73]. Some of these hepatotoxicants had, earlier, already passed preclinical toxicology assessment and only showed hepatoxicity in the clinic.

In another chip system inhabiting endothelial cells, macrophages, stellate cells and hepatocytes embedded in a collagen hydrogel, Vernetti et al. demonstrated stable albumin and urea production under perfusion for over 28 days as well [74]. In a chip established by Toh et al., no extracellular matrix is used, but the cells are caught by a pillar structure [75]. Toh et al. showed higher sensitivity to detect toxicity of some substances (e.g. acetaminophen and rifampin) of cells cultured in this system compared to cells cultured in a multiwellplate [75]. Ong et al. used the system of Toh et al. to demonstrate improved differentiation of progenitor cells to hepatocyte-like cells under flow conditions compared to static cultures. Cells differentiated in the chip system showed increased albumin and urea production [76].

There are also approaches to culture 3-dimensional liver spheroids under perfusion [77, 78]. Tostoes et al. demonstrated viability and activity of phase I and phase II enzymes over a period of 3-4 weeks in spheroids under perfusion [77]. Kim et al. cultured liver spheroids and colorectal tumor microtissues in one perfused system and replicated the liver-induced activation of the predrug cyclophosphamide [79]. Plenty of systems have been developed to model organ-organ-interactions involving a liver compartment [80-88]. Since this thesis focuses on a single-organ-chip of the liver, these systems are not described in detail. One other upside of perfusion is that it

enables the establishment of physiological gradients inside the culture chamber. In the liver, especially the oxygen gradient is important for the liver-specific zonation [89]. Zonation-specific protein expression and hepatocyte-function was reproduced in microfluidic chips by induction with exogenous hormones or modulating of oxygen concentration [90-92].
Most of the mentioned systems are single-compartment chip systems and have only low throughput. However, there are a few platforms, which enable parallelized experiments [78, 93-98]. These platforms are mainly designed in multiwellplate format and have 11 to 96 independent cell culture chambers [78, 93-97]. If not designed in multiwellplate format, a custom build periphery system enables parallelization [98, 99].

As described, microfluidic systems show improved hepatocyte-function in comparison to conventional in vitro systems and some systems even enable parallelization. Still, a broad use of organ-on-chip systems by non-expert end-users has not yet been established. This is due to different drawbacks in chip material, laborious setting up of perfusion, no in vivo-like medium flow and non-favorable dimensions of cell aggregates as well as tedious handling. Many devices are manufactured from polydimethyl siloxane (PDMS) which is known to absorb hydrophobic substances like small molecule drugs [100-102]. Complex tubing makes handling complicated while tubeless perfusion on rocker-platforms only enables unphysiological bidirectional medium flow. In addition, cell aggregates in many organ-on-chip systems do not replicate the physiological dimensions. Last but not least, the handling of most chip systems is not automatable and requires a high expertise of the respective end-user. To tackle these challenges, the HepaChip multiwellplate (HepaChip-MP) was developed.

1.3.3 HepaChip-MP

The HepaChip-MP has been developed to meet features an adequate organ-on-chip system of the liver should have to be routinely used. These features include liver-specific dimensions of cell aggregates and undisturbed mass transfer of substances in the cellular microenvironment. Cellular gene expression, function and cell responses after challenges with substances should be comparable to cells in vivo for a few weeks of culture. This feature probably can be supported by co-culturing the different cell types of the liver (as already described). Medium flow should mimic

physiologic flow conditions to enable the development of physiologic gradients. Last but not least, the chip handling should be easily integrated in common workflows and allow for parallelized experiments.[31, 103]

To develop an organ-on-chip system to be used by pharmaceutical industry and academic non-expert end-users, a microfluidic platform in 96-wellplate format with 24 independent chambers was designed – the HepaChip-MP [104-106]. It consists of a cyclic olefin polymer (COP) which shows low adsorbance of compounds. By additionally coating the channels and cell culture chamber with pluronic F-127, the adsorbance of compounds is further lowered [105, 107]. Patterned Collagen I coating enables specific seeding of cells [105]. Integrated electrodes and the dimensions of the chamber enable cell assembly by dielectrophoresis [108]. The cell culture areas are 850 µm long and 60 µm wide and thus, per design, enable an automated assembly of cell aggregates in similar dimensions to the liver sinusoid in vivo. Since there is no membrane or hydrogel needed for the cell assembly, cells are in direct contact to the medium, allowing for undisturbed mass transfer. Shear forces at the cell culture areas are low to protect hepatocytes from unphysiological mechanical stress [109]. Capillary stop valves enable reproducible filling of the cell culture chambers [110]. Priming of the chip and cell assembly is performed with a pipetting robot. This increases reproducibility as well as ease of handling and thus, supports the adaptation by non-expert end-users.

2 Objective of the thesis

The overall aim of this thesis was to establish the HepaChip-MP as an easy-to-use microfluidic platform to mimic liver specific behavior and by this, to provide a convenient tool to assess cell metabolism as well as toxicity after substance treatment. To reach this aim, the thesis was divided in three objectives:

1. Optimize and establish easy-to-perform procedures to handle the HepaChip-MP
2. Demonstrate cell vitality and liver-specific cell function of cells cultured in the HepaChip-MP
3. Establish a read-out method focusing on oxygen consumption to enable the analysis of substance-induced changes in cell metabolism

Based on proof-of-concept experiments [104, 106, 111], this work aimed to establish, optimize and adapt robust cell culture procedures in the HepaChip-MP to subsequently make use of them to analyze cell function.

In a first step, it was intended to improve cell culture chamber filling as well as cell assembly to optimize chip performance. Aspects to be optimized were the occurrence of air bubbles in the channels and the full coverage of the cell culture ridges with cells. The protocols were performed with a common pipetting robot to enable the integration in common workflows.

In the next step, it was attempted to establish read-out methods specifically adapted to the chip system to enable the analysis of cell vitality and cell function, especially focusing on CYP activity and induction as one of the most important liver function in relation to drug metabolism. As a proof-of-concept, cells cultured on the HepaChip-MP were treated with substances known to induce an effect, e.g. loss in cell vitality to demonstrate adequate performance of the assays. To increase physiologic relevance, a co-culture with primarly human liver endothelial cells was investigated. This included optimization of cell assembly and immunocytochemistry experiments.

To more deeply analyze cell responses after substance treatment, oxygen sensors were implemented in the HepaChip-MP. The goal was to first use them to demonstrate known effects of substance-treatment on the electron transport chain. By this, it should be demonstrated that the oxygen sensors are functional and the PHH cultured in the HepaChip-MP show physiologic cellular respiration. Finally, oxygen consumption of

cultured cells treated with different substances was analyzed to get more detailed insights into their mechanisms of action.

3 Results I: Cell culture and assay development in the HepaChip-MP

To enable reproducible cell culture experiments in the HepaChip-MP, the automated processes to prepare the chip and to assemble the cells were optimized. Primary human hepatocytes (PHH) and primary human liver endothelial cells were used in the HepaChip-MP to establish a co-culture. Commonly used assays to measure cell vitality (calcein staining, resazurine assay and ATP assay), protein expression (immunocytochemistry) and cell function (CYP-activity) were adapted to the HepaChip-MP and used, e.g. after substance treatment. In addition, different cell culture media were tested to support long-term cell culture.

For assays which lyse the cells (BCA assay and ATP assay), scripts were written to being able to perform this experiments automated and parallelized with the pipetting robot under pressure driven flow (for scripts, see Suppl.Fig. 1 and Suppl.Fig. 2). Online assays or assays which require unchanged cell morphology (e.g. calcein staining or immunostaining) were carried out with gravitational driven flow. This ensures that the cells are not exposed to more shear stress than during routine culture, which may change their morphology.

3.1 Priming of HepaChip-MP and routine culture

Starting this thesis, automated and parallelized processes to fill the chambers of the HepaChip-MP and to assemble the cells were optimized. The main objectives were to prevent the formation of air bubbles while filling and to cover the cell culture ridges with cells as completely as possible. After optimization of the initial filling process, the average yield of bubble free chambers was 77% for all chips prepared during the time of this thesis (see Appendix I, Appendix Table 1). This equals more than 18 chambers per chip to perform experiments. Next, the cell assembly was optimized to reach compact elongated cell aggregates on the assembly ridges. The developed process is described in detail in Busche et al., Appendix II. Busche et al., Appendix II, Suppl.Fig. 5 examplarily shows endothelial cells which were assembled with different frequencies (Busche et al., Appendix II, Suppl.Fig. 5). This demonstrates that the frequency for assembling new cell types in the HepaChip-MP has to be evaluated before using them routinely. Also, the used volume of the cell suspension and the waiting period between

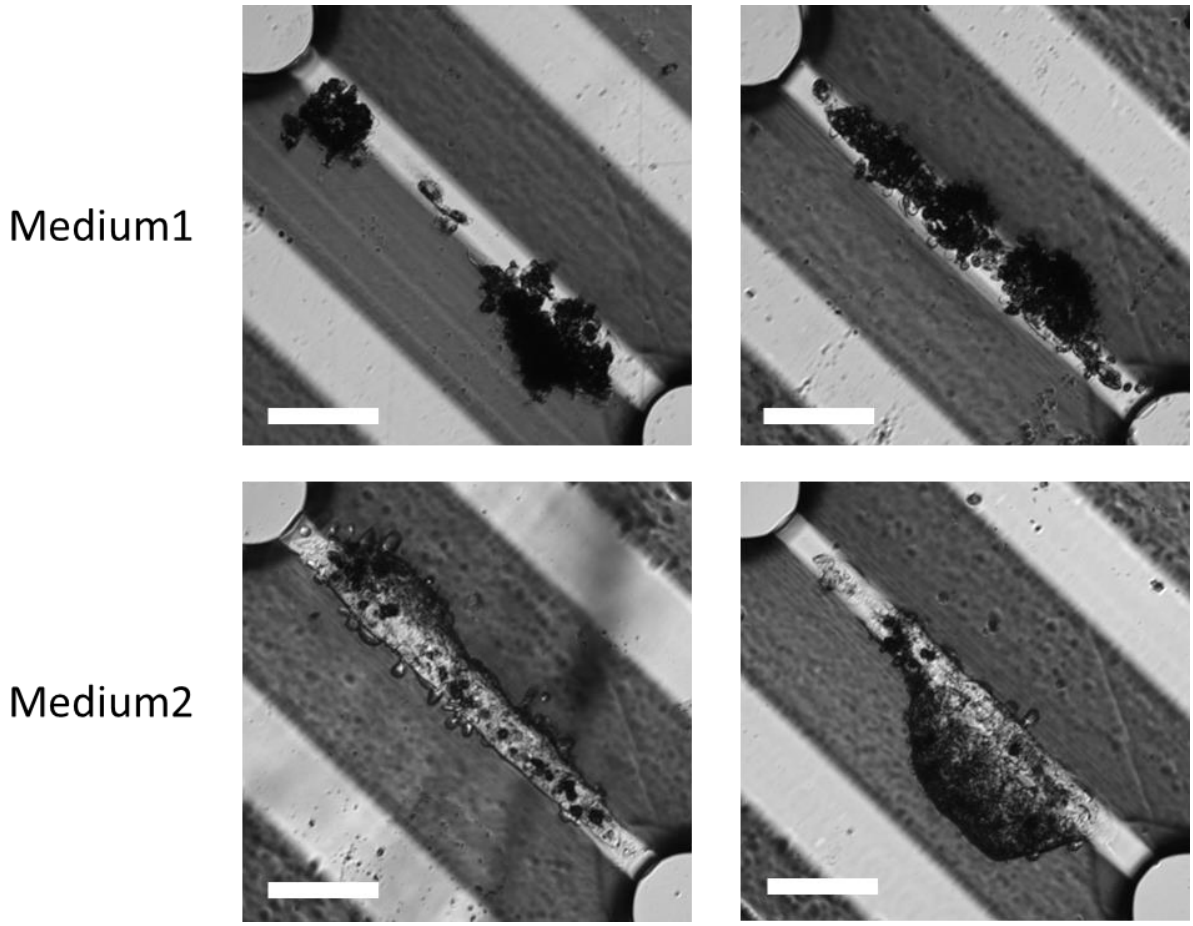

Figure 2: Represenative microscopic pictures of primary human hepatocytes cultured on the middle ridges in two different media on day 12 after cell assembly. Cells cultured in Medium1 appear to be black aggregates of cells (top panel). Cells cultured in Medium2 build a dense structure with observable borders at the interface to the medium (bottom panel). Also, cells cultured in Medium2 seem to show more adherent cell morphology than cells cultured in Medium1 on day 12 of culture (observable by the more transparent appearance) (scale bar equals 200 µm).

two pumping steps were optimized. By repeating cycles of setting up the pressure for pumping 1 µl and waiting for 15 sec, the flow velocity during the waiting period between two pumps decreases. Hence, the flow includes perfusion velocities, which are high enough to push all the non-adherent cells through the chamber, so they do not clog the channels. Likewise, the flow includes perfusion velocities which are low enough to enable efficient cell assembly by electrophoresis. After improving the technical aspects of the cell assembly, different media were tested to enable long-term culture of the cells. Medium1 denotes Williams E supplemented with 10% FBS, 15 mM HEPES, 1 mM Na-pyruvate, 1% non-essential amino acids, 1 µg/mL dexamethasone, 1 µg/mL human insulin and primocin. Medium2 was composed of Medium1 plus 0.55 µg/mL human transferrin, 0.5 ng/mL Na-selen and 5.35 µg/mL linoleic acid. Medium2 preserved better cell morphology over a culture period of 12 days (Figure 2). In

addition, Medium2 tended to support CYP2C9 and CYP3A4 activity over time better than Medium1 (Busche et al., Appendix II, Table 2). Thus, all future experiments were carried out with Medium2 if not stated differently.

At the beginning of the culture, cells built elongated structures over almost the whole cell culture ridges. Over time, the cells on the middle cell culture ridge built more contracted structures (Busche et al., Appendix II, Fig. 4). This might be due to stronger cell-cell-interactions than cell-substrate-interaction. Cells on the outer ridges tended to migrate towards the periphery (Busche et al., Appendix II, Fig. 4). This demonstrates that the cells are sensitive to minute hydrodynamic forces which are caused by a slight lateral flow (Busche et al., Appendix II, Suppl. Fig. 4; Busche et al., Appendix III, Fig. 2).

3.2 Cell vitality

For assessing the cell vitality of PHH cultured in the HepaChip-MP a resazurine assay and an ATP assay were established. The cell vitality in the HepaChip-MP was analyzed over the first six days of culture and after substance treatment. A resazurine assay performed on day 1, 3 and 6 of culture showed no changes over time in signal for non-treated cells while the signal for cells treated with 2 mM diclofenac at day 2 decreased to 40-70% of the value at day 1 (Busche et al., Appendix II, Fig. 3). This demonstrates that non-treated cells do not loose vitality over the first six days of culture. If not depicted differently, the analyses in this thesis were performed in the first six days of culture.

To enable testing of drugs or other substances for toxicity, different vitality tests are needed. Vitality tests generally measure one cell function, but different substances can cause non-identical cell response and some assays may be more sensitive for detecting the effect of a specific substance. That is why in general, to assess the influence of the substance of interest in detail, more than one vitality assay should be performed. The resazurine assay measures the redox potential while the ATP assay measures the concentration of ATP. The performed ATP assay showed higher sensitivity than the resazurine assay to detect diclofenac toxicity (see Figure 3). Toxicity of acetaminophen was demonstrated with the ATP assay as well. Diclofenac and acetaminophen toxicity was measured to exemplarily demonstrate the possibility to analyze dose-dependent influences on cell vitality and function on one single HepaChip-MP (see Figure 3 and Busche et al., Appendix II, Fig. 6).

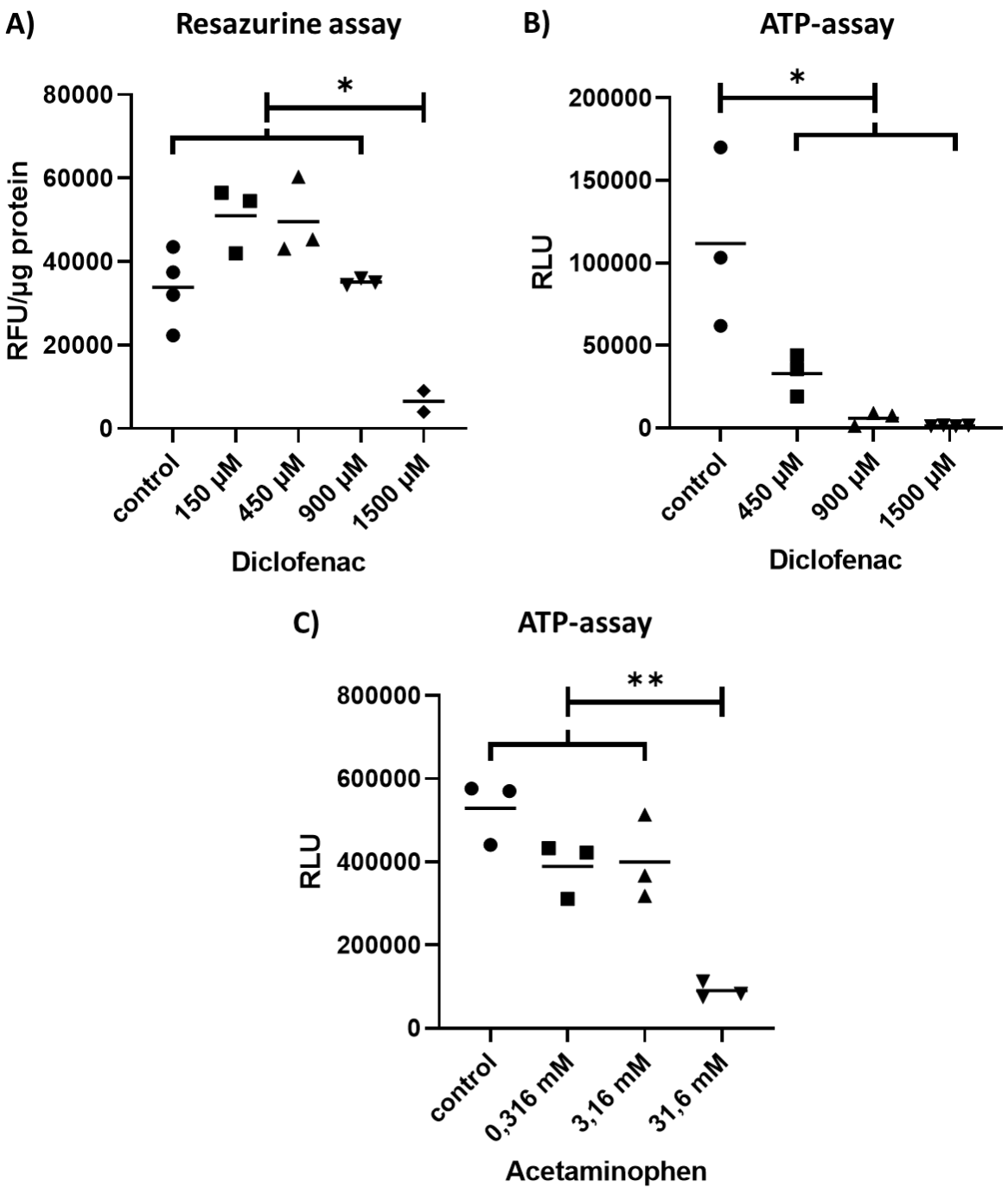

*Figure 3: Assessment of dose-dependent effects of diclofenac (A, B) and acetaminophen (C) analyzed with a resazurine assay (A) and an ATP-assay (B, C). Significances were calculated by one-way ANOVA and posthoc Tukey test (significances: * equals p<0.05, ** equals p>0.01).*

3.3 Hepatocyte-specific function

Next to cell vitality, cell specific function is an important marker to be analyzed. By demonstrating cell type-specific function, the relevance of the respective in vitro model can be verified. For hepatocytes, cytochrome P450 (CYP) activity is a very important

function to be evaluated in a cell model (see 1.2.1). CYP2C9 and CYP3A4 belong to the three CYP enzymes which are responsible for modifications of 63% of clinical used drugs [13]. Hence, the activity of these enzymes was evaluated in the HepaChip-MP. Basal activity of CYP2C9 and CYP3A4 was preserved over at least six days of culture (Busche et al., Appendix II, Fig. 4, Table 2). Also, induction with rifampicin showed the expected upregulation of enzyme activity (Busche et al., Appendix II, Fig. 5). Induced activity was 3.4-higher for CYP3A4 and 3.3-fold higher for CYP2C9. This demonstrates that basal as well as regulation of CYP activity after substance treatment can be analyzed in the HepaChip-MP.

3.4 Co-culture

Endothelial cells were introduced to the model system to add complexity and improve *in vitro – in vivo* correlation (see also 1.2.2 'Intrahepatic anatomical structure'). Endothelial cells make up 15-20% of the cells of the liver and are after hepatocytes the most prevalent cells in this organ [112]. Liver sinusoidal endothelial cells have a very high endocytosis capacity and a plethora of different functions in liver disease, liver regeneration, inflammation and infection [18, 112]. Amongst other things, they secrete paracrine factors, sense shear stress and present antigens to immune cells.

To add primary human liver endothelial cells (HuLEC) to the system, the adequate frequency for the assembly via DEP had to be determined. It was found that they need a higher frequency than PHH to be assembled efficiently (HuLEC: 620 kHz; PHH: 360 kHz; Busche et al., Appendix II, Suppl. Fig. 5). If non-optimal frequencies were used, the respective cells were diverted to the cell culture ridges less efficiently. A process was established to assemble primary human liver endothelial cells and primary human hepatocytes in one HepaChip-MP (see Busche et al., Appendix II). After assembling both cell types in the HepaChip-MP, cell type specific protein markers were stained by immunocytochemistry. Hepatocytes were stained for cytokeratin (CK18) and endothelial cells were stained for Cluster of Differentiation 31 (CD31) [113]. Cells positive for CK18 as well as cells positive for CD31 were found in the cell culture chamber at day 3 of culture (Busche et al., Appendix II, Fig. 7). This demonstrates that the HepaChip-MP is suitable for assembling and co-culturing different cell types to improve complexity and thus

relevance of the model. To support cell vitality and function of both cell types, a 50/50 mixture of the respective cell-type specific media was used.

4 Results II: Continuous, non-invasive monitoring of oxygen consumption in the HepaChip-MP provides novel insight into the response to nutrients and drugs of primary human hepatocytes

Molecular oxygen plays a pivotal role in the metabolism of mammalian cells. In the respiratory chain, it is used as an electron acceptor to oxidize NADH. The released energy is used to pump protons from the mitochondrial matrix into the intermembrane space. Thus, a concentration gradient of protons is built at the inner mitochondrial membrane. This gradient is utilized to produce ATP by oxidative phosphorylation. Thus, measuring the oxygen consumption (OC) of cells can give insights in cell vitality and mitochondrial (dis)function. Oxygen sensors were integrated into the HepaChip-MP at the inlet and the outlet of each cell culture chamber by colleagues of Associate Professor Torsten Mayr at the Graz University of Technology (Busche et al., Appendix III, Fig. 1). The chip material (COP) has low oxygen permeability [114]. Thus, by calculating the difference between inlet and outlet sensor, respectively, the consumed oxygen in the chamber can be determined.

It was demonstrated that the OC decreases with slower perfusion rates (Busche et al., Appendix III, Fig. 2; Busche et al., Appendix III, Suppl. Fig.1). Non-cellular effects to explain this finding like oxygen loss through the plastic ware or a flow-dependence of the sensors were ruled out by comparing chambers inhabiting cells to chambers without assembled cells. Chambers without assembled cells show negligible and unchanged OC over time (Busche et al., Appendix III, Suppl. Fig. 2). This demonstrates the applicability to use the integrated oxygen sensors to measure cellular OC.

4.1 Fructose

To test the acute cell response in OC on challenge with substances, fructose was used to treat PHH. Fructose treatment resulted in an immediate decrease of OC to less than 50% and a subsequent increase of OC to nearly initial levels after approx. 120 minutes (Busche et al., Appendix III, Fig. 3). This effect was not observed for cells treated with glucose, lactate or glycerol as control substances. Glucose is a C6-carbohydrate like fructose and consists of the same atoms with only small differences in the molecular structure. Lactate and glycerol are C3-carbohydrates and

products of the metabolism of fructose. Since neither lactate or glycerol showed the observed effect of fructose on OC, this suggests a fructose-specific effect in OC after treatment. Fructose is known to be phosphorylated by hepatocytes very fast and thereby intracellular concentration of ATP decreases [115]. As expected, in the HepaChip-MP, the ATP concentration of PHH was significantly lower 20 min after the start of fructose treatment compared to non-treated cells (Busche et al., Appendix III, Fig. 3). However, even after the apparent equilibration of OC close to initial levels, the ATP concentration of fructose-treated cells did not increase. Instead, it stayed at the same level as measured 20 minutes after fructose-application. This was an unexpected finding. The assumption was that when OC levels are reaching close to initial levels, also ATP levels should have been increased again to restore the initial equilibrium (see also 5.3).

4.2 System stability

The robustness and repeatability of measured responses is an important aspect to verify for in vitro systems. By demonstrating this, treatments and readouts have not necessarily to be carried out at exactly the same time point after starting the experiment to be able to compare cell responses. In addition, repeated-dose experiments can be carried out if the system is stable over a period of time.

The stability of oxygen sensing in the HepaChip-MP was evaluated by repeatedly treating PHH with fructose on day in vitro (DIV) 2 and DIV 3. The fructose-specific change in OC described above was reproduced on the same day with two hours break in between and on subsequent days (Busche et al., Appendix III, Fig. 4). This demonstrates the robustness of the readout system and the cellular regeneration of the cultured PHH. All described experiments in this thesis involving measurement of OC were carried out on DIV 2 or DIV 3.

4.3 Mitochondrial respiration

Known effects on OC are observed after subsequent dosing of oligomycin A, FCCP and rotenone/antimycin A [116]. The treatment with those substances gives a deeper insight into mitochondrial respiration and function. In the HepaChip-MP, the effect of oligomycin A, FCCP and rotenone/antimycin A were reproduced as expected

(Busche et al., Appendix III, Fig. 5). Oligomycin inhibits the ATP synthase and treatment lowered the OC under the basal level. FCCP is an uncoupling agent and OC rapidly rose to a plateau after treatment. Rotenone/antimycin A inhibits the electron transfer chain and the treatment led to a decrease of the OC under the level of the oligomycin A-treated cells. This allows for further experiments, which analyze differences in cell responses to the above mentioned substances after pretreatment with various other substrates. Differences in cell responses could then give insights into the mechanism of action of the substance of the pretreatment.

4.4 Getting insights into toxicity of ammonium chloride and diclofenac

To demonstrate the usability of our system to get deeper insights into substance effects on cellular OC and metabolic equilibrium, we treated PHH with ammonium chloride and diclofenac. Neither ammonium chloride nor diclofenac treatment showed an immediate effect on the OC of cultured cells like observed for fructose (data not shown). Although the specific mechanism of action is still unclear, ammonium chloride is known to have toxic effects on different tissues and cells including hepatic mitochondria [117, 118]. In the HepaChip-MP, PHH pretreated with 80 mM ammonium chloride showed the same cell response as untreated cells on treatment with oligomycin A and rotenone+antimycin A (Busche et al., Appendix III, Fig. 5). However, FCCP treatment resulted in different cell responses. While the OC of untreated cells immediately increases quickly to reach a plateau, the OC of ammonium chloride treated cells rose in a sigmoidal-shaped curve (Busche et al., Appendix III, Fig. 5). The level of the plateau did not differ, though. This effect on OC after FCCP treatment was not observed for other substances tested in this thesis. Thus, the described effect of ammonium chloride may be a substance-specific disturbance of the cellular equilibrium and might act as a starting point for further analyses of the mechanism of action of ammonium toxicity.

Next, the influence of diclofenac on OC of PHH was analyzed. Diclofenac is known to be associated with DILI and damage of mitochondria [119]. Syed et al. also demonstrated that diclofenac inhibits oxidative phosphorylation in isolated rat liver mitochondria [120]. In the HepaChip-MP, pretreating of PHH with 450 µM diclofenac resulted in a significant reduction of maximal respiration and reserve

capacity (Busche et al., Appendix III, Fig. 6). Treatment with 50 µM and 150 µM did not cause differences in OC in comparison to non-treated cells. Cells pretreated with 1500 µM diclofenac did not show any response to the treatment with oligomycin A, FCCP and rotenone+antimycin A (Busche et al., Appendix III, Suppl. Fig. 5). This suggests that the cells are dead after treatment with 1500 µM diclofenac, as described previously (Busche et al., Appendix III, Fig. 6). In conclusion, the system can be used to detect substance-induced toxicity and get insights into mechanisms of action.

5 General Discussion & Outlook

In this thesis, a parallelized and perfused in vitro system of the liver sinusoid was established and used to analyze the effect of different substances on primary human liver cells. For this, processes for chip filling, cell assembly, routine culture and analyzing cell function were optimized, applied and partly automatized. Assays to evaluate cell function include vitality assays, activity and induction of cytochrome P450 enzymes, immunocytochemistry and measuring oxygen consumption.

5.1 Parallelization and handling of the HepaChip-MP in comparison to other commercialized systems

As described in the introduction, one aspect that hinders broad adaption of organ-on-chip systems is the usability by non-expert end-users and lack of parallelization. With 24 independently usable cell culture chambers on one microwellplate, the HepaChip-MP enables parallelization and the execution of e.g. a dose-response curve on one chip (see Figure 3). In addition, various required controls can be used with the same cell preparation on the same chip. In comparison to other commercialized system, the degree of parallelization of the HepaChip-MP settles somewhere in the middle. It comprises more chambers than InSpheros (11 chambers; [78]) and CNBios (12 chambers; [94, 97]) platform, but fewer chambers than Emulates (48 chambers; [98, 99]) and Mimetas' (96 chambers; [95]) platforms. Often, chambers are not usable due to air bubbles or clogged channels and the vendors of the commercialized systems do not mention the actually usable chambers per chip and cell preparation. Nevertheless, Emulates and Mimetas' platform probably allow for more experiments in parallel than the HepaChip-MP. One drawback of Mimetas' platform is that it uses a rocker platform to establish the perfusion. By this, a bidirectional flow is initiated. In contrast to the unidirectional flow in the HepaChip-MP, bidirectional flow does not lead to more physiologic homogenous shear forces, constant delivery of nutrients or removal of waste products. Emulates platform enables parallelization by using a combination of periphery systems where single chips can be inserted. This is a great feature for routine culture, but for performing experiments with different treatments etc. each single chip has to be handled by itself which prolongs manual handling procedures. The HepaChip-MP, however, employs 24 chambers on

one single chip whose medium reservoirs are easily accessible by conventional pipetting processes like in commonly used well plates. In addition, assays in the HepaChip-MP can be performed by conventional automation systems like pipetting robots. This decreases manual handling steps and thus eases the handling. Hence, the HepaChip-MP combines various advantages of currently commercialized organ-on-chip systems in terms of parallelization, ease-of-use and mode of perfusion.

5.2 General aspects of cell culture in the HepaChip-MP

One important aspect of organ-on-chip systems is to sustain organ-specific cell function over a sufficient long time. For this, coculture with non-parenchymal cells and the supply with an appropriate medium to support cell vitality and function may be advantageous (see 1.3.1 and 1.3.2). In this thesis, it was demonstrated that the usage of medium2 leads to a better cell morphology on day 12 of culture than medium1 (Figure 2). Medium2 additionally includes human transferrin, Na-selen and linoleic acid in comparison to Medium1. These are supplements often used in literature [45, 66, 92, 121, 122]. Transferrin is a transporter for Fe^{3+}-ions and an antioxidant. Thus, it contributes to the equilibrium of iron metabolism and supports the detoxification of reactive oxygen species (ROS). Selen is an essential trace element, which is rarely supplemented in common cell culture media. It is an important part of enzymes contributing to the detoxification of ROS. ROS production is known to be elevated during and after surgery and hepatocyte isolation [123]. Miller et al. reported that moderate ROS production during and shortly after isolation can be beneficial for cell survival [123]. But Miller et al. are using healthy rodent livers for isolating hepatocytes, while in the existing study hepatocytes of diseased human livers are used. Boghal et al. demonstrated that hepatocytes isolated from diseased human liver tissue show higher ROS production than hepatocytes isolated from healthy livers [124]. Hence, the hepatocytes used in the present thesis are assumed to produce more ROS than the amount which would be beneficial for cell survival as reported by Miller et al [123]. Thus, the usage of transferrin and selen as medium supplements supports the vitality of cells by inhibiting negative effects of ROS. Linoleic acid is an essential ω-6 fatty acids and by supporting membrane integrity, it shields cells against shear forces [125]. This effect of linoleic acid may especially be advantageous in perfused culture systems.

In general, further development of media for perfused systems is postulated to improve organ-specific cell function [122]. Currently used media are optimized for proliferation of cells. Hence, the media comprise a surplus of nutrients and nutrient concentrations decline between two medium exchanges in static cell culture systems. However, in organ-on-chip systems with unidirectional perfusion, medium in the cell microenvironment is constantly exchanged. In addition, the medium-to-cell ratio is often higher in organ-on-chip systems than e.g. in 2D culture systems. Hence, the cells are constantly experiencing a high concentration of nutrients. This does not reflect the in vivo situation and to emulate physiological conditions better, the medium should be adapted to this new situation. One further development would be a blood surrogate, which can be used for different organ systems cultivated in a row in one system. Media generally support proliferation and function of a specific cell type and comprise certain nutrients and growth factors. However, a medium for a multi-organ chip should support all the different organ-function and thus, has other demands for medium supplements. If the respective multi-organ chip has sufficient hormone and growth factor producing organs implemented, it can also be assumed that a very basic medium would be suited. In such a system, it could be possible that an equilibrium is developing between production and usage of hormones and growth factors which leads to physiologic organ function. In such a system the relation of organs in terms of cell number and position in the circulatory system has to be taken into account.

It was demonstrated that cells on the outer cell culture ridges of the Hepachip-MP migrate to the periphery of the chamber (Busche et al., Appendix II, Fig. 4). This possibly is due to minute medium flow over the outer cell culture ridges (Busche et al., Appendix II, Suppl. Fig. 4). This is in line with investigations by Polacheck et al., who demonstrated that minute medium flow induces directed cell migration [126]. Polacheck et al. showed in a 3D collagen matrix system that cells seeded in high density migrate with the flow and that cells seeded in low density migrate against the flow direction. In the HepaChip-MP, the density of the cell aggregates is probably more similar to the high density situation investigated by Polacheck et al and hence, the cells migrate with the flow. This unintentional and lateral medium flow could be prevented by slightly changing the design of the cell culture chambers in future projects. Another observation was that cells on the cell culture ridges tend to contract to form a more spheroid-like structure (Busche et al., Appendix II, Fig. 4). One possible reason for that

is that the cell-cell-interaction becomes stronger than the cell-surface-interaction. Maybe, cells even build proteinases which destroy the collagen on the surface and therefore, the interaction with the surface is decreasung. This could possibly either be counteracted by using other molecules, proteins or protein-combinations to mediate stronger and more durable adhesion or by inhibiting the proteinases.

In this work, the co-culture of PHH and HuLEC was established (Busche et al., Appendix II, Fig. 7) to demonstrate the possibility to assemble different cell types in one cell culture chamber of the HepaChip-MP. In future projects, this enables the setting up of a system which inhabits the required cell types for a specific question of interest. It has to be taken into consideration though that due to differences in the dielectrophoretic properties of different cell types, different cell types might need different frequencies to be assembled efficiently in the HepaChip-MP (see also 3.4).

5.3 Cell function and effect of substances

Due to the low cell number per chamber, sensitive assays are required to quantify cell function in the HepaChip-MP. Nevertheless, readouts like cell vitality after substance treatment as well as analyses of enzyme regulation can be performed in this system (see 3.2 and 3.3).

It was demonstrated that CYP2C9 as well as CYP3A4 can be induced in the HepaChip-MP (Busche et al., Appendix II, Fig. 5). This is an important aspect to be shown in liver models and indicates physiologic enzyme regulation [22]. In the following, the basal CYP activity will be compared to results from other labs. The PHH used in this study were purchased from CYTES Biotechnologies S.L. (Barcelona, Spain). CYTES tests all the PHH they sell in-house in a sandwich culture built out of collagen I and matrigel. Unfortunately, they did not provide any information about CYP2C9 activity. Our project partner Primacyt GmbH (Schwerin, Germany) used cells from the same donor as utilized in this thesis in a spheroid model to test CYP2C9 activity as well as CYP3A4 activity. They found a very similar basal activity of CYP2C9 (Busche et al., Appendix III, Fig. 5; Table 1). Since CYP3A4 is the most important CYP enzyme in terms of drug metabolism [13], the activity data for this enzyme is compared in more detail to other studies in the following. For the donor used in this thesis, CYTES found a basal CYP3A4 activity approximately 12 times higher in their sandwich culture than in the HepaChip-MP (Table 1). Our project partner Primacyt

GmbH (Schwerin, Germany) found activities approximately 10 times higher than in the HepaChip-MP in their spheroid model (Busche et al., Appendix III, Fig. 5; Table 1). In line with these findings, Foster et al. found approximately 60 times higher CYP3A4 activity in spheroids compared to an organ-on-chip system [127]. On the other hand, Vinci et al. showed a roughly 20 times higher CYP3A4 activity in a perfused system compared to a static system [128]. In general, reported values for CYP3A4 activity show high variability of about 5 times in magnitude (Table 1). The values are often normalized to cell count. Since this type of normalization is not easily executed in our chip system, we normalized on mg protein per chamber. To compare values normalized on cell number and total protein amount, cell numbers were converted to total protein amount (Table 1). CYP3A4 activities in the HepaChip-MP are one to six orders of magnitude higher than in the cited literature (Table 1). In general, CYP activity depends on many factors like the donor, the culture system, co-cultured cell types, day of measurement, media supplements as well as the incubation time of the substrate may influence the determined activity. This various interdependencies may explain the high variability in reported values for CYP3A4 activity in literature. To be able to better compare studies in the future, standardized assay protocols should be established and used by scientists (if applicable in the respective system).

Three different assays to evaluate diclofenac toxicity were performed in this thesis: a resazurine assay (Figure 3, Busche et al., Appendix II, Fig. 6), an ATP-assay (Figure 3) and measuring mitochondrial respiration after substance treatment (Busche et al., Appendix III, Fig. 3-6). While the resazurine assay demonstrates significant cell damage only after treatment with 1500 µM diclofenac, the other two assays already show diminished cell vitality/activity after treatment with 450 µM. This demonstrates that different assays may have varying sensitivity to detect toxicity of a substance. In general, assays may interfere with the compound, measure different cell functions and should be chosen based on the design of the study [132]. Syed et al. found an IC_{50} value of 19.5 µM for diclofenac in isolated rat mitochondria [120]. Additionally, they demonstrated the protective effect of GSH. While isolated rat mitochondria do not contain GSH, PHH do. This may explain the higher doses of diclofenac needed to induce cell damage in PHH as demonstrated in this study.

Table 1: Basal CYP3A4 activity for different culture systems from literature. The first three lines correspond to experiments performed with the same donor. To compare values normalized on cell number and total protein amount, cell number was converted to total protein amount. For this, it was assumed that the concentration of proteins is 0.2 g/ml in cells [129] and that PHH roughly have an average volume of 8000 µm³ [130]. This leads to a total protein content of 1.6 ng per primary human hepatocyte.

	culture system	cell types	day of culture	Basal activity (pmol/min/mg protein)	original unit
this work	**HepaChip-MP**	**PHH**	**5**	**0.532**	**ng/min/ mg protein**
Primacyt	**spheroid**	**PHH**	**9**	**5.165**	**ng/min/ mg protein**
CYTES Biotechnologies	**Collagen I-Matrigel sandwich**	**PHH**	**4**	**6.42**	**pmol/min/ mg protein**
Bell, 2018 [63]	**spheroid**	**PHH**	**5**	**0.016**	**pmol/h/ 10^6 cells**
	Collagen I-Matrigel sandwich	**PHH**	**5**	**$4.688*10^{-3}$**	**pmol/h/ 10^6 cells**
Foster, 2019 [127]	**Spheroid**	**PHH + NPC**	**4**	**0.016**	**pmol/min/ 10^6 cells**
	Organ-on-chip	**PHH + LSEC**	**3**	**$2.5*10^{-4}$**	**pmol/min/ 10^6 cells**
Vinci, 2011 [128]	**Organ-on-chip dynamic**	**PHH**	**7**	**$4.688*10^{-3}$**	**nmol/h/ 10^6 cells**
	Organ-on-chip static	**PHH**	**7**	**$2.083*10^{-4}$**	**nmol/h/ 10^6 cells**
Novik, 2010 [70]	**Organ-on-chip**	**PHH + NPC**	**1**	**$1.125*10^{-3}$**	**pmol/min/ 10^6 cells**
Prodanov, 2016 [71]	**Organ-on-chip**	**PHH + NPC**	**7**	**$1.736*10^{-5}$**	**pmol/d/ 10000 cells**
Zeilinger, 2011 [131]	**hollow fiber bioreactor**	**PHH + NPC**	**5**	**$6.51 * 10^{-7}$**	**µmol/d/ 10^7 cells**

We demonstrated significant lower ATP concentration in cell cultures after treatment with 31.5 mM acetaminophen (Figure 3). Minsart et al. detected a decrease to over 50% of cell viability after treatment with concentrations higher than 10 mM acetaminophen in HepaRG cells [133]. Xie et al. demonstrated cell damage of primary human hepatocytes after treatment with 5 mM acetaminophen and higher [134]. Hence, the concentrations for acetaminophen-induced cell damage found in this study stand in line with literature data.

Measuring cellular oxygen consumption after treatment with oligomcyin, FCCP and R/A is known to give insight into mitochondrial function and disfunction [116]. The expected cell response after challenge with these substances was demonstrated in the HepaChip-MP in this thesis (Busche et al., Appendix III, Fig. 5). This indicates physiologic regulation of oxygen usage and enables in depth analysis of substances impeding mitochondrial respiration. Analysis of mitochondrial respiration by PHH pretreated with ammonium chloride and diclofenac demonstrated the feasibility to get more insights into mechanism of action (Busche et al., Appendix III, Fig. 5+6). The main differences in cell responses in oxygen consumption of pretreated PHH compared to control cells were found after treatment with FCCP. Cell response on FCCP treatment is dependent on nutrient supply and metabolic status of the cell [135]. Thus, FCCP-treatment in combination with changing the microenvironment of the cell (by e.g. challenge with substances) supports deeper analysis of equilibrium changes inside the cell. The demonstrated effects of ammonium chloride and diclofenac may serve as starting points to better understand the mechanism of action of these substances.

In this thesis, a very specific acute effect of fructose on cellular respiration of PHH was demonstrated (Busche et al., Appendix III, Fig. 3). The oxygen consumption initially drops after starting the fructose-treatment and rises again to basal levels within approximately two hours. This effect was not observed for glucose, lactate and glycerol. This effect of fructose has also not been described in recent literature. Though, Ylikahri et al. demonstrated the biphasic effect of fructose in 1971 in perfused rat livers [136]. These authors proposed that the oxygen consumption initially drops due to a depletion of P_i followed by inhibition of oxidative phosphorylation. When the P_i concentration increases again, oxidative phosphorylation is induced and ATP regenerated. However, in our experiments, we found that the ATP concentration stayed low even though the cellular oxygen consumption reached initial levels after two hours of fructose-treatment (Busche et al., Appendix III, Fig. 3). One explanation for this observation could be that the regenerated ATP is immediately used to phosphorylate the fructose. Another explanation could be that this suggests a different mechanism than ATP and P_i depletion for the fructose-induced effect on oxygen consumption. In future experiments, these mechanisms should be analyzed in combination with the metabolization of fructose.

5.4 Potential future use of HepaChip-MP system

In general, the use of organ-on-chip systems and the HepaChip-MP depends on the question of interest. A perfused system which is more expensive and more complicated to handle than simple 2D monolayers is not needed to find out that high concentrations of a toxic agent may damage cells. But when it comes to the more detailed analysis of mechanisms of action, a perfused and more physiologic system in terms of dimensions can be of big advantage. In addition, it has been demonstrated, that results generated in organ-on-chip systems may be better translatable to human than results from animal studies (for a review, see [137]). Nevertheless, not all relevant parameters for preclinical research can currently be reproduced in an organ-on-chip system (e.g. cognition or behavior). Hence, organ-on-chip systems may serve as preclinical model systems which will reduce animal studies in some extend, but might not fully replace them.

The HepaChip-MP especially has the advantages over other perfused systems that it does not need a hydrogel or a membrane to assemble the cells. Hence, the cells are in direct contact to the medium and delivery of nutrients/substances as well as removal of waste products is not hindered by diffusion through physical hurdles. Also, the fact that the cell culture ridges in the HepaChip-MP have the same dimensions like the cell sheets in the acinus of the liver may be an important feature for some applications. However, long-term and stable adhesion of cell aggregates on the cell culture ridges still has to be optimized (see 5.5).

The integrated oxygen sensors are a special feature of the HepaChip-MP. The two commercialized benchmark systems to measure respiration rates in vitro are the MitoXpress platform and the seahorse XF analyser [138, 139], both from Agilent (Santa Clara, CA, United States). These systems enable measurement of oxygen concentration in closed and static chambers. Thus, they measure the depletion of oxygen in the medium and at the end of the measurement, the cellular microenvironment may be hypoxic. This is an artificial and non-physiologic situation. The HepaChip-MP, however, enables online measurements of oxygen concentration under the same perfusion conditions as employed during routine culture. Hence, the cells and the cellular microenvironment is not disturbed because of the measurement. In addition, exchange of medium is not possible in the MitoXpress. The seahorse XF analyser enables up to four consecutive substance injections without exchanging the

medium. In the HepaChip-MP, the continuous perfusion removes the tested substances and easily enables numerous consecutive treatments. Hence, for measuring oxygen consumption, the HepaChip-MP has several advantages over currently commercialized systems.

5.5 Further chip and process development

To enable convenient usage of the HepaChip-MP and adoption by other labs, cellular function and handling processes should be optimized further. Concerning processes of chip priming, the occurrence of air bubbles in the chamber still has to be reduced. This would enable reliable design of experiments and improve the costs/data point relation. The cell assembly process may further be optimized to waste less cells which do not attach on the ridges, but flow through the chamber without being used afterwards. Since primary cells may be a limiting factor when in vitro systems are used even more extensively, saving cells would be of advantage and reduce costs. To enable repeated dosing experiments or simply analyze cells over a longer period of time, a long-term culture has to be established. This may be realized by media optimization, co-culture with e.g. non-parenchymal or feeder cells or modified coating of the cell culture ridges. The modified coating may counteract the tendency to build more spheroid-like structures on the cell culture ridges and lead to stable elongated cell aggregates on the cell culture ridges mimicking the cell sheets in the liver sinusoid. In addition, the minute flow over the cell culture ridges (see Busche et al., Appendix II, Fig. 4 + Discussion) has to be prevented by changing the chamber design. By this, cells may stay longer especially on the outer cell culture ridges.

To lay the foundation for a broad adoption of new systems, validation experiments have to be carried out. In this thesis, proof-of-concept experiments have been carried out and they show promising results. In the next steps, results should be reproduced with different donors and in different laboratories. This would demonstrate the robustness of the system. One step in this direction has already been executed during the time of this thesis by setting up a pipetting robot to handle the HepaChip-MP in the laboratories of the cooperation partner Primacyt GmbH (Schwerin, Germany). Also, more experiments to compare cell behavior in the HepaChip-MP with other in vitro systems like 2D monolayers and spheroids should be carried out to be able to better compare the different systems.

More detailed further developments have to be focused on the application of interest. In general, normalization should be taken into consideration. Chambers of organ-on-chip systems are mostly closed and not all cells put into the systems adhere and stay there over the culture time. Since it is also difficult to count cells in three-dimensional constructs, the exact cell count is not determined reliably and easily. One possible normalization procedure is to measure the total protein amount per chamber. This normalization was carried out in this thesis. However, every tiny residue of medium disturbs the determination of protein concentration and it is tedious to wash the chambers and channels adequately. For future applications, integrated sensors or algorithm-based normalization procedures may facilitate the normalization.

5.6 Conclusion

Current preclinical model systems of the liver sinusoid fail to predict substance effects in humans reliably. Organ-on-chip systems are a promising technology addressing current drawbacks of preclinical model systems, however, still pose challenges in terms of their scalability, low parallelization and automation of work processes as well as fit for purpose analysis methods.

In this thesis, the HepaChip-MP was established as a parallelized microfluidic platform to mimic liver specific cell behaviour and substance-induced toxicity. This was reached by a) optimizing and establishing easy-to-perform and partly automated procedures to handle the HepaChip-MP, b) demonstrating cell viability and liver-specific cell function of cells cultured in it and c) establishing oxygen sensors and analyzing oxygen consumption of cells treated with different substances.

The parallelization and automation of filling and cell assembly processes with a pipetting robot enables broad usage of the HepaChip-MP by non-expert end-users. Optimization of cell culture processes, including media composition, enabled the prolonged culture periods necessary to establish processes to study cell vitality and function. After validating established handling and cell culture processes with different donors and in other laboratories, the HepaChip-MP can readily be used for various applications in academia and industry, like substance testing.

In pharmaceutical industry, especially CYP activity and its physiological regulation is an important function to be emulated. Basal CYP activity and induction has successfully been demonstrated in this thesis (see 3.3). In addition, substance-induced

toxicity is an important aspect to be evaluated in pharmaceutical research. With the resazurine assay, the ATP-assay and the measurement of cellular oxygen consumption, three assays have been established in the HepaChip-MP to analyze the toxicity of a substance (see 3.2 and 4.4). The oxygen sensors also enable more detailed analysis of mitochondrial respiration and oxidative phosphorylation which opens possibilities to get a deeper insight into the mechanism of action of substances. For example, the effect detected for fructose on cellular ATP concentration and cellular respiration indicates a new finding in relation to ATP production for metabolism of fructose other than via oxidative phosphorylation (see 4.1 and 5.3). In addition, the different cell responses after FCCP treatment of PHH pretreated with diclofenac and ammonium chloride may be a starting point to better understand the mechanisms of action of these substances. Future experiments should analyze the substance-induced changes in mitochondrial oxygen usage in more detail.

To summarize, the results of this thesis provide the basis and the proof-of-concept for various future applications of the HepaChip-MP in academia and industry. In addition, exciting substance-induced effects were demonstrated with integrated oxygen sensors which have not been described in literature, yet.

Literature

1. Lacoste-Roussillon, C., et al., *Incidence of serious adverse drug reactions in general practice: a prospective study.* Clin Pharmacol Ther, 2001. **69**(6): p. 458-62.
2. McNaughton, R., G. Huet, and S. Shakir, *An investigation into drug products withdrawn from the EU market between 2002 and 2011 for safety reasons and the evidence used to support the decision-making.* BMJ Open, 2014. **4**(1): p. e004221.
3. Zhang, W., et al., *Pharmacogenetics of drugs withdrawn from the market.* Pharmacogenomics, 2012. **13**(2): p. 9.
4. Ichai, P. and D. Samuel, *Epidemiology of liver failure.* Clin Res Hepatol Gastroenterol, 2011. **35**(10): p. 610-7.
5. Licata, A., *Adverse drug reactions and organ damage: The liver.* Eur J Intern Med, 2016. **28**: p. 9-16.
6. Björnsson, E.S., *Global Epidemiology of Drug-Induced Liver Injury (DILI).* Current Hepatology Reports, 2019. **18**(3): p. 274-279.
7. Scannell, J.W., et al., *Diagnosing the decline in pharmaceutical R&D efficiency.* Nat Rev Drug Discov, 2012. **11**(3): p. 191-200.
8. Harrison, R.K., *Phase II and phase III failures: 2013-2015.* Nat Rev Drug Discov, 2016. **15**(12): p. 817-818.
9. Paul, S.M., et al., *How to improve R&D productivity: the pharmaceutical industry's grand challenge.* Nat Rev Drug Discov, 2010. **9**(3): p. 203-14.
10. Franzen, N., et al., *Impact of organ-on-a-chip technology on pharmaceutical R&D costs.* Drug Discov Today, 2019. **24**(9): p. 1720-1724.
11. Blumgart, L., *Surgery of the liver, biliary tract and pancreas*. 4th ed. 2016: Saunders. 2008.
12. Abdel-Misih, S.R. and M. Bloomston, *Liver anatomy.* Surg Clin North Am, 2010. **90**(4): p. 643-53.
13. Zanger, U.M. and M. Schwab, *Cytochrome P450 enzymes in drug metabolism: regulation of gene expression, enzyme activities, and impact of genetic variation.* Pharmacol Ther, 2013. **138**(1): p. 103-41.
14. Zanger, U.M., et al., *Functional pharmacogenetics/genomics of human cytochromes P450 involved in drug biotransformation.* Anal Bioanal Chem, 2008. **392**(6): p. 1093-108.
15. Barbarino, J.M., et al., *PharmGKB summary: very important pharmacogene information for UGT1A1.* Pharmacogenet Genomics, 2014. **24**(3): p. 177-83.
16. Welsch, U. and T. Deller, *Leber und Gallenwege*, in *Sobotta Lehrbuch Histologie*. 2010, Urban&Fischer in Elsevier.
17. Wilkinson, A.L., M. Qurashi, and S. Shetty, *The Role of Sinusoidal Endothelial Cells in the Axis of Inflammation and Cancer Within the Liver.* Frontiers in Physiology, 2020. **11**.
18. Shetty, S., P.F. Lalor, and D.H. Adams, *Liver sinusoidal endothelial cells - gatekeepers of hepatic immunity.* Nat Rev Gastroenterol Hepatol, 2018. **15**(9): p. 555-567.
19. Nagy, P., S.S. Thorgeirsson, and J.W. Grisham, *Organizational Principles of the Liver*, in *The Liver*. 2020. p. 1-13.
20. Atkins, J.T., et al., *Pre-clinical animal models are poor predictors of human toxicities in phase 1 oncology clinical trials.* Br J Cancer, 2020. **123**(10): p. 1496-1501.

21. Van Norman, G.A., *Limitations of Animal Studies for Predicting Toxicity in Clinical Trials: Is it Time to Rethink Our Current Approach?* JACC Basic Transl Sci, 2019. **4**(7): p. 845-854.
22. Baudy, A.R., et al., *Liver microphysiological systems development guidelines for safety risk assessment in the pharmaceutical industry.* Lab Chip, 2020. **20**(2): p. 215-225.
23. Schwartz, R.E., et al., *Pluripotent stem cell-derived hepatocyte-like cells.* Biotechnol Adv, 2014. **32**(2): p. 504-13.
24. Zeilinger, K., et al., *Cell sources for in vitro human liver cell culture models.* Exp Biol Med (Maywood), 2016. **241**(15): p. 1684-98.
25. Zhao, X., et al., *Hepatic Differentiation of Stem Cells in 2D and 3D Biomaterial Systems.* Bioengineering (Basel), 2020. **7**(2).
26. Luckert, C., et al., *Comparative analysis of 3D culture methods on human HepG2 cells.* Arch Toxicol, 2017. **91**(1): p. 393-406.
27. Gerets, H.H., et al., *Characterization of primary human hepatocytes, HepG2 cells, and HepaRG cells at the mRNA level and CYP activity in response to inducers and their predictivity for the detection of human hepatotoxins.* Cell Biol Toxicol, 2012. **28**(2): p. 69-87.
28. Lee, J.H., K.L. Ho, and S.K. Fan, *Liver microsystems in vitro for drug response.* J Biomed Sci, 2019. **26**(1): p. 88.
29. Poloznikov, A., et al., *In vitro and in silico liver models: Current trends, challenges and opportunities.* ALTEX, 2018. **35**(3): p. 397-412.
30. Tetsuka, K., M. Ohbuchi, and K. Tabata, *Recent Progress in Hepatocyte Culture Models and Their Application to the Assessment of Drug Metabolism, Transport, and Toxicity in Drug Discovery: The Value of Tissue Engineering for the Successful Development of a Microphysiological System.* J Pharm Sci, 2017. **106**(9): p. 2302-2311.
31. Lauschke, V.M., et al., *Novel 3D Culture Systems for Studies of Human Liver Function and Assessments of the Hepatotoxicity of Drugs and Drug Candidates.* Chem Res Toxicol, 2016. **29**(12): p. 1936-1955.
32. Deng, J., et al., *Engineered Liver-on-a-Chip Platform to Mimic Liver Functions and Its Biomedical Applications: A Review.* Micromachines (Basel), 2019. **10**(10).
33. Asha, S. and M. Vidyavathi, *Role of human liver microsomes in in vitro metabolism of drugs-a review.* Appl Biochem Biotechnol, 2010. **160**(6): p. 1699-722.
34. Gomez-Lechon, M.J., et al., *Human hepatocytes as a tool to study toxicity and drug metabolism.* Current Drug Metabolism, 2003. **4**: p. 21.
35. Block, G.D., et al., *Population expansion, clonal growth, and specific differentiation patterns in primary cultures of hepatocytes induced by HGF/SF, EGF and TGF alpha in a chemically defined (HGM) medium.* J Cell Biol, 1996. **132**(6): p. 1133-49.
36. Ferrini, J.-B., et al., *Long-term primary cultures of adult human hepatocytes.* Chemico-Biological Interactions, 1997. **107**: p. 15.
37. Runge, D.M., et al., *Epidermal growth factor- and hepatocyte growth factor-receptor activity in serum-free cultures of human hepatocytes.* J Hepatol, 1999. **30**(2): p. 265-74.
38. Runge, D., et al., *Serum-free, long-term cultures of human hepatocytes: maintenance of cell morphology, transcription factors, and liver-specific functions.* Biochem Biophys Res Commun, 2000. **269**(1): p. 46-53.

39. Ullrich, A., et al., *Use of a standardised and validated long-term human hepatocyte culture system for repetetive analyses of drugs: Repeated administrations of acetaminophen reduces albumin and urea secretion.* ALTEX, 2006. **24**: p. 6.
40. Xiang, C., et al., *Long-term functional maintenance of primary human hepatocytes in vitro.* Science, 2019. **364**(6438): p. 399-402.
41. Levy, G., et al., *Long-term culture and expansion of primary human hepatocytes.* Nat Biotechnol, 2015. **33**(12): p. 1264-1271.
42. Zhou, M., et al., *Long-term maintenance of human fetal hepatocytes and prolonged susceptibility to HBV infection by co-culture with non-parenchymal cells.* J Virol Methods, 2014. **195**: p. 185-93.
43. Kostadinova, R., et al., *A long-term three dimensional liver co-culture system for improved prediction of clinically relevant drug-induced hepatotoxicity.* Toxicol Appl Pharmacol, 2013. **268**(1): p. 1-16.
44. Khetani, S.R. and S.N. Bhatia, *Microscale culture of human liver cells for drug development.* Nat Biotechnol, 2008. **26**(1): p. 120-6.
45. March, S., et al., *Micropatterned coculture of primary human hepatocytes and supportive cells for the study of hepatotropic pathogens.* Nat Protoc, 2015. **10**(12): p. 2027-53.
46. Dunn, J.C.Y., R.G. Tompkins, and M.L. Yarmush, *Long-Term in Vitro Function of Adult Hepatocytes in a Collagen Sandwich Configuration.* Biotechnology Progress, 1991. **7**(3): p. 237-245.
47. Dunn, J.C., R.G. Tompkins, and M.L. Yarmush, *Hepatocytes in collagen sandwich: evidence for transcriptional and translational regulation.* J Cell Biol, 1992. **116**(4): p. 1043-53.
48. LeCluyse, E.L., K.L. Audus, and J.H. Hochman, *Formation of extensive canalicular networks by rat hepatocytes cultured in collagen-sandwich configuration.* Am J Physiol, 1994. **266**(6 Pt 1): p. C1764-74.
49. Liu, X., et al., *Partial Maintenance of Taurocholate Uptake by Adult Rat Hepatocytes Cultured in a Collagen Sandwich Configuration.* Pharmaceutical Research, 1998. **15**(10): p. 1533-1539.
50. Yanni, S.B., et al., *In vitro investigation of the hepatobiliary disposition mechanisms of the antifungal agent micafungin in humans and rats.* Drug Metab Dispos, 2010. **38**(10): p. 1848-56.
51. Yang, K., et al., *Sandwich-Cultured Hepatocytes as a Tool to Study Drug Disposition and Drug-Induced Liver Injury.* J Pharm Sci, 2016. **105**(2): p. 443-459.
52. Kern, A., et al., *Drug metabolism in hepatocyte sandwich cultures of rats and humans.* Biochem Pharmacol, 1997. **54**(7): p. 761-72.
53. Miranda, J.P., et al., *Extending hepatocyte functionality for drug-testing applications using high-viscosity alginate-encapsulated three-dimensional cultures in bioreactors.* Tissue Eng Part C Methods, 2010. **16**(6): p. 1223-32.
54. Yamada, M., et al., *Controlled formation of heterotypic hepatic micro-organoids in anisotropic hydrogel microfibers for long-term preservation of liver-specific functions.* Biomaterials, 2012. **33**(33): p. 8304-15.
55. Chang, T.T. and M. Hughes-Fulford, *Monolayer and spheroid culture of human liver hepatocellular carcinoma cell line cells demonstrate distinct global gene expression patterns and functional phenotypes.* Tissue engineering. Part A, 2009. **15**(3): p. 559-567.

56. Ramaiahgari, S.C., et al., *A 3D in vitro model of differentiated HepG2 cell spheroids with improved liver-like properties for repeated dose high-throughput toxicity studies.* Archives of Toxicology, 2014. **88**(5): p. 1083-1095.
57. No da, Y., et al., *Functional 3D human primary hepatocyte spheroids made by co-culturing hepatocytes from partial hepatectomy specimens and human adipose-derived stem cells.* PLoS One, 2012. **7**(12): p. e50723.
58. Bell, C.C., et al., *Characterization of primary human hepatocyte spheroids as a model system for drug-induced liver injury, liver function and disease.* Sci Rep, 2016. **6**: p. 25187.
59. Messner, S., et al., *Multi-cell type human liver microtissues for hepatotoxicity testing.* Archives of toxicology, 2013. **87**(1): p. 209-213.
60. Proctor, W.R., et al., *Utility of spherical human liver microtissues for prediction of clinical drug-induced liver injury.* Arch Toxicol, 2017. **91**(8): p. 2849-2863.
61. Vorrink, S.U., et al., *Prediction of Drug-Induced Hepatotoxicity Using Long-Term Stable Primary Hepatic 3D Spheroid Cultures in Chemically Defined Conditions.* Toxicol Sci, 2018. **163**(2): p. 655-665.
62. Li, F., et al., *Three-Dimensional Spheroids With Primary Human Liver Cells and Differential Roles of Kupffer Cells in Drug-Induced Liver Injury.* Journal of Pharmaceutical Sciences, 2020. **109**(6): p. 1912-1923.
63. Bell, C.C., et al., *Comparison of Hepatic 2D Sandwich Cultures and 3D Spheroids for Long-term Toxicity Applications: A Multicenter Study.* Toxicol Sci, 2018. **162**(2): p. 655-666.
64. Ma, X., et al., *Deterministically patterned biomimetic human iPSC-derived hepatic model via rapid 3D bioprinting.* Proceedings of the National Academy of Sciences, 2016. **113**(8): p. 2206-2211.
65. Grix, T., et al., *Bioprinting Perfusion-Enabled Liver Equivalents for Advanced Organ-on-a-Chip Applications.* Genes (Basel), 2018. **9**(4).
66. Nguyen, D.G., et al., *Bioprinted 3D Primary Liver Tissues Allow Assessment of Organ-Level Response to Clinical Drug Induced Toxicity In Vitro.* PLoS One, 2016. **11**(7): p. e0158674.
67. Chang, R., et al., *Biofabrication of a three-dimensional liver micro-organ as an in vitro drug metabolism model.* Biofabrication, 2010. **2**(4): p. 045004.
68. Ma, L., et al., *Current Advances on 3D-Bioprinted Liver Tissue Models.* Adv Healthc Mater, 2020. **9**(24): p. e2001517.
69. Dash, A., et al., *Hemodynamic flow improves rat hepatocyte morphology, function, and metabolic activity in vitro.* Am J Physiol Cell Physiol, 2013. **304**(11): p. C1053-63.
70. Novik, E., et al., *A microfluidic hepatic coculture platform for cell-based drug metabolism studies.* Biochem Pharmacol, 2010. **79**(7): p. 1036-44.
71. Prodanov, L., et al., *Long-term maintenance of a microfluidic 3D human liver sinusoid.* Biotechnol Bioeng, 2016. **113**(1): p. 241-6.
72. Rennert, K., et al., *A microfluidically perfused three dimensional human liver model.* Biomaterials, 2015. **71**: p. 119-131.
73. Ewart, L., et al., *Performance assessment and economic analysis of a human Liver-Chip for predictive toxicology.* Communications Medicine, 2022. **2**(1): p. 154.
74. Vernetti, L.A., et al., *A human liver microphysiology platform for investigating physiology, drug safety, and disease models.* Exp Biol Med (Maywood), 2016. **241**(1): p. 101-14.

75. Toh, Y.C., et al., *A microfluidic 3D hepatocyte chip for drug toxicity testing.* Lab Chip, 2009. **9**(14): p. 2026-35.
76. Ong, L.J.Y., et al., *A pump-free microfluidic 3D perfusion platform for the efficient differentiation of human hepatocyte-like cells.* Biotechnol Bioeng, 2017. **114**(10): p. 2360-2370.
77. Tostoes, R.M., et al., *Human liver cell spheroids in extended perfusion bioreactor culture for repeated-dose drug testing.* Hepatology, 2012. **55**(4): p. 1227-36.
78. Kim, J.Y., et al., *96-well format-based microfluidic platform for parallel interconnection of multiple multicellular spheroids.* J Lab Autom, 2015. **20**(3): p. 274-82.
79. Kim, J.Y., et al., *3D spherical microtissues and microfluidic technology for multi-tissue experiments and analysis.* J Biotechnol, 2015. **205**: p. 24-35.
80. Sung, J.H., C. Kam, and M.L. Shuler, *A microfluidic device for a pharmacokinetic–pharmacodynamic (PK–PD) model on a chip.* Lab on a Chip, 2010. **10**(4): p. 446-455.
81. Viravaidya, K., A. Sin, and M.L. Shuler, *Development of a Microscale Cell Culture Analog To Probe Naphthalene Toxicity.* Biotechnology Progress, 2004. **20**(1): p. 316-323.
82. Mahler, G.J., et al., *Characterization of a gastrointestinal tract microscale cell culture analog used to predict drug toxicity.* Biotechnol Bioeng, 2009. **104**(1): p. 193-205.
83. van Midwoud, P.M., et al., *A microfluidic approach for in vitro assessment of interorgan interactions in drug metabolism using intestinal and liver slices.* Lab Chip, 2010. **10**(20): p. 2778-86.
84. Choucha-Snouber, L., et al., *Investigation of ifosfamide nephrotoxicity induced in a liver-kidney co-culture biochip.* Biotechnol Bioeng, 2013. **110**(2): p. 597-608.
85. Chang, S.Y., et al., *Human liver-kidney model elucidates the mechanisms of aristolochic acid nephrotoxicity.* JCI Insight, 2017. **2**(22).
86. Maschmeyer, I., et al., *A four-organ-chip for interconnected long-term co-culture of human intestine, liver, skin and kidney equivalents.* Lab Chip, 2015. **15**(12): p. 2688-99.
87. Theobald, J., et al., *Liver-Kidney-on-Chip To Study Toxicity of Drug Metabolites.* ACS Biomater Sci Eng, 2018. **4**(1): p. 78-89.
88. Vernetti, L., et al., *Functional Coupling of Human Microphysiology Systems: Intestine, Liver, Kidney Proximal Tubule, Blood-Brain Barrier and Skeletal Muscle.* Sci Rep, 2017. **7**: p. 42296.
89. Kietzmann, T., *Metabolic zonation of the liver: The oxygen gradient revisited.* Redox Biol, 2017. **11**: p. 622-630.
90. McCarty, W.J., O.B. Usta, and M.L. Yarmush, *A Microfabricated Platform for Generating Physiologically-Relevant Hepatocyte Zonation.* Sci Rep, 2016. **6**: p. 26868.
91. Kang, Y.B., et al., *Metabolic Patterning on a Chip: Towards in vitro Liver Zonation of Primary Rat and Human Hepatocytes.* Scientific Reports, 2018. **8**(1).
92. Lee-Montiel, F.T., et al., *Control of oxygen tension recapitulates zone-specific functions in human liver microphysiology systems.* Exp Biol Med (Maywood), 2017. **242**(16): p. 1617-1632.

93. Tan, K., et al., *A high-throughput microfluidic microphysiological system (PREDICT-96) to recapitulate hepatocyte function in dynamic, re-circulating flow conditions.* Lab Chip, 2019. **19**(9): p. 1556-1566.
94. Dash, A., et al., *Liver tissue engineering in the evaluation of drug safety.* Expert Opin Drug Metab Toxicol, 2009. **5**(10): p. 1159-74.
95. Bircsak, K.M., et al., *A 3D microfluidic liver model for high throughput compound toxicity screening in the OrganoPlate(R).* Toxicology, 2021. **450**: p. 152667.
96. Rubiano, A., et al., *Characterizing the reproducibility in using a liver microphysiological system for assaying drug toxicity, metabolism, and accumulation.* Clin Transl Sci, 2020.
97. Domansky, K., et al., *Perfused multiwell plate for 3D liver tissue engineering.* Lab Chip, 2010. **10**(1): p. 51-8.
98. Jang, K.-J., et al., *Reproducing human and cross-species drug toxicities using a Liver-Chip.* Science Translational Medicine, 2019. **11**(517): p. eaax5516.
99. *Emulate - Our technology*. 2021 26.07.2022; Available from: https://emulatebio.com/products-services/instruments-and-accessories/.
100. Li, N., M. Schwartz, and C. Ionescu-Zanetti, *PDMS compound adsorption in context.* J Biomol Screen, 2009. **14**(2): p. 194-202.
101. Toepke, M.W. and D.J. Beebe, *PDMS absorption of small molecules and consequences in microfluidic applications.* Lab Chip, 2006. **6**(12): p. 1484-6.
102. van Meer, B.J., et al., *Small molecule absorption by PDMS in the context of drug response bioassays.* Biochem Biophys Res Commun, 2017. **482**(2): p. 323-328.
103. Yu, F., et al., *A perfusion incubator liver chip for 3D cell culture with application on chronic hepatotoxicity testing.* Sci Rep, 2017. **7**(1): p. 14528.
104. Beer, M., et al., *A novel microfluidic 3D platform for culturing pancreatic ductal adenocarcinoma cells: comparison with in vitro cultures and in vivo xenografts.* Scientific Reports, 2017. **7**(1): p. 1325.
105. Schuette, J., *Dielectrophoretic assembly of in vivo-like artificial liver sinusoids in a microfluidic device*, in *Faculty of applied sciences*. 2012, Albert-Ludwigs-University Freiburg: Tuebingen. p. 99.
106. Tomilova, O., *Optimierung und Charakterisierung eines mikrofluidischen 3D in vitro Lebermodels mit 24 Kammern im MTP-Format*, in *Faculty of Applied Sciences*. 2016, University Esslingen: Reutlingen. p. 88.
107. Schütte, J., et al., *A method for patterned in situ biofunctionalization in injection-molded microfluidic devices.* Lab Chip, 2010. **10**(19): p. 2551-8.
108. Holzner, F., et al., *Numerical modelling and measurement of cell trajectories in 3-D under the influence of dielectrophoretic and hydrodynamic forces.* ELECTROPHORESIS, 2011. **32**(17): p. 2366-2376.
109. Hagmeyer, B., et al. *Tailoring microfluidic systems for organ-like cell culture applications using multiphysics simulations*. in *Microfluidics, BioMEMS, and Medical Microsystems XI*. 2013. San Francisco,California,USA: SPIE;.
110. Hagmeyer, B., F. Zechnall, and M. Stelzle, *Towards plug and play filling of microfluidic devices by utilizing networks of capillary stop valves.* Biomicrofluidics, 2014. **8**(5): p. 056501.
111. Godoy, P., et al., *Recent advances in 2D and 3D in vitro systems using primary hepatocytes, alternative hepatocyte sources and non-parenchymal liver cells and their use in investigating mechanisms of hepatotoxicity, cell signaling and ADME.* Arch Toxicol, 2013. **87**(8): p. 1315-530.

112. Poisson, J., et al., *Liver sinusoidal endothelial cells: Physiology and role in liver diseases.* J Hepatol, 2017. **66**(1): p. 212-227.
113. Kegel, V., et al., *Protocol for Isolation of Primary Human Hepatocytes and Corresponding Major Populations of Non-parenchymal Liver Cells.* J Vis Exp, 2016(109): p. e53069.
114. Ochs, C.J., et al., *Oxygen levels in thermoplastic microfluidic devices during cell culture.* Lab Chip, 2014. **14**(3): p. 459-62.
115. Latta, M., et al., *ATP-Depleting Carbohydrates Prevent Tumor Necrosis Factor Receptor 1-Dependent Apoptotic and Necrotic Liver Injury in Mice.* Journal of Pharmacology and Experimental Therapeutics, 2007. **321**(3): p. 875-883.
116. Divakaruni, A.S., et al., *Chapter Sixteen - Analysis and Interpretation of Microplate-Based Oxygen Consumption and pH Data*, in *Methods in Enzymology*, A.N. Murphy and D.C. Chan, Editors. 2014, Academic Press. p. 309-354.
117. Dasarathy, S., et al., *Ammonia toxicity: from head to toe?* Metab Brain Dis, 2017. **32**(2): p. 529-538.
118. Niknahad, H., et al., *Ammonia-induced mitochondrial dysfunction and energy metabolism disturbances in isolated brain and liver mitochondria, and the effect of taurine administration: relevance to hepatic encephalopathy treatment.* Clin Exp Hepatol, 2017. **3**(3): p. 141-151.
119. Boelsterli, U.A., *Diclofenac-induced liver injury: a paradigm of idiosyncratic drug toxicity.* Toxicol Appl Pharmacol, 2003. **192**(3): p. 307-22.
120. Syed, M., C. Skonberg, and S.H. Hansen, *Mitochondrial toxicity of diclofenac and its metabolites via inhibition of oxidative phosphorylation (ATP synthesis) in rat liver mitochondria: Possible role in drug induced liver injury (DILI).* Toxicol In Vitro, 2016. **31**: p. 93-102.
121. Ehrlich, A., et al., *Microphysiological flux balance platform unravels the dynamics of drug induced steatosis.* Lab Chip, 2018. **18**(17): p. 2510-2522.
122. Maass, C., et al., *Establishing quasi-steady state operations of microphysiological systems (MPS) using tissue-specific metabolic dependencies.* Sci Rep, 2018. **8**(1): p. 8015.
123. Miller, I.P., et al., *Beneficial Role of ROS in Cell Survival: Moderate Increases in H(2)O(2) Production Induced by Hepatocyte Isolation Mediate Stress Adaptation and Enhanced Survival.* Antioxidants (Basel), 2019. **8**(10).
124. Bhogal, R.H., et al., *Reactive oxygen species mediate human hepatocyte injury during hypoxia/reoxygenation.* Liver Transplantation, 2010. **16**(11): p. 1303-1313.
125. Butler, M., et al., *Linoleic acid improves the robustness of cells in agitated cultures.* Cytotechnology, 1999. **30**(1-3): p. 27-36.
126. Polacheck, W.J., J.L. Charest, and R.D. Kamm, *Interstitial flow influences direction of tumor cell migration through competing mechanisms.* Proc Natl Acad Sci U S A, 2011. **108**(27): p. 11115-20.
127. Foster, A.J., et al., *Integrated in vitro models for hepatic safety and metabolism: evaluation of a human Liver-Chip and liver spheroid.* Arch Toxicol, 2019. **93**(4): p. 1021-1037.
128. Vinci, B., et al., *Modular bioreactor for primary human hepatocyte culture: Medium flow stimulates expression and activity of detoxification genes.* Biotechnology Journal, 2011. **6**(5): p. 554-564.
129. Milo, R., *What is the total number of protein molecules per cell volume? A call to rethink some published values.* BioEssays, 2013. **35**(12): p. 1050-1055.

130. Morales-Navarrete, H., et al., *A versatile pipeline for the multi-scale digital reconstruction and quantitative analysis of 3D tissue architecture.* Elife, 2015. **4**.
131. Zeilinger, K., et al., *Scaling down of a clinical three-dimensional perfusion multicompartment hollow fiber liver bioreactor developed for extracorporeal liver support to an analytical scale device useful for hepatic pharmacological in vitro studies.* Tissue Eng Part C Methods, 2011. **17**(5): p. 549-56.
132. Aslantürk, Ö.S., *In Vitro Cytotoxicity and Cell Viability Assays: Principles, Advantages, and Disadvantages*, in *Genotoxicity - A Predictable Risk to Our Actual World*, M.L. Larramendy and S. Soloneski, Editors. 2018, IntechOpen.
133. Minsart, C., et al., *New insights in acetaminophen toxicity: HMGB1 contributes by itself to amplify hepatocyte necrosis in vitro through the TLR4-TRIF-RIPK3 axis.* Sci Rep, 2020. **10**(1): p. 5557.
134. Xie, Y., et al., *Mechanisms of acetaminophen-induced cell death in primary human hepatocytes.* Toxicol Appl Pharmacol, 2014. **279**(3): p. 266-274.
135. Zhdanov, A.V., et al., *Availability of the key metabolic substrates dictates the respiratory response of cancer cells to the mitochondrial uncoupling.* Biochim Biophys Acta, 2014. **1837**(1): p. 51-62.
136. Ylikahri, R.H., I.E. Hassinen, and M.T. Kähönen, *Metabolic interactions of fructose and ethanol in perfused liver of normal and thyroxine-treated rats.* Metabolism, 1971. **20**(6): p. 555-67.
137. Ingber, D.E., *Is it Time for Reviewer 3 to Request Human Organ Chip Experiments Instead of Animal Validation Studies?* Advanced Science, 2020. **7**(22): p. 2002030.
138. Ferrick, D.A., A. Neilson, and C. Beeson, *Advances in measuring cellular bioenergetics using extracellular flux.* Drug Discov Today, 2008. **13**(5-6): p. 268-74.
139. Hynes, J., et al., *In vitro analysis of cell metabolism using a long-decay pH-sensitive lanthanide probe and extracellular acidification assay.* Anal Biochem, 2009. **390**(1): p. 21-8.

Declaration

Ich erkläre hiermit, dass ich die zur Promotion eingereichte Arbeit mit dem Titel "*HepaChip-MP: a microfluidic liver model in multiwellplate format for the assessment of metabolism, toxicity and modeling of disease as an example of microfluidic in vitro models to mimic physiological organ behaviour*" selbstständig verfasst, nur die angegebenen Quellen und Hilfsmittel benutzt und wörtlich oder inhaltlich übernommene Zitate also solche gekennzeichnet habe. Ich erkläre, dass die Richtlinien zur Sicherung guter wissenschaftlicher Praxis der Universität Tübingen beachtet wurden. Ich versichere an Eides statt, dass diese Angaben wahr sind und dass ich nichts verschwiegen habe. Mir ist bekannt, dass die falsche Angabe einer Versicherung an Eides statt mit Freiheitsstrafe bis zu drei Jahren oder mit Geldstrafe bestraft wird.

Ort, Datum

Marius Busche

Appendices

Appendix I: Supplementary Information

Appendix Table 1: Air-bubble free chambers, total chambers and consequent percentage of air-bubble free chambers of the chips used during the thesis.

Chip Nr.	Air-bubble free chambers	chambers total	Percentage
1	19	24	79,1666667
2	11	12	91,6666667
3	11	24	45,8333333
4	22	24	91,6666667
5	14	24	58,3333333
6	14	24	58,3333333
7	22	24	91,6666667
8	24	24	100
9	22	24	91,6666667
10	21	24	87,5
11	16	16	100
12	23	24	95,8333333
13	19	24	79,1666667
14	16	18	88,8888889
15	22	24	91,6666667
16	22	24	91,6666667
17	18	24	75
18	20	24	83,3333333
19	22	24	91,6666667
20	22	24	91,6666667
21	20	24	83,3333333
22	17	24	70,8333333
23	19	24	79,1666667
24	17	24	70,8333333
25	14	24	58,3333333
26	19	24	79,1666667
27	21	24	87,5
28	13	24	54,1666667
29	16	24	66,6666667
30	14	24	58,3333333
31	20	24	83,3333333
32	21	24	87,5
33	12	24	50
34	19	24	79,1666667
35	11	24	45,8333333
36	18	24	75
37	20	24	83,3333333
38	12	24	50
39	21	24	87,5
40	17	23	73,9130435
41	18	24	75
42	17	24	70,8333333
43	20	24	83,3333333
44	19	24	79,1666667
45	21	24	87,5
46	16	24	66,6666667
47	14	24	58,3333333
48	11	24	45,8333333
49	15	24	62,5
50	19	24	79,1666667
51	18	24	75
52	23	24	95,8333333
53	21	24	87,5
54	21	24	87,5
55	19	24	79,1666667
56	19	24	79,1666667
57	16	24	66,6666667
58	16	24	66,6666667
59	17	24	70,8333333
60	14	18	77,7777778
61	22	24	91,6666667

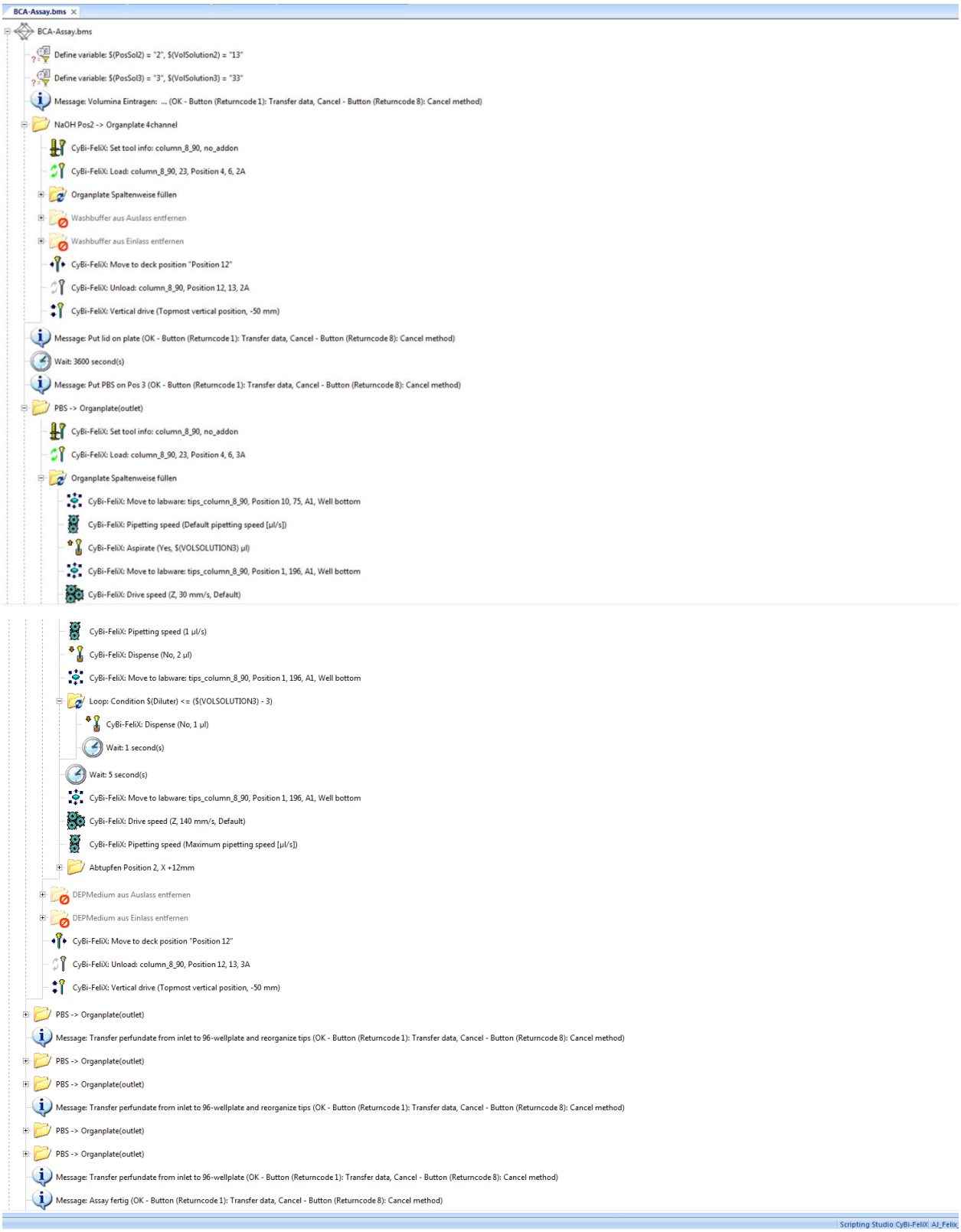

Suppl.Fig. 1: Script to perform the cell lysis for the BCA assay in the HepaChip-MP with the FeliX pipetting robot. First NaOH is pipetted in the chamber to induce cell lysis (NaOH Pos2 → Organpolate 4channel). After one hour of incubation (Wait 3600 second(s)), the lysate is pushed out of the chamber with PBS (PBS → Organplate (Outlet)). In the figure, one folder of PBS pipetting is opened exemplarily. The other folders to pipet PBS contain the same steps.

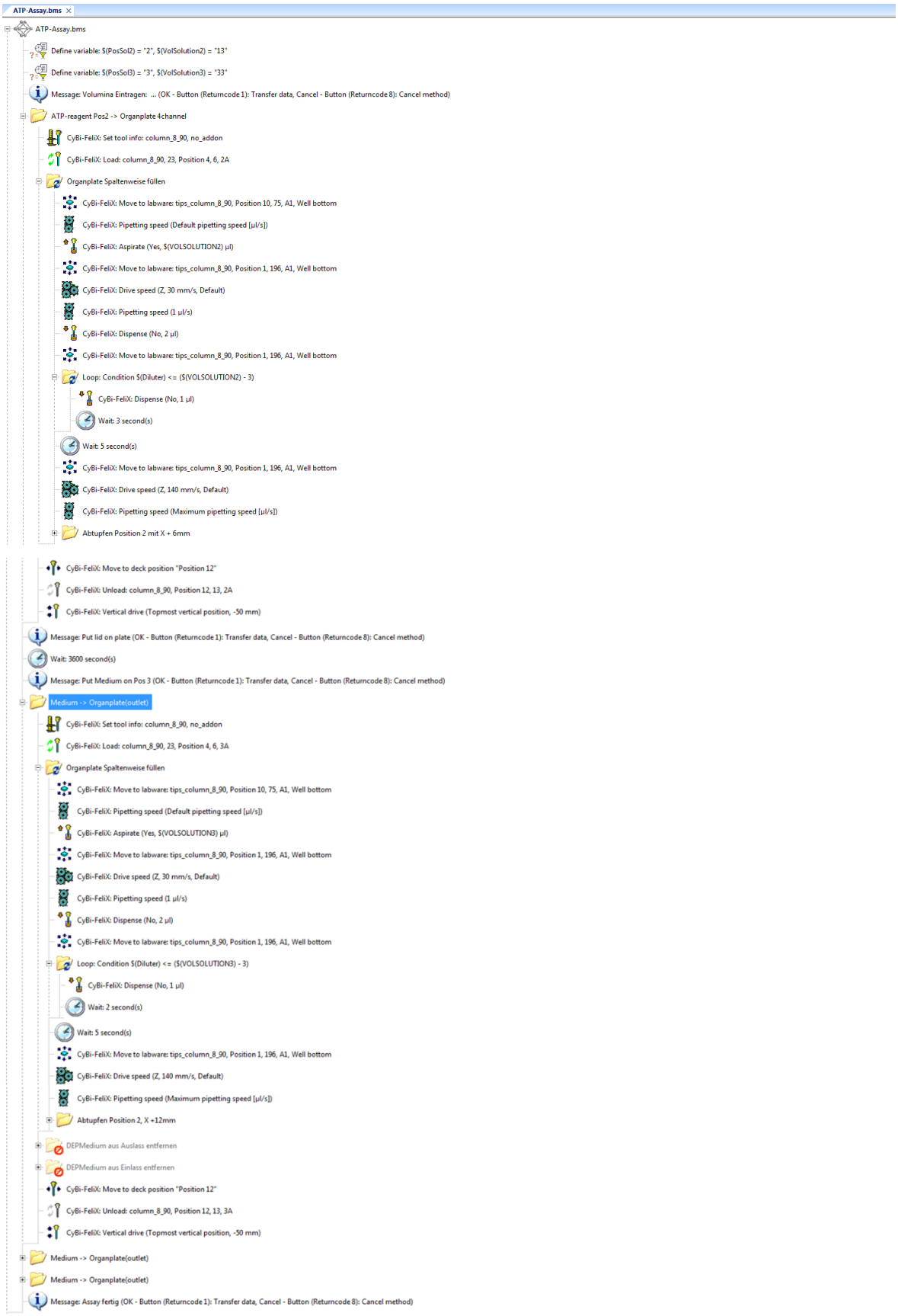
ATP-Assay.bms
ATP-Assay.bms
Define variable: $(PosSol2) = "2", $(VolSolution2) = "13"
Define variable: $(PosSol3) = "3", $(VolSolution3) = "33"
Message: Volumina Eintragen: ... (OK - Button (Returncode 1): Transfer data, Cancel - Button (Returncode 8): Cancel method)
ATP-reagent Pos2 -> Organplate 4channel
CyBi-FeliX: Set tool info: column_8_90, no_addon
CyBi-FeliX: Load: column_8_90, 23, Position 4, 6, 2A
Organplate Spaltenweise füllen
CyBi-FeliX: Move to labware: tips_column_8_90, Position 10, 75, A1, Well bottom
CyBi-FeliX: Pipetting speed (Default pipetting speed [µl/s])
CyBi-FeliX: Aspirate (Yes, $(VOLSOLUTION2) µl)
CyBi-FeliX: Move to labware: tips_column_8_90, Position 1, 196, A1, Well bottom
CyBi-FeliX: Drive speed (Z, 30 mm/s, Default)
CyBi-FeliX: Pipetting speed (1 µl/s)
CyBi-FeliX: Dispense (No, 2 µl)
CyBi-FeliX: Move to labware: tips_column_8_90, Position 1, 196, A1, Well bottom
Loop: Condition $(Diluter) <= ($(VOLSOLUTION2) - 3)
CyBi-FeliX: Dispense (No, 1 µl)
Wait: 3 second(s)
Wait: 5 second(s)
CyBi-FeliX: Move to labware: tips_column_8_90, Position 1, 196, A1, Well bottom
CyBi-FeliX: Drive speed (Z, 140 mm/s, Default)
CyBi-FeliX: Pipetting speed (Maximum pipetting speed [µl/s])
Abtupfen Position 2 mit X + 6mm
CyBi-FeliX: Move to deck position "Position 12"
CyBi-FeliX: Unload: column_8_90, Position 12, 13, 2A
CyBi-FeliX: Vertical drive (Topmost vertical position, -50 mm)
Message: Put lid on plate (OK - Button (Returncode 1): Transfer data, Cancel - Button (Returncode 8): Cancel method)
Wait: 3600 second(s)
Message: Put Medium on Pos 3 (OK - Button (Returncode 1): Transfer data, Cancel - Button (Returncode 8): Cancel method)
Medium -> Organplate(outlet)
CyBi-FeliX: Set tool info: column_8_90, no_addon
CyBi-FeliX: Load: column_8_90, 23, Position 4, 6, 3A
Organplate Spaltenweise füllen
CyBi-FeliX: Move to labware: tips_column_8_90, Position 10, 75, A1, Well bottom
CyBi-FeliX: Pipetting speed (Default pipetting speed [µl/s])
CyBi-FeliX: Aspirate (Yes, $(VOLSOLUTION3) µl)
CyBi-FeliX: Move to labware: tips_column_8_90, Position 1, 196, A1, Well bottom
CyBi-FeliX: Drive speed (Z, 30 mm/s, Default)
CyBi-FeliX: Pipetting speed (1 µl/s)
CyBi-FeliX: Dispense (No, 2 µl)
CyBi-FeliX: Move to labware: tips_column_8_90, Position 1, 196, A1, Well bottom
Loop: Condition $(Diluter) <= ($(VOLSOLUTION3) - 3)
CyBi-FeliX: Dispense (No, 1 µl)
Wait: 2 second(s)
Wait: 5 second(s)
CyBi-FeliX: Move to labware: tips_column_8_90, Position 1, 196, A1, Well bottom
CyBi-FeliX: Drive speed (Z, 140 mm/s, Default)
CyBi-FeliX: Pipetting speed (Maximum pipetting speed [µl/s])
Abtupfen Position 2, X +12mm
DEPMedium aus Auslass entfernen
DEPMedium aus Einlass entfernen
CyBi-FeliX: Move to deck position "Position 12"
CyBi-FeliX: Unload: column_8_90, Position 12, 13, 3A
CyBi-FeliX: Vertical drive (Topmost vertical position, -50 mm)
Medium -> Organplate(outlet)
Medium -> Organplate(outlet)
Message: Assay fertig (OK - Button (Returncode 1): Transfer data, Cancel - Button (Returncode 8): Cancel method)

Suppl.Fig. 2: Script to perform the cell lysis for the ATP-assay in the HepaChip-MP with the FeliX pipetting robot. First the assay reagent is pipetted into the chamber (ATP-reagent Pos2 → Organplate 4channel). After one hour incubation time (Wait 3600 second(s)), medium is used to flush the lysate out of the chamber (Medium → Organplate). In the figure, one folder of medium pipetting is opened exemplarily. The other folders to pipet medium contain the same steps.

Appendix II: Busche M, et al., HepaChip-MP - a twenty-four chamber microplate for a continuously perfused liver coculture model. Lab Chip. 2020;20:2911-26. doi: 10.1039/d0lc00357c

Lab on a Chip

PAPER

View Article Online
View Journal | View Issue

Check for updates

Cite this: *Lab Chip*, 2020, **20**, 2911

HepaChip-MP – a twenty-four chamber microplate for a continuously perfused liver coculture model†

Marius Busche,*[a] Olena Tomilova,[a] Julia Schütte,[a] Simon Werner,[a] Meike Beer,[a] Nicola Groll,[a] Britta Hagmeyer,[a] Michael Pawlak,[a] Peter D. Jones,[a] Christian Schmees,[a] Holger Becker,[b] Juliane Schnabel,[b] Karsten Gall,[c] Roland Hemmler,[c] Madlen Matz-Soja,[de] Georg Damm,[f] Simon Beuck,[g] Tobias Klaassen,[g] Jana Moer,[h] Anett Ullrich,[h] Dieter Runge,[h] Katja Schenke-Layland,[aijk] Rolf Gebhardt[del] and Martin Stelzle*[a]

HepaChip microplate (HepaChip-MP) is a microfluidic platform comprised of 24 independent culture chambers with continuous, unidirectional perfusion. In the HepaChip-MP, an automated dielectrophoresis process selectively assembles viable cells into elongated micro tissues. Freshly isolated primary human hepatocytes (PHH) and primary human liver endothelial cells (HuLEC) were successfully assembled as cocultures aiming to mimic the liver sinusoid. Minimal quantities of primary human cells are required to establish micro tissues in the HepaChip-MP. Metabolic function including induction of CYP enzymes in PHH was successfully measured demonstrating a high degree of metabolic activity of cells in HepaChip-MP cultures and sufficient sensitivity of LC-MS analysis even for the relatively small number of cells per chamber. Further, parallelization realized in HepaChip-MP enabled the acquisition of dose–response toxicity data of diclofenac with a single device. Several unique technical features should enable a widespread application of this *in vitro* model. We have demonstrated fully automated preparation of cell cultures in HepaChip-MP using a pipetting robot. The tubeless unidirectional perfusion system based on gravity-driven flow can be operated within a standard incubator system. Overall, the system readily integrates in workflows common in cell culture labs. Further research will be directed towards optimization of media composition to further extend culture lifetime and study oxygen gradients and their effect on zonation within the sinusoid-like microorgans. In summary, we have established a novel parallelized and scalable microfluidic *in vitro* liver model showing hepatocyte function and anticipate future in-depth studies of liver biology and applications in pre-clinical drug development.

Received 8th April 2020,
Accepted 25th June 2020

DOI: 10.1039/d0lc00357c

rsc.li/loc

[a] *NMI Natural and Medical Sciences Institute, University of Tübingen, Reutlingen, Germany. E-mail: martin.stelzle@nmi.de*
[b] *Microfluidic ChipShop GmbH, Jena, Germany*
[c] *Ionovation GmbH, Bissendorf, Germany*
[d] *Section of Hepatology, Clinic and Polyclinic for Gastroenterology, Hepatology, Infectiology, Pneumology, University Clinic Leipzig, Leipzig, Germany*
[e] *Rudolf-Schönheimer-Institute of Biochemistry, Leipzig University, Leipzig, Germany*
[f] *Department of Hepatobiliary Surgery and Visceral Transplantation, University Hospital, Leipzig University, Leipzig, Germany*
[g] *A & M Labor fuer Analytik und Metabolismusforschung Service GmbH, Bergheim, Germany*
[h] *PRIMACYT Cell Culture Technology GmbH, Schwerin, Germany*
[i] *Department of Women's Health, Research Institute for Women's Health, Eberhard Karls University Tübingen, Tübingen, Germany*
[j] *Cluster of Excellence iFIT (EXC 2180) "Image-Guided and Functionally Instructed Tumor Therapies", Eberhard Karls University Tübingen, Germany*
[k] *Department of Medicine/Cardiology, Cardiovascular Research Laboratories (CVRL), University of California (UCLA), Los Angeles, CA, USA*
[l] *InViSys-Tübingen GbR, Leipzig, Germany*
† Electronic supplementary information (ESI) available. See DOI: 10.1039/d0lc00357c

Introduction

Drug-induced liver injury represents a major cause for the failure of drug candidates.[1] Current test systems including cell culture and animal models offer insufficient predictivity of drug-induced hepatotoxicity.[2–6] Fundamentally new models are needed to address this challenge.[7] Consensus exists that these models should i) use human cells (PHH or induced pluripotent stem cell (iPSC)-derived hepatocyte-like cells), ii) exhibit organ-like morphology, iii) provide an organ-specific microenvironment including appropriate extracellular matrix and non-parenchymal cells, and iv) allow for continuous perfusion to enable the establishment of proper chemical gradients within the culture.[8–10]

Numerous *in vitro* models developed to mimic liver function have provided important insights into the biological function and physiology.[2,11–19] The addition of growth factors

and medium supplements as well as coculture of feeder cells or non-parenchymal cells with primary hepatocytes have been shown to extend the useful culture time and to maintain liver-specific functions of the hepatocytes.[2,11–16] Also, culture in a three-dimensional (3D) environment stabilize hepatic functions, but still show a delayed dedifferentiation.[17] Spheroid-based models have been shown to exhibit higher sensitivity to toxic substances than two-dimensional (2D) models,[18,19] which has been comprehensively reviewed.[20–22] These reviews highlight organ-on-chip systems, which add perfusion and associated physiological shear stress to the culture systems. The latter aids in maintaining hepatocytes in their differentiated state. Dash *et al.* showed enhanced albumin and urea production as well as enhanced expression and activity of CYP enzymes of primary hepatocytes under shear stress.[23] This underlines the importance of a 3D culture and the presence of shear stress to achieve a truly *in vivo*-like physiology within an *in vitro* system of the liver.

Employing microfluidic technologies has enabled long-term coculture of hepatocytes with non-parenchymal cells or feeder cells under dynamic conditions in 3D.[27–30] In these systems, cells exhibited gene expression patterns that suggest a more physiological state. Clearance of xenobiotic substances as well as responses after drug treatment compared favorably to *in vivo* data. In particular, enhanced metabolic activity was detected[31–33] even for compounds normally metabolized slowly.[34] Reduced albumin production was observed upon treatment with bosentan at a lower dose of the drug.[35] Also, cell response towards hormones was recapitulated in a more *in vivo* like manner[36] in perfused systems when compared to static 2D models.

While these systems have demonstrated the power of microfluidic technology to mimic the *in vivo* situation more closely than possible with static models, certain shortcomings hampering widespread application remain to be overcome.

Mostly, devices with single or only a few micro tissues have been demonstrated.[40] However, parallelization represents a critical prerequisite to gaining robust and statistically valid data sets in a cost-effective manner. Unfortunately, this has been demonstrated by only a few systems so far. Kim *et al.* introduced the platform of InSphero with eleven parallelized cultures, each comprising a row of six spheroids.[41] Jang *et al.* used the Mimetas OrganoPlate with 40 independent chambers to differentiate HepaRG cells and analyzed their function.[42] However, both systems use tilting platforms to generate bidirectional flow, which prohibits the development of physiological gradients of substances inside the chamber. Domansky *et al.* developed a system that used integrated pneumatic pumps on a device in multiwell plate format comprising 12 chambers to coculture primary rat hepatocytes and liver sinusoidal endothelial cells (LSECs).[43]

Perfusion is often achieved by applying flow using syringe pumps. While this enables precise control of flow rate, establishing proper fluidic connections tends to be complex and prone to the introduction of air bubbles. Bubbles can damage micro tissues or interrupt flow and therefore must be avoided. Also, large scale parallelization is not feasible utilizing these systems.

Many devices have been manufactured from polydimethylsiloxane (PDMS) by soft lithography. PDMS provides for favorable biocompatibility, transparency and relative ease of manufacturing of individual devices. However, PDMS also is known to absorb hydrophobic compounds.[44–46] Reliable dose–response data often cannot be obtained in such systems, given the inherently large surface-to-volume ratio of microfluidic devices and the hydrophobicity of many drug candidates.

Often, organ-on-chip cultures do not resemble the actual 3D morphology of the organ tissue but rather represent perfused 2D or randomly organized 3D cellular arrangements. While immobilization of cells within gels enables arrangement in a 3D structure, gels may influence diffusion within the microtissue. This also applies to the assembly of cells on membranes with properties differing from physiological tissue.

Therefore, the objective of this work was the development of a parallelized, microfluidic platform for cocultures of hepatocytes and endothelial cells resembling liver sinusoid morphology. Metabolic activity as well as toxicological response to a known compound were to be assessed as a proof of sufficient sensitivity and compatibility of the used assays and physiologic cell function.

To enable integration into common cell culture workflows, we designed a plate following the SBS-standard 96-well plate format with 24 independent microorgans. We chose a cyclic olefin polymer (COP) as a material with excellent optical transparency and low absorbance of compounds. This enables the use of conventional microscopy and state-of-the-art biochemical assays. Further, COP allows for seamless upscaling of manufacturing by micro-injection molding. A high degree of parallelization along with ease-of-use was achieved by continuous, tubeless, gravity-driven, unidirectional flow at physiological rates.

In addition, liver cells were to be assembled in elongated structures closely mimicking the physiological dimension with respect to length and width of the natural human liver sinusoid. Only viable cells were actively assembled by dielectrophoretic forces generated by integrated electrodes.

A complete workflow from priming of the microplate to cell assembly was realized using a pipettor system. A miniaturized, 24-channel, incubator-compatible pump system was developed which can be used to continuously transfer culture media from outlet to inlet reservoirs thus enabling constant reperfusion.

In summary, we present an automated system allowing for parallelized culture of cells mimicking the liver sinusoid both with respect to physical dimensions as well as function. In particular, we demonstrate compatibility with common biological workflows in terms of usability and readout methods.

Materials & methods

Reagents were purchased from Merck KGaA (Darmstadt, Germany) unless stated otherwise.

i) Microplate manufacture

HepaChip microplates (HepaChip-MPs) were jointly developed and are now manufactured by microfluidic ChipShop (Jena, Germany).

The HepaChip-MP (Fig. 1) consists of cyclic olefin polymer (COP) and was manufactured by micro injection molding. The mold was generated using ultra-precision micro milling. Prior to bonding, electrodes were fabricated by evaporation of titanium (10 nm) and gold (approx. 100 nm) through a shadow mask. These electrodes are intended for generating a high-frequency electric field within the cell chambers for dielectrophoretic assembly of cells onto the assembly ridges (see Fig. 1). Prior to bonding the assembly ridges were illuminated through a shadow mask by short wavelength (185 nm) UV light using a low-pressure mercury lamp (Heraeus Noblelight, Hanau, Germany, NIQ lamp, quartz tube, 5 W lamp), thereby introducing acid groups on the assembly ridges.[47] Finally, microplates were bonded with a COP foil (188 μm thickness). Openings in the foil were positioned to enable electrical access to the electrode connection pads on the bottom face of the microplate.

ii) Peripheral instrumentation

A CyBio FeliX pipetting system (Analytic Jena AG, Fig. 2B) was modified to hold a dielectrophoresis (DEP) fixture (Fig. 2C) for the HepaChip-MP comprising LED illumination and electrical connectors for the electrodes located on the bottom face of the microplate. The metallic encasing provides

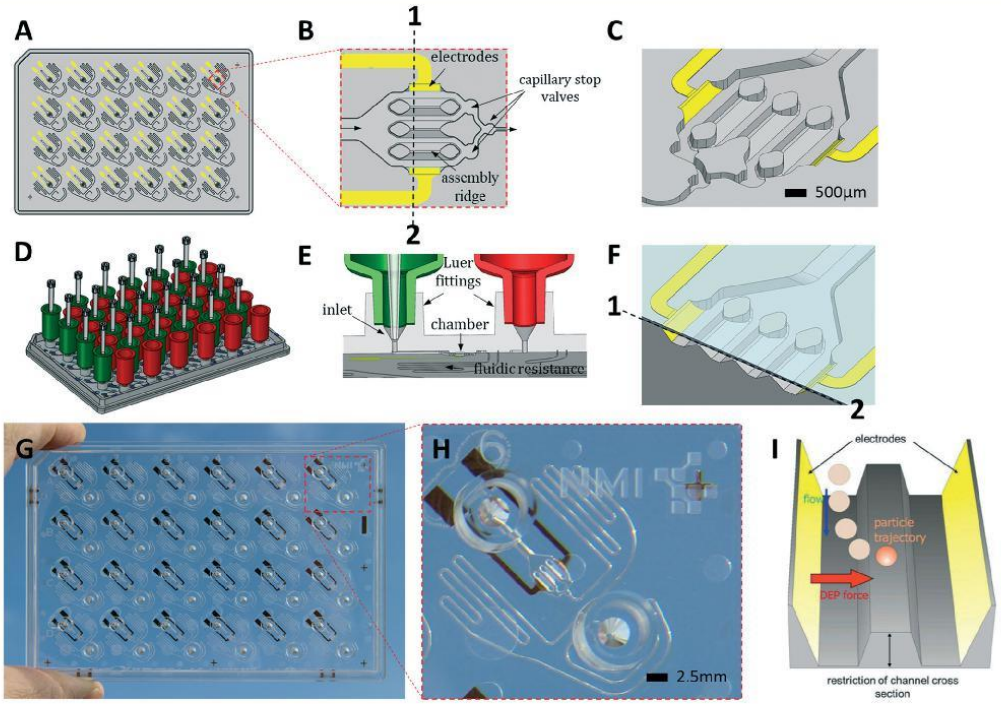

Fig. 1 The HepaChip-MP design. A) Layout of the microplate made of COP (grey) in ANSI/SBS format with electrodes (yellow). B) Close-up of an individual chamber showing electrodes at the periphery of the chamber, three assembly ridges and capillary stop valves for bubble-free filling. The direction of flow is from left to right. C) 3D view of a chamber. D) HepaChip-MP shown with tanks (reservoirs) on inlets (green) and outlets (red) as well as pipette tips reaching into the tanks. E) Tank connectors fit into Luer fittings. Gravity-driven flow may be bypassed by a pipette positioned in the conical inlet, thus tightly sealing and enabling defined flow for process steps such as cell assembly or fast media exchange. F) A cross-section along 1–2 in (B) including the cover foil which leaves a gap of about 50 μm height above the assembly ridges where cell aggregates mimicking sinusoids are formed. G) HepaChip-MP made by micro injection molding of COP and evaporation of gold electrodes. H) Close-up of an individual unit showing Luer fittings, cell chamber, electrodes, and meandering fluid resistor. I) Schematic illustration of the dielectrophoretic (DEP) force which draws cells onto the assembly ridges.

electromagnetic shielding of the high frequency electric fields applied during DEP assembly of cells. Openings on the bottom of the DEP fixture allow optical access of cell chambers by an imaging system to monitor chamber priming and cell assembly. Two different pipetting heads can be attached automatically by program control and either hold 24 or 4 pipetting tips. Batch programs for automated procedures were implemented to render robust and reproducible operation of the HepaChip-MP system.

iii) Automated priming, functionalization, cell assembly and cell culture workflow in HepaChip-MP

Chambers were primed with Pluronic F127 in HEPES, pH 7.4. In order to coat collagen on the assembly ridges a solution of Pluronic F127 (1 mg mL^{-1}) and collagen (100 μg mL^{-1}) in HEPES, pH 4, was pumped through the chambers. The collagen selectively binds to areas previously activated by UV illumination (see Fig. S2†). At the same time, non-activated, hydrophobic surfaces were coated by a monolayer of Pluronic to reduce cell adhesion and substance adsorption (see Fig. S6†). The procedure has been reported in detail previously.[47] Chambers were incubated with collagen solution overnight at room temperature under slow perfusion by filling the inlets with 500 μL of collagen/Pluronic solution.

After removing the collagen solution from inlet and outlet, the culture chambers were filled with low conductivity DEP medium (see v) to allow for positive DEP of cells. The cells were suspended in DEP medium immediately prior to the assembly routine (see v). The pipetting robot infused the cell suspension at 4 μL min^{-1}, while a high-frequency electric field was applied across the electrodes (80 V_{pp}, 360 kHz for hepatocytes, 80 V_{pp}, 620 kHz for endothelial cells) to assemble the cells.

Details of the chamber design resulting in an inhomogeneous electric field distribution, including multiphysics simulations of electric fields and DEP forces on cells have been reported previously.[48] A video showing cell assembly by DEP is in the ESI† (Video S2).

After completion of the assembly process, the high-frequency voltage was turned off. DEP medium was rinsed out of the cell culture chamber by perfusion with cell culture medium. Cells not assembled over the assembly ridge but attached to the periphery of the cell aggregate were thereby also rinsed out of the chamber. Finally, cells that were rinsed into the outlet were removed by pipetting. Fluid ports were routinely checked for the presence of cells prior to any assays to prevent interference by residual cells located in either the inlet or outlet. Shear forces in a HepaChip chamber were

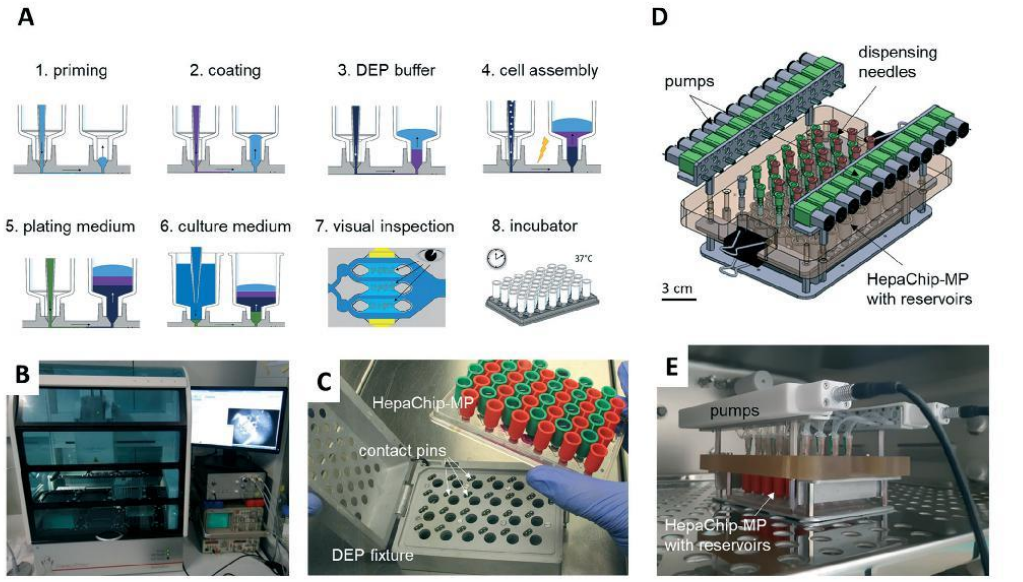

Fig. 2 Automated workflow and perfusion system for cell culture in HepaChip-MP. A) Schematic depiction of the workflow. Each process step except for the incubation is performed by a pipetting robot (B). During automated chamber priming, cell assembly and medium exchange, the HepaChip-MP is mounted in the DEP fixture (C), which establishes electrical contact between the integrated electrodes and a high-frequency generator to arrange cells by dielectrophoresis. D) The pump system is compatible with microfluidic microplates with fluid ports in the 96-well pattern and enables re-circulation by pumping medium from the outlet reservoirs (red) to the inlet reservoirs (green). The system comprises 24 peristaltic pumps and mounts directly on the HepaChip-MP. E) The pump system may be operated within an incubator.

calculated by multiphysics simulation and have been reported previously.[49]

iv) Perfusion system

A perfusion system was built to enable continuous reperfusion of cell culture medium (Fig. 2D and E). It comprises 24 miniature peristaltic pumps (Takasago Electric Inc., Nagoya, Japan) with cannulas reaching into inlet and outlet reservoirs on the microplate. These pumps transfer medium from the outlet to the inlet reservoir, in this way maintaining a defined pressure difference and flow rate. The absence of a pressure-tight fluidic connection between the perfusion system and the microfluidic device ensures that flow is completely gravity driven. This design furthermore eliminates the risk of bubbles, as any air possibly introduced in the tubing will not be pumped into the microfluidic device. The pumps are operated every 150 min for 4 min to transfer medium perfused during this period (approx. 75 to 100 μL) back to the inlet reservoir. The level difference and flow rate can be adjusted by varying the vertical position of the cannula which draws medium out of the outlet reservoir.

The HepaChip-MP also may be operated as stand-alone device which indeed was the mode of use routinely employed in this study. With inlet reservoirs filled with approximately 900 μL, continuous flow at rates decreasing from about 60 μL h^{-1} to 5 μL h^{-1} can be maintained over a period of at least 12 h (Fig. S1†), after which time period the medium can be re-perfused manually or by use of a pipetting robot.

v) Cell culture and media formulations

Fresh and cryopreserved primary human hepatocytes (PHH) (Donor BHuf16068, Cytes Biotechnologies, Barcelona) as well as cryopreserved primary human liver endothelial cells (HuLEC) were used in our experiments.

Fresh PHH and HuLEC were isolated from liver tissue samples by a two-step EDTA/collagenase perfusion technique as described elsewhere.[50] Liver tissue samples were obtained from macroscopically healthy tissue that remained from resected human liver of patients with primary or secondary liver tumors or benign local liver diseases. Informed consent of the patients for the use of tissue for research purposes was obtained according to the ethical guidelines of Leipzig University Hospital (ethics vote 006/17-ek). Fresh hepatocytes were stored on ChillProtect Plus and shipped overnight on ice.

The appropriate HuLEC cell number for cryopreservation was centrifuged at 300 × *g* for 4 min at 4 °C and the HuLEC pellet was re-suspended in a cryopreservation medium consisting of 70% ChillProtec Plus medium (Biochrom, Berlin, Germany), 20% FBS and 10% dimethyl sulfoxide (DMSO; Carl Roth, Karlsruhe, Germany) whereby a maximum concentrations of 2–10 × 10^6 HuLEC per mL medium are recommended. The resulting cell suspension was transferred into CryoPure vials. The vials were inverted briefly, placed as soon as possible in a Mr. Frosty Freezing Container (Thermo Fisher Scientific, Waltham, USA) and transferred to −80 °C for at least 24 h. Cryopreserved cells were shipped on dry ice overnight.

Cryopreserved PHH were thawed using a thawing kit (Primacyt) according to instructions and cell number and viability were determined with the trypan blue exclusion test. Next, 3–4 million cells were centrifuged at 4 °C and 50 × *g* for 5 min. Cells were re-suspended in 2 mL of DEP medium. DEP stock solution was prepared by dissolving 1 g glucose, 57.9 mg sodium pyruvate, 28.4 mg $CaCl_2$ and 24.6 mg $MgSO_4$ in 100 mL diH_2O. To obtain the final DEP medium, 10 mL of DEP stock was diluted in 100 mL diH_2O, 9.5 g saccharose was added and the medium was sterilized by filtration. After re-suspending cells in DEP medium, the suspension was placed in the pipetting robot and used for cell assembly in the HepaChip-MP.

Fresh PHH used in HepaChip-MP cultures were washed twice with ice-cold PBS (centrifugation 50 × *g*, 5 min, 4 °C). Subsequently, cells were re-suspended in culture medium and cell number and viability were determined with the trypan blue exclusion test. For culturing PHH different medium formulations were used. Medium 1 denotes Williams E (with GlutaMAX; Thermo Fisher Scientific) supplemented with 10% FBS, 15 mM HEPES (Thermo Fisher Scientific), 1 mM Na-pyruvate, 1% non-essential amino acids (Thermo Fisher Scientific), 1 μg mL^{-1} dexamethasone, 1 μg mL^{-1} human insulin and primocin (Invivogen, San Diego, CA, USA). Medium 2 was composed of medium 1 plus 0.55 μg mL^{-1} human transferrin, 0.5 ng mL^{-1} Na-selen and 5.35 μg mL^{-1} linoleic acid. After determination of cell number and viability, 3–4 million cells were centrifuged at 4 °C and 50*g* for 5 min and re-suspended in 2 mL of DEP medium. Then, the cell suspension was placed in the pipetting robot and for cell assembly in the HepaChip-MP.

For co-culture experiments, HuLEC were assembled at day 1 after assembly of hepatocytes. Cryopreserved HuLEC were transferred to 10 mL prewarmed EGM2 (Promocell, Heidelberg, Germany) and then centrifuged at 300*g* for 5 min at room temperature. Cells were re-suspended in EGM2 and cell number and viability were determined by trypan blue exclusion test. HuLEC concentration employed for assembly in the HepaChip-MP was 0.5 × 10^6 cells per ml.

For spheroid cultures, cryopreserved PHH from a single donor (BHuf16068, Cytes Biotechnologies, Barcelona) were thawed following the distributor's manual. Cells were re-suspended in 3D-HMM (Primacyt) and cell number and viability were determined with the trypan blue exclusion test. Cells were seeded into ULA U-bottom 96-well plates (Greiner Bio-One, Kremsmünster, Austria) in 70 μL 3D-HMM at a density of 2500 cells per well. To aid sedimentation of cells and formation of spheroids, plates were centrifuged once at 500 × *g* for 2 min. Spheroids were cultured at 37 °C with 5% CO_2 for 6 days until a spheroid with regular shape was formed. On day 3 fresh 3D-HMM (30 μL) was added to each well.

Induction of cytochrome P450 (CYP) enzymatic activity was performed in 3D spheroid cultures and HepaChip-MP cultures in the presence of 3D-HMM medium (Primacyt). For

the coculture of PHH and HuLEC, medium 2 and EGM2 were used at a ratio of 1 : 1. For all other experiments medium 2 was used if not stated differently.

vi) Assays

Calcein staining. Cell culture medium in inlet reservoirs was replaced by calcein AM solution (4 μg mL^{-1} in PBS, 500 μL per inlet reservoir; Thermo Fisher Scientific). The solution was perfused through the chamber by gravity-driven flow for 60 min thereby exchanging the chamber volume more than 20 times. Thereafter, the calcein AM solution was removed and replaced with 900 μl of cell culture medium and allowed to perfuse for at least 15 min to remove any calcein AM solution from the chambers. Subsequently, microscopic images were obtained using a FITC filter (Axiovert 200, Carl Zeiss AG, Oberkochen, Germany).

Immunostaining. All washing steps described in this paragraph were performed by filling the inlet with 900 μl of PBS and allowing for at least 15 min of perfusion thereby exchanging the chamber volume at least 10–15 times. Cells were fixed with paraformaldehyde (PFA) by completely removing cell culture medium from inlet and outlet followed by the addition of 500 μL 4% PFA in PBS. After 20 min incubation, the PFA solution was removed and the inlet was filled with PBS for washing. PBS was removed and cells were permeabilized and antigens were blocked by filling the inlet with 0.1% Triton-X100/5% BSA in PBS. After perfusion for 30 min, cells were washed. Primary fluorescent antibodies were used, diluted in 5% BSA in PBS (see Table 1) and 250 μL of antibody solution was used per inlet and incubated overnight at room temperature. Afterward, cells were washed and nuclei were stained with DAPI. For DAPI staining, PBS was removed, the inlet was filled with 5 μg mL^{-1} DAPI in PBS and incubated for 45 min. Afterward, cells were washed with PBS and kept in PBS until microscopic inspection.

Basal CYP activity and induction of CYP enzymes in spheroid and HepaChip-MP cultures. To directly compare the two liver models, cryopreserved cells obtained from a single donor (BHuf16068, Cytes Biotechnologies, Barcelona) were used. Stock solution of rifampicin as an inducer for both CYP2C9 and CYP3A4 was diluted to 20 μM in the respective cell culture medium.

In HepaChip-MP cultures, the induction of CYP enzymes was started at day 2 of culture and carried out for 72 h by perfusing medium containing 20 μM rifampicin. Thereafter, solutions of the CYP substrate in the respective cell culture medium were perfused for 5 h through the chamber (50 μM diclofenac for CYP2C9; 15 μM midazolam for CYP3A4). Sample volumes of approx. 150 μL were obtained. After transferring the sample to tubes, 15 μL of 10% acetic acid were added and samples were stored at −80 °C until analysis by liquid chromatography-mass spectrometry (LC-MS).

For induction experiments in spheroid cultures, medium was removed from wells and spheroids were treated with 70 μL of 20 μM rifampicin for 72 h starting on day 6, whereby the induction solution was replaced every day. At day 9, spheroids were washed twice with PBS and incubated with 90 μL substrate solution (50 μM diclofenac for CYP2C9; 15 μM midazolam for CYP3A4) for 5 h. After incubation with substrates, the supernatant of two wells was pooled (final volume 180 μL), and the samples were transferred into tubes containing 18 μL of 10% acetic acid in 3D-HMM. Samples were stored at −80 °C until analysis by LC-MS.

Cell lysis and BCA-assay. To determine protein amount per cell chamber, cells were lysed *in situ* and the lysate was retrieved and analyzed by a BCA assay. For this purpose, cell culture medium was removed from outlet and inlet. The inlet was filled with 800 μL PBS to completely remove any cell culture medium from the system which otherwise would interfere with protein quantification. After 45 min of rinsing by gravity-driven flow, PBS was removed from outlet and inlet. Tanks were removed and inlet and outlet were washed 3 times with 50 μL of PBS. Subsequently, 10 μL of 0.1 M NaOH solution was pipetted into the cell culture chamber by tightly contacting a 100 μL pipette to the inlet and actively pumping the solution into the chamber. The chambers were incubated for 60 min at room temperature. To extract the lysates from the cell chambers, 3 × 50 μL were pipetted into the outlet. The 3 × 50 μL were retrieved from the inlet and transferred to a 96-well plate.

For cell lysis in spheroid cultures, spheroids were washed once with PBS and incubated with 0.1 M NaOH for 15–20 min. Cell lysates of two spheroids were pooled and stored at −80 °C until protein analysis.

Samples from HepaChip-MP and spheroid cultures were analyzed by a BCA-protein assay kit for low concentrations (Abcam, ab207002) according to its instructions.

Liquid chromatography-mass spectrometry. All reagents and chemicals used were of analytical or LC-MS grade.

Preparation of stock and working solutions, calibration standards and QC samples. Stock solution of 4′-hydroxydiclofenac (HDC) and the respective internal standard (4′-hydroxydiclofenac-$^{13}C_6$; HDC-$^{13}C_6$) were prepared by accurate weighing of the reference item and dissolution in a mixture of dimethylsulfoxide and acetonitrile (7 + 3, v + v) to yield a final concentration of 1 mg mL^{-1}. A commercially available, certified stock solution of 1 mg mL^{-1} in methanol

Table 1 Antibodies used for staining different cell types in the HepaChip-MP

Antigen	Fluorescent label	Vendor	Catalog#	Host species	Reactivity	Dilution
CD31	Alexa Fluor 488	Abcam	ab215911	Mouse	Human	1 : 500
CK18	Alexa Fluor 647	Abcam	ab206269	Rabbit	Human	1 : 500

was used for HMDZ and its internal standard (1′-hydrixymidazolam-d_4; HDMZ-d_4). Working solutions for spiking of matrix samples were prepared by serial dilution of the stock solutions in a mixture of water and methanol (1 + 1, v + v).

Calibration standards were prepared freshly on each day of analysis by the addition of 10 μL of spiking solution to 100 μL of pre-acidified blank matrix (neat cell culture medium, *i.e.* 3D-HMM, +10% aqueous acetic acid, 100 + 10, v + v). QC samples in pre-acidified blank matrix were prepared in bulk in advance and stored at ≤−18 °C until use.

Sample processing. Fifty (50) μL of pre-acidified sample (blank matrix, calibration standard, QC, or cell culture incubate) were pipetted into a preconditioned OASIS HLB μElution plate (96 well format, Waters, Eschborn, Germany) and mixed with 50 μL of water + formic acid (100 + 1, v + v) and 10 μL of internal standard working solution (conc. of HDC-$^{13}C_6$ and HMDZ-d_4, and approx. 250 ng mL^{-1}). After washing of the loaded sample with water + formic acid (100 + 1, v + v), the analytes were eluted with 50 μL of acetonitrile + water + formic acid (90 + 10 + 1, v + v + v) into a 96 well collection plate. The eluate was concentrated under a gentle stream of nitrogen at approx. 40 °C for 10 min and the residue was reconstituted in 35 μL of acetonitrile + water + formic acid (20 + 80 + 1, v + v + v). The plate was sealed and 15 μL of the processed sample were injected for LC-MS analysis.

LC-MS method. LC-MS analysis was performed on an 1100 Series high-performance liquid chromatography system (Agilent Technologies, Waldbronn, Germany) coupled to a TSQ Vantage mass spectrometer (Thermo Fisher Scientific, Dreieich, Germany). Chromatographic separation was achieved on a Reprospher 100 C18-DE analytical column (2.0 × 50 mm, 1.8 μm particle size; Dr. Maisch, Ammerbruch, Germany) equipped with a Security Guard cartridge precolumn (C18, 4 × 2.0 mm; Phenomenex, Aschaffenburg, Germany), maintained at 40 °C. Mobile phases consisted of 10 mM ammonium carbamate in water (A) and in a mixture of methanol and acetonitrile (80 + 20; B). The following gradient elution was carried out at a constant flow rate of 250 μL min^{-1} [% A (min)]: 99 (0.0), 99 (0.3), 30 (4.0), 20 (6.0), 0 (6.01), 0 (7.0), 99 (7.01), 99 (10.0). The MS was operated in positive ESI mode (HESI II probe), applying a spray voltage of 4500 V and a vaporizer temperature of 200 °C. Argon was used as collision gas.

Protonated analytes were detected after collision induced dissociation (collision gas: argon) in multiple reaction monitoring mode using the following ion transitions (*m*/*z*–*m*/*z*, collision energy [V], S-lens [V]): 312.0–230.0, 35, 80 (HDC), 318.0–236.0, 35, 80 (HDC-$^{13}C_6$), 342.0–324.0, 21, 130 (HMDZ), 346.0–328.0, 21, 130 (HMDZ-d_4).

Quantification and analytical acceptance criteria. The concentrations of HDC and HDMZ in cell culture incubations were determined using the corresponding calibration functions with weighting of the measured results (weighting $1/conc^2$). HDC-$^{13}C_6$ and HMDZ-d_4 were used as respective internal standards. The chromatograms were recorded and integrated in peak area mode by use of the LCquan software (Thermo Fisher Scientific, Dreieich, Germany). Quantification of the analytes was conducted in accordance with the current guidelines on bioanalytical method validation (EMA guideline and FDA guidance for industry).

The calibration range was set from 0.200 ng mL^{-1} (lower limit of quantification, LLOQ) to 200 ng mL^{-1} (upper limit of quantification, ULOQ). An explorative calibration standard at 0.100 ng mL^{-1} was analyzed within each run and included into regression analysis, if higher sensitivity was required. The volume of the acetic acid solution added to each individual sample was corrected during quantification.

One set of calibration standards (including one blank sample and zero calibration standard each) was analyzed at the start of the analytical run and one at the end. Each set of calibration standards consisted of at least eight non-zero standards distributed over the calibration range. Calibration standards were excluded from linear regression if the accuracy of an individual standard was outside the limits of ±20% (±25% at the LLOQ). No more than 25% of the calibration standards were excluded from each series of calibration standards. At least one sample at the LLOQ and the ULOQ level had to meet the specifications.

At least six QC samples (three different levels as duplicates) were analyzed within each run. At least 67% of all QCs per run and at least 50% of the QCs of one concentration level had to meet the acceptance criteria for QC samples (bias of each individual QC sample concentration of max. ±20%).

Assessment of cytotoxicity and viability over the course of 6 days using a resazurin assay. Toxicity was assessed by a resazurin assay using the alamarBlue reagent (Bio-Rad, Hercules, CA, USA). Cells were seeded as described above. At day one of culture, the cells were treated with different concentrations of diclofenac (0, 150, 450, 900, 1500 μM). These concentrations were chosen based on literature showing toxicity on hepatocytes in this range.[51] Diclofenac was directly dissolved into medium 2. After 24 h of drug treatment, the medium including diclofenac was discarded and replaced by medium 2 with 10% alamarBlue reagent. After 12 h, 100 μL of the perfused medium were transferred into a black 96-well plate and fluorescence was measured (Ex.: 540 nm, Em.: 580 nm).

In order to determine track viability, a resazurine assay was carried out on day 1, day 3 and day 6 of culture in the HepaChip-MP as described above. A stock solution of resazurine in medium 2 was prepared, aliquoted and stored at 4 °C until the respective day of experiment. As a negative control, cells were treated with 2 mM diclofenac starting at day 2 of culture.

vii) Statistics

Values are given as mean and standard deviation (mean ± SD). As the results presented here are intended to demonstrate various assays in this new platform, the results include technical rather than biological replicates. The results of the induction experiment of CYP2C9 and CYP3A4 were analyzed for statistical significance by an unpaired

t-test. For the cytotoxicity test, a one-way ANOVA with *post hoc* Tukey was carried out. Statistics software GraphPad Prism (GraphPad Software, USA, California, San Diego) was used. *P*-Values are provided in the figure description.

Results

1. Hepachip-MP microfluidic design

The HepaChip-MP was designed at NMI and manufactured by microfluidic ChipShop in conformity with ANSI/SBS standards for outer dimensions and position of fluid ports (Fig. 1). Each HepaChip-MP has 24 culture chambers (Fig. 1B and C), which contain three assembly ridges with dimensions similar to the human liver sinusoid (approx. 30 cells or 900 μm in length[52]) on which cells can adhere. The chamber is 4.3 mm long, 2.3 mm wide and has a height of 0.19 mm. The resulting chamber volume is approximately 0.85 μl. As fluid enters through the inlet and flows along the assembly ridges, capillary stop valves sequentially arranged within the chamber ensure reproducible priming and efficiently prevent trapping of bubbles (Video S1†).[53] Electrodes on the chamber sides are employed to generate high frequency electric fields across the assembly ridges for assembly of cells by DEP. Maximum field strengths are achieved in the vertical gaps between the assembly ridges and the cover (Fig. 1C). Electrical field distribution, hydrodynamic flow and cell trajectories resulting thereof have been reported previously.[48]

Both inlets and outlets have Luer fittings to enable versatile connections. Tanks attached to these Luer fittings (Fig. 1D) enable continuous gravity-driven flow when the inlet (green) and outlet tanks (red) are filled to different levels. A fluid resistor (width: 100 μm, length: approx. 140 mm) at the outlet of the culture chamber defines a flow rate ranging from approximately 1 to 0.1 μL min^{-1} over a period of 12 h (Fig. S1†).

Conical structures at the bottom of the Luer fittings allow for pressure-tight connection of pipette tips (Fig. 1E). This mode of operation is used during priming and cell assembly to achieve flow rates which are constant or different from those that can be achieved by gravity-driven flow. This mode allows infusion of minute amounts of fluids such as staining solutions or test samples at any time, temporarily suspending the flow of medium contained in the tank. Thus, automated assays such as viability tests or immunohistochemical staining may be performed. Upon retraction of the pipette tip, gravity-driven medium flow resumes without delay.

We designed the fluid resistance such as to enable *in vivo*-like perfusion. To this end, the number of cells in the chamber and their oxygen consumption was considered. As gas permeability of COP is quite small[54] diffusion of oxygen through the polymer may be neglected. The tank volume of 900 μL allows continuous perfusion for at least 12 h without user intervention or the perfusion system. With 500–1000 cells per chamber consuming 0.3–8 fmol min^{-1} per cell,[55–57] this flow rate was expected to provide sufficient oxygen while allowing for the development of an appropriate oxygen gradient along the sinusoid structures. Perfusion by gravity-driven flow was measured with medium at 37 °C (Fig. S1†). As expected, the flow rate decreases over time as levels within the inlet and outlet tank equilibrate. This perfusion mode was employed in the experiments described in this study.

However, to also enable constant flow rates, we developed an incubator-compatible perfusion system (Fig. 2D and E) which can be used to continually pump media from outlet reservoirs back into the inlet reservoirs, thus maintaining constant pressure differences and flow rates. This device enables long-term perfusion without user attention and thus can enhance overall system usability.

2. Process development and cell assembly

The priming of chambers was evaluated. Only chambers completely filled without any air bubbles were considered usable. Priming with a pipetting rate of 1.11 μL min^{-1} properly filled an average >80% of the chambers.

Selective coating of only the assembly ridges with ECM protein by perfusion of a collagen I/Pluronic F127 mixture was confirmed using collagen labelled with rhodamine (RITC). The selective deposition of RITC-labelled collagen on assembly ridges was verified by fluorescence microscopy (Fig. S2†).

The fraction of cells assembled on the assembly ridges *vs.* cells passing through the chamber strongly depends on the flow rate as reported previously.[48] Lower flow rate results in lower hydrodynamic drag forces and higher efficiency of cell assembly by DEP. However, cells can sediment and clog the microfluidic channels if flow rates are too low. The pipettor provides a higher degree of precision and thus reproducibility than manual pipetting. A video showing the automated priming and cell assembly process is provided in the ESI† (Video S1).

Cells assembled on the assembly ridges adhere due to the collagen I coating and the reduced shear forces present in this region of the chamber.[48] In contrast, higher hydrodynamic forces wash out cells which may have been collected incorrectly in the chamber (Fig. 4).

3. Liver cultures in HepaChip-MP

3.1 Morphology and viability

PHH monoculture. All experiments reported here were carried out using PHH. Cell culture experiments using the HepaChip-MP confirmed the desired formation of elongated structures on the assembly ridges. Cells adhered to the assembly ridges and started to build compact structures within two days (Fig. 4). Fig. S3† shows images obtained from a larger number of chambers of several HepaChip-MP demonstrating reproducibility of cell assembly on the assembly ridges. The development of compact structures can be observed from the dense grouping of cells on the assembly ridges. In addition, a barrier-like structure can be seen at the interface between the microtissue and the flow channel. At DIV5, these structures became more compact and shorter and broadened. This process continued until day 12 of culture. The viability of cells up until day 8 was confirmed by calcein staining (Fig. 4). Cells which are initially not part

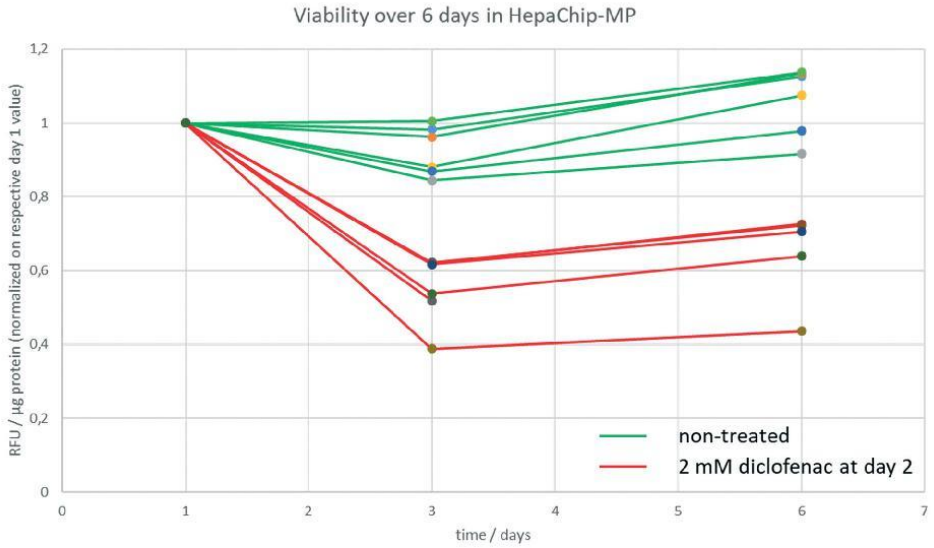

Fig. 3 Viability of PHH during 6 days in HepaChip-MP. The viability was measured by a resazurine assay at day 1, 3 and 6 of culture. Non-treated PHH show no significant change of RFU values during 6 days of culture (green lines) whereas the RFU values of PHH treated with 2 mM diclofenac decline to 40–70% (red lines). Six chambers of a single HepaChip-MP of both non-treated and treated samples are shown.

of the compact structure are flushed out or integrated into the cell structures (Fig. 4, day 0 to day 5).

Unexpectedly, cells assembled on the outermost assembly ridges (denoted by "L" and "R" in Fig. 4), were observed to collectively migrate over time towards the periphery of the chamber. As a minute, previously unnoticed cross flow was suspected to be responsible, the movement of fluorescent microparticles (diameter 5 µm) under flow in the chamber was studied. Indeed, movement of particles indicated flow perpendicular to the chamber axis, including crossflow traversing the left and right assembly ridges (Fig. S4†). Hydrodynamic forces of this flow pattern, as minute as they may be considering small pressure and flow rates present in the chamber during culture, may lead to the dislocation of the assembled cells. Additional study in future experiments may guide a redesign of the culture chamber to ensure flow strictly parallel to the assembly ridges.

To track viability of PHH cultured in HepaChip-MP over a culture period of 6 days, a resazurine assay was carried out on days 1, 3 and 6 of culture (Fig. 3). Non-treated PHH show constant viability over the duration of the experiment (green lines). PHH treated with 2 mM diclofenac at day 2 show RFU values declining to about 40–70% of the initial values (red lines).

3.2 Metabolic activity

Basal CYP activities during culture. Basal activities of CYP2C9 and CYP3A4 of cultures of fresh PHH (donor: female, 55 years, hemangioma) were evaluated on day 3 and day 6 in the HepaChip-MP with two different cell culture media (Table 2). CYP2C9 was equally active at day 3 and 6 in medium 1 (ratio of 1.05 ± 0.18) and slightly more active at day 6 in medium 2 (ratio of 1.38 ± 0.14). CYP3A4 activity was higher on day 6 *vs.* day 3 in either medium 1 (ratio of 1.39 ± 0.21) or medium 2 (ratio of 1.62 ± 0.05).

CYP activity in HepaChip-MP in comparison to 3D-spheroid culture. We evaluated xenobiotic metabolism of PHH in the HepaChip-MP and in spheroids as a benchmark system (Fig. 5). Induction was carried out by incubation with rifampicin for 72 h. The activity of CYP3A4 and CYP2C9 was measured by substrate turnover after 5 h of substrate incubation using LC-MS analysis of metabolites in the perfusates. In spheroids, induced activity *vs.* basal activity was 6.6-fold higher for CYP3A4 and 2.1-fold higher for CYP2C9. In the HepaChip-MP cultures, induced activity was 3.4-fold higher for CYP3A4 and 3.3-fold higher for CYP2C9. The measured conversion rates of CYP2C9 were of the same order of magnitude in both the spheroid and HepaChip-MP. The conversion rates observed for CYP3A4 were more than 20-fold lower in HepaChip-MP than in the spheroid model, while induction ratios were similar.

3.3 Vitality assessment after drug treatment using HepaChip-MP. The effect of diclofenac on PHH vitality was assessed using a resazurin assay (Fig. 6). The measurement was carried out at day 3 with a culture of fresh PHH of a male donor (63 years, cholangiocellular carcinoma) after 24 h of treatment with diclofenac. At concentrations of 150 µM or 450 µM, the signal was increased by 50% *vs.* the control (0 µM). No difference was observed for 900 µM treatment. Upon

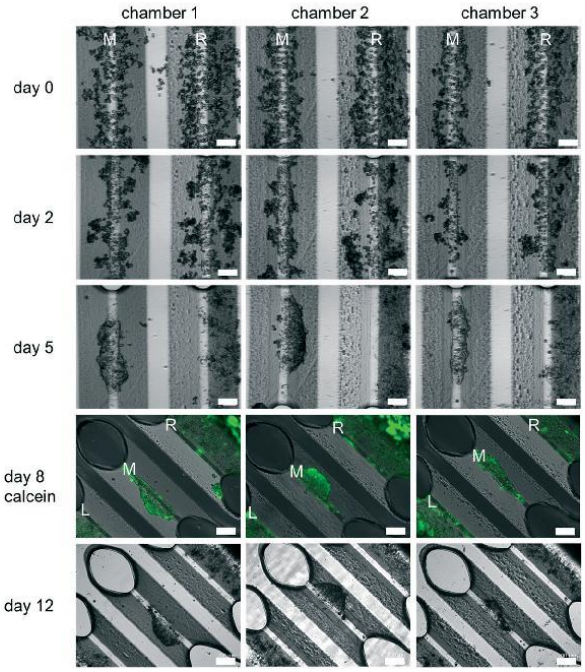

Fig. 4 Representative microscopic images obtained from three different cultivation chambers showing cultures of fresh PHH in the HepaChip-MP over a period of twelve days. Images from day 0 to 5 show the middle assembly ridge (M) and the right assembly ridge (R). Images on day 8 and twelve (rotated by 45 degrees) show the middle assembly ridge (M), the right assembly ridge (R) and a part of the left assembly ridge (L). The cells can be assembled on the assembly ridges (day 0) and a compact elongated structure forms there within 2 days. After 5 days the cells on the middle assembly ridge are still in a compact elongated but more contracted structure. The cells on the right assembly ridge collectively migrate to the right. All cells are still viable on day 8 as shown with calcein staining. Throughout the culture, the cells on the middle assembly ridge are contracting to form a more spheroid-like structure (scale bar day 0, day 2 and day 5: 300 μm; scale bar day 8 and day 12: 200 μm, n = 8).

treatment with 1500 μM the signal decreased by 81%. We explain the reason for this non-monotonic behavior in the discussion below.

3.4 Coculture of hepatocytes and endothelial cells. Cryopreserved PHH (cPHH) (donor BHuf 16068, Cytes Biotechnologies, Barcelona) and cryopreserved HuLEC (cHuLEC) were cocultured in the HepaChip-MP. The endothelial cells were assembled after the hepatocytes aiming to mimic the physiological arrangement in which endothelial cells build a barrier between hepatocytes and blood stream.[58] The two cell types require different DEP frequencies (see methods section and Fig. S5†). Immunocytochemical staining using antibodies against cell-type-specific markers (hepatocytes: CK18; endothelial cells: CD31)[59] showed CK18-positive cells as well as CD31-positive cells at day 3 of culture (Fig. 7). The cocultured cells also built compact elongated structures on the assembly ridges. As expected, the cPHH built the core of the elongated structures, with endothelial cells located mostly on their outer surfaces.

Table 2 Basal CYP activity in HepaChip-MP. Ratios at day 6 and day 3 of metabolites 4-hydroxydiclofenac (HDC) and 1-hydroxymidazolam (HMDZ), representing the activity of CYP2C9 and CYP3A4, respectively. These basal values are the mean ratios ± standard deviation based on four chambers for each time point

Ratio day6/day3	HDC	HMDZ
Medium 1	1.05 ± 0.18	1.39 ± 0.21
Medium 2	1.38 ± 0.14	1.62 ± 0.05

Discussion

Here, we have demonstrated a perfusable liver-on-a-chip platform in SBS/ANSI microplate format which enables i) active assembly and coculture of PHH and HuLEC; ii) continuous unidirectional gravity-driven flow; iii) integration in common testing workflows and iv) automation using comprehensive instrumentation (pipetting robot, perfusion system). We expect that this platform will facilitate the use of an organ-on-chip system by end users without particular proficiency in microfluidic technology. Demonstrative experiments confirmed

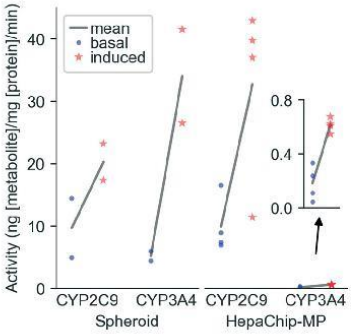

Fig. 5 CYP induction in spheroids and HepaChip-MP. Primary human hepatocytes (PHH) (donor BHuf 16068) were cultured *in vitro* and CYP activity was induced with 20 μM rifampicin from day 2 to day 5 (HepaChip-MP) or day 6 to day 9 (3D spheroid cultures). Basal and induced CYP activities were determined after 5 h of substrate incubation with spheroids and HepaChip-MP cultures. Data represent the metabolite formation normalized to protein content. For the spheroids, each incubation condition included four spheroids of which two were pooled for metabolite and protein analysis as technical replicates. In case of the HepaChip-MP cultures, samples from four to five cell culture chambers (technical replicates) were analyzed for each condition. Means of values obtained from basal and induced activity of cells were analyzed by an unpaired *t*-test for each enzyme and *in vitro* system. *P*-Values are the following. CYP2C9 spheroid: 0.1985; CYP3A4 spheroid: 0.0618; CYP2C9 HepaChip-MP: 0.0236; CYP3A4 HepaChip-MP: 0.0008.

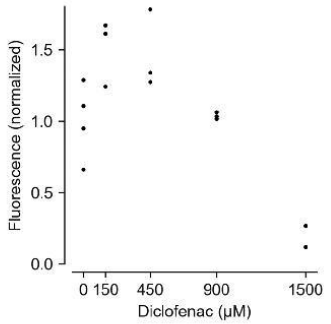

Fig. 6 Assessment of dose-dependent effects of diclofenac on PHH vitality. Cells from a male donor (63 years, cholangiocellular carcinoma) were cultivated in the HepaChip-MP. Fluorescence values from the resazurin assay were normalized *vs.* protein mass and the control without diclofenac. Three to four chambers were analyzed for 0–900 μM diclofenac; two chambers were analyzed for 1500 μM diclofenac. Individual data points of technical replicates are shown. Test for statistical significance by ANOVA showed statistical significant differences between the different conditions (*p*-value = 0.0005). *Post hoc* comparisons using Tukey's showed statistical significant differences between 0 and 1500 μM (*p*-value = 0.0118), 150 and 1500 μM (*p*-value = 0.0005), 450 and 1500 μM (*p*-value = 0.0006) as well as 900 and 1500 μM diclofenac (*p*-value = 0.0123).

important biological functions and assays, namely xenobiotic metabolism (*via* LC/MS) including induction, viability assay, assessment of drug-induced toxicity and immunostaining of marker proteins.

While we regard the HepaChip-MP model as an important step towards fully workflow-compatible microphysiological systems, our study also shows that certain improvements will be required to fully attain this goal. These will be subject to further research and development as outlined below.

Chamber priming and parallelization

Priming successfully fills more than 80% of chambers without air bubbles, enabling 20 independent experiments with the same cell preparation on a single microplate. Working with primary cells with high donor variability requires such parallelization to reproducibly obtain valid data. While successful priming demonstrates the proper function of capillary stop valves in the chamber,[48] optimization of the process and possibly of the design of the capillary stop features is required to attain success rates approaching 100%.

A single HepaChip-microplate can acquire a complete dose–response curve. Robustness of operation is attained by process automation using a pipetting robot. Open access of the medium reservoirs enables handling comparable to standard microplates. These features will facilitate the integration of microfluidic microplates such as the HepaChip-MP into common pharmaceutical and biological workflows.

Technical and biological features

In contrast to other *in vitro* systems, HepaChip-MP has distinct advantages with respect to usability and biologic mimicry. While microfluidic microplate platforms using a rocker to induce gravity-driven perfusion this flow is bi-directional.[41,42] In contrast, HepaChip-MP cultures are unidirectionally perfused to enable generation of *in vivo*-like chemical gradients and a more *in vivo*-like shear stress along micro tissues. The HepaChip-MP platform can be handled like a common microplate while microfluidic models with chip-integrated peristaltic pumps require connection to external periphery.[60]

Most importantly, the assembly of cells by DEP exclusively selects viable cells. Non-viable cells do not maintain the difference in intra- and extracellular conductivity which is fundamental in DEP for the generation of a dipole moment.[48] As a consequence, non-viable cells simply pass through the chamber. Furthermore, DEP allows sequential assembly of multiple cell types to mimic physiological structures. This paradigm of controlled assembly of cells into micro tissues in specifically designed cell chambers can be generalized to other organ systems and we present liver sinusoids in the HepaChip-MP as a representative example (Fig. 4).

The feasibility of controlled assembly of cells into micro tissues in the desired structure is a general advantage of microfluidic systems when compared to spheroid models. In spheroids, cells are assembled randomly in spherical structures. Hepatocytes in the HepaChip-MP are assembled

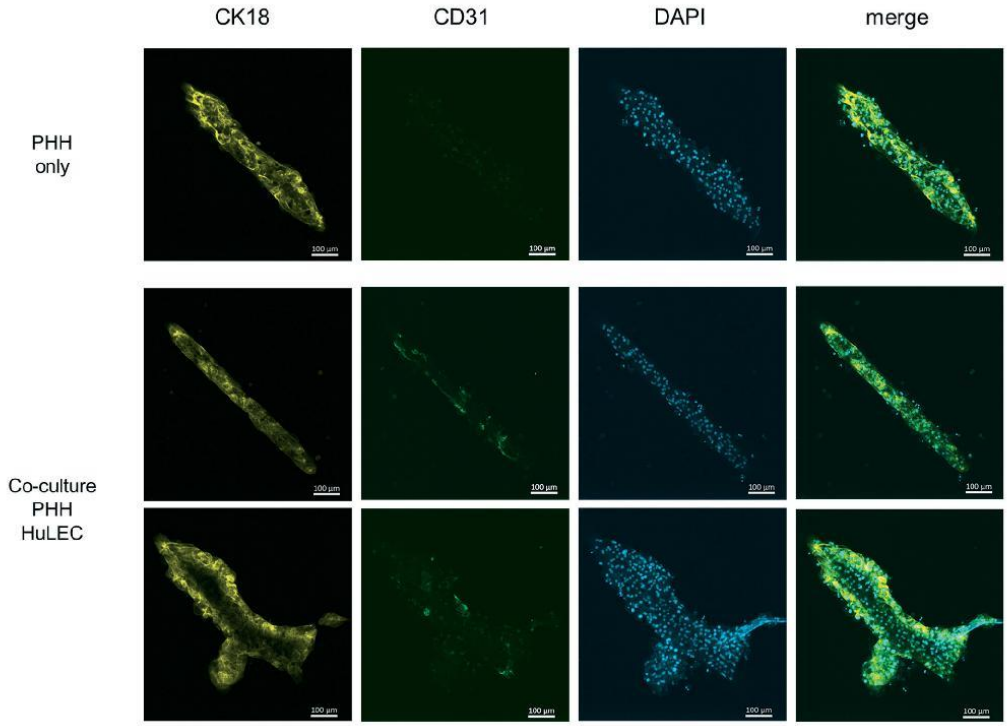

Fig. 7 Fluorescence micrographs of a monoculture of cryopreserved PHH (first row) and cocultures with cryopreserved HuLEC (second and third rows) at day 3 of culture. CK18 indicates PHH (yellow) and CD31 labels endothelial cells (green). DAPI staining shows cell nuclei. The monoculture used medium 2. The coculture used a 1 : 1 mixture of medium 2 and EGM2. These images of single assembly ridges are representative of at least three chambers for each condition. Scale bar: 100 µm.

in compact elongated structures (Fig. 4), which resembles the structure of the liver sinusoid more closely than spheroid structures and perfused monolayers. We have observed that initially elongated structures contract over time (Fig. 4). Cell–cell interactions may become stronger than their adhesion (*via* collagen coating) on the assembly ridges. Further experiments will investigate alternative ECM coatings to influence cell adhesion and long-term development of the organoid structure and function.

In terms of mimicking the liver sinusoid in all its complexity, there is still a long way to go.[20,21] *In vivo*, there are additional cell types present when compared to current test systems including HepaChip-MP. Cell functionality, protein expression and physical dimensions as well as the microenvironment differ from model systems.[20,21] Some *in vitro* models include non-parenchymal cells and thereby achieve promising results in terms of improved long term culture with hepatocyte specific functionality, disease modelling and drug response.[2,17,30] However, these models do not reproduce the dimensions and physiologic microenvironment of the liver sinusoid.

Therefore, the cell culture chamber of the HepaChip-MP was designed to enable the cultivation of hepatocytes along with non-parenchymal cells in elongated cell aggregates with physical dimensions of the liver sinusoid (see Results section and ref. 52). Also, cells are in direct contact to the perfused medium as no hydrogel or membrane is required for the assembly of cells. In this study we also demonstrate seeding and coculture of HuLEC and PHH in the HepaChip-MP (Fig. 7). In future experiments, additional non-parenchymal cell types will be included in order to reach at a relevant cellular complexity as reported previously,[2,17,30] yet cultured in cell aggregates mimicking the physical dimensions of the liver sinusoid more closely.

Migration of organoids to the periphery

The observation of migration of cells on the outer assembly ridges towards the periphery suggests that cells may be sensitive to even minute, yet continuous hydrodynamic forces which they experience due to the design of the cell culture

chamber (see Fig. S4†). This finding will inform future designs of flow chambers.

Metabolic activity

So far, PHH cultured in the HepaChip-MP were shown to exhibit xenobiotic metabolism over at least six days (Table 2). This is an important feature in model systems for toxicity testing and drug development since many substances are detoxified or activated by CYP enzymes of PHH. Induction of CYP2C9 and CYP3A4 in the HepaChip-MP (Fig. 5) indicates physiological enzyme regulation, which is also an important feature of a liver model.[8,61] Future experiments will analyze the stability of CYP activity and induction over time. Other authors demonstrated the possibility to measure CYP activity of PHH *in vitro* co-cultured with non-parenchymal cells over 14 to 90 days.[2,27,62–64] It was also shown that the coculture of PHH with primary Kupffer cells does not influence the CYP activity.[65] Consequently, the coculture of PHH with HuLEC and stellate cells in HepaChip-MP is expected to enhance CYP activity even in future long term cultures.

Our experiments of CYP induction demonstrate that the HepaChip-MP allows quantification of physiological liver cell function and enzyme activity despite the relatively low cell count per chamber. This enables the efficient use of primary cells which are costly and have limited availability. Analysis of cell behavior using the HepaChip-MP nevertheless requires sufficiently sensitive assays.

When compared to 3D spheroids, HepaChip-MP cultures showed similar basal CYP2C9 activity. In contrast to a report by Foster *et al.* that basal CYP2C9 activity in spheroids was more than 20 times higher than in a microfluidic liver model with hepatocytes and non-parenchymal cells.[66] To this end, the potential influence of non-parenchymal cells on metabolic activity remains to be evaluated in the HepaChip-MP as well as in our spheroid model. We observed basal CYP3A4 activity approximately 25 times higher in spheroids than in HepaChip-MP cultures. Foster *et al.* observed 60-times-higher CYP3A4 activity in spheroids compared to a microfluidic liver model.[66] These findings stand in contrast to results of Vinci *et al.* who found an upregulation of CYP expression as well as CYP activity of CYP2C9, CYP3A4, and other CYP enzymes under flow conditions.[67] However, Vinci *et al.* only evaluated the influence of medium flow on the cells. They used exactly the same culture conditions (seeding, plates, model system) whereas Foster *et al.* and the present study investigated two different model systems (3D spheroid and microfluidic chip). In spheroids and microfluidic liver models, cell assembly and microenvironment around the cells also differ, which may explain the differences between the cited reports.

Assessment of cell vitality after drug treatment

Feasibility of measuring cell vitality after drug treatment using HepaChip-MP was demonstrated with a resazurin (alamarBlue) assay (Fig. 6). Using cells from a single donor yielded a dose–response curve of cell vitality after treatment with diclofenac. While low vitality at high concentrations (1500 μM) was observed, cells showed an increased vitality at intermediate concentrations (150 and 450 μM).

At high concentrations, diclofenac induces oxidative stress leading to cell damage and death.[68,69] However, non-monotonic dose–response curves in resazurin assays can result from changed NADPH production rates. Cells attempt to counteract oxidative stress with reduced glutathione (GSH), the regeneration of which requires NADPH.[70] NADPH produced to regenerate GSH also reduces resazurine. This can lead to apparent vitality above 100% as seen with 150 and 450 μM diclofenac.

While this interference is undesirable, an advantage of the resazurin assay is that it may be carried out at multiple time points during culturing. Such results can be complemented by end-point viability assays.

Manufacturing and availability of organ-on-chip systems

Adoption of organ-on-chip systems requires scalable fabrication and the availability of devices for validation of results. Microinjection molding enables mass production of devices with consistent properties, in comparison with methods based on soft lithography or photolithography. Use of COP achieves good optical properties and low substance adsorption, as shown by a panel of hydrophobic drugs (Fig. S6†).

Future research will investigate the predictivity of the HepaChip-MP with comprehensive tests of substances with known effects. Also, we will attempt to establish and measure the oxygen gradient inside the culture chambers and assess a zonation[24–26,37–39] of protein expression. Further, the influence of endothelial or stellate cells on hepatocyte function will be analyzed in cocultures. Finally, the optimization of medium composition to attain long-term stable cultures and the establishment of disease models will be undertaken.

Conclusions

We have designed, fabricated and evaluated a microfluidic model of the liver in a parallelized and scalable format. Towards industrial relevance, we focused on injection molding of COP microfluidics in the ANSI/SBS microplate format. The formation of functional structures resembling liver sinusoids demonstrated the successful active assembly of cocultures in 3D culture chambers. Evaluation of physiological function confirmed both the vitality and specific enzyme activity of sinusoidal structures as well as the compatibility of this microfluidic model with established cell-based assays. The HepaChip-MP has significant potential as an *in vitro* liver model, and furthermore presents a new technological approach to create organ-on-a-chip models of additional organ systems.

Author contributions

M. S., H. B., R. G. conceived the concept of HepaChip-MP. H. B., J. S. developed chip fabrication technology. B. H. performed multiphysics simulation and fluidic design. S. W. contributed to chip design and periphery instrumentation. M. P. contributed to the multiwellplate design of the chip. M. Bu., O. T., J. S., M. Be. conducted cell culture experiments with Hepachip-MP. S. B., T. K. performed LC/MS analysis of samples. K. G., R. H. developed the automated pipetting system. A. U., J. M., and D. R. developed and evaluated a spheroid model and conducted benchmarking experiments and contributed to discussion and manuscript writing. G. D., M. M. provided human hepatocytes and non-parenchymal cells. M. S., R. G., C. S., N. G., K. S. guided research. M. S., M. Bu, P. J., C. S. wrote the manuscript.

Conflicts of interest

H. B. is CSO of microfluidic ChipShop GmbH, which developed HepaChip-MP jointly with NMI and currently manufactures these devices. M. S., J. S., B. H., and S. W. are inventors in patents covering HepaChip-MP technology.

Acknowledgements

We thank Prof. Dr. med Daniel Seehofer and his team of the Department of Hepatobiliary Surgery and Visceral Transplantation, Leipzig University for liver tissue samples. Funding for this research provided (in part) by the German ministry for education and research (BMBF) through grants no. 01GG0729, 031A121, 031B0481 is gratefully acknowledged.

References

1 M. D. Leise, J. J. Poterucha and J. A. Talwalkar, Drug-induced liver injury, *Mayo Clin. Proc.*, 2014, **89**(1), 95–106.
2 R. Kostadinova, *et al.*, A long-term three dimensional liver co-culture system for improved prediction of clinically relevant drug-induced hepatotoxicity, *Toxicol. Appl. Pharmacol.*, 2013, **268**(1), 1–16.
3 M. Chen, J. Borlak and W. Tong, High lipophilicity and high daily dose of oral medications are associated with significant risk for drug-induced liver injury, *Hepatology*, 2013, **58**(1), 388–396.
4 N. Kaplowitz, Avoiding idiosyncratic DILI: Two is better than one, *Hepatology*, 2013, **58**(1), 15–17.
5 S. Babai, L. Auclert and H. Le-Louët, Safety data and withdrawal of hepatotoxic drugs, *Therapie*, 2018, DOI: 10.1016/j.therap.2018.02.004, in press.
6 L. Kuna, *et al.*, Models of Drug Induced Liver Injury (DILI) - Current Issues and Future Perspectives, *Curr. Drug Metab.*, 2018, **19**(10), 830–838.
7 V. Y. Soldatow, *et al.*, In vitro models for liver toxicity testing, *Toxicol. Res.*, 2013, **2**(1), 23–39.
8 A. R. Baudy, *et al.*, Liver microphysiological systems development guidelines for safety risk assessment in the pharmaceutical industry, *Lab Chip*, 2020, **20**(2), 215–225.
9 K. Tetsuka, M. Ohbuchi and K. Tabata, Recent Progress in Hepatocyte Culture Models and Their Application to the Assessment of Drug Metabolism, Transport, and Toxicity in Drug Discovery: The Value of Tissue Engineering for the Successful Development of a Microphysiological System, *J. Pharm. Sci.*, 2017, **106**(9), 2302–2311.
10 A. Poloznikov, *et al.*, In vitro and in silico liver models: Current trends, challenges and opportunities, *ALTEX*, 2018, **35**(3), 397–412.
11 S. R. Khetani and S. N. Bhatia, Microscale culture of human liver cells for drug development, *Nat. Biotechnol.*, 2008, **26**(1), 120–126.
12 J.-B. Ferrini, *et al.*, Long-term primary cultures of adult human hepatocytes, *Chem.-Biol. Interact.*, 1997, **107**, 31–45.
13 A. Ullrich, *et al.*, Long term cultures of primary human hepatocytes as an alternative to drug testing in animals, *ALTEX*, 2009, **26**(4/09), 295–302.
14 D. R. Berger, *et al.*, Enhancing the functional maturity of induced pluripotent stem cell-derived human hepatocytes by controlled presentation of cell-cell interactions in vitro, *Hepatology*, 2015, **61**(4), 1370–1381.
15 S. March, *et al.*, Micropatterned coculture of primary human hepatocytes and supportive cells for the study of hepatotropic pathogens, *Nat. Protoc.*, 2015, **10**(12), 2027–2053.
16 M. Zhou, *et al.*, Long-term maintenance of human fetal hepatocytes and prolonged susceptibility to HBV infection by co-culture with non-parenchymal cells, *J. Virol. Methods*, 2014, **195**, 185–193.
17 C. C. Bell, *et al.*, Characterization of primary human hepatocyte spheroids as a model system for drug-induced liver injury, liver function and disease, *Sci. Rep.*, 2016, **6**, 25187.
18 Y. Edling, *et al.*, Increased sensitivity for troglitazone-induced cytotoxicity using a human in vitro co-culture model, *Toxicol. In Vitro*, 2009, **23**(7), 1387–1395.
19 W. R. Proctor, *et al.*, Utility of spherical human liver microtissues for prediction of clinical drug-induced liver injury, *Arch. Toxicol.*, 2017, **91**(8), 2849–2863.
20 V. M. Lauschke, *et al.*, Novel 3D Culture Systems for Studies of Human Liver Function and Assessments of the Hepatotoxicity of Drugs and Drug Candidates, *Chem. Res. Toxicol.*, 2016, **29**(12), 1936–1955.
21 J. Deng, *et al.*, Engineered Liver-on-a-Chip Platform to Mimic Liver Functions and Its Biomedical Applications: A Review, *Micromachines*, 2019, **10**(10), 676.
22 J. H. Lee, K. L. Ho and S. K. Fan, Liver microsystems in vitro for drug response, *J. Biomed. Sci.*, 2019, **26**(1), 88.
23 A. Dash, *et al.*, Hemodynamic flow improves rat hepatocyte morphology, function, and metabolic activity in vitro, *Am. J. Physiol., Cell Physiol.*, 2013, **304**(11), C1053–C1063.
24 F. T. Lee-Montiel, *et al.*, Control of oxygen tension recapitulates zone-specific functions in human liver microphysiology systems, *Exp. Biol. Med.*, 2017, **242**(16), 1617–1632.

25 J. W. Allen and S. N. Bhatia, Formation of steady-state oxygen gradients in vitro: application to liver zonation, *Biotechnol. Bioeng.*, 2003, **82**(3), 253–262.
26 J. Hellkamp, *et al.*, Modulation by oxygen of the glucagon-dependent activation of the phosphoenolpyruvate carboxykinase gene in rat hepatocyte cultures, *Eur. J. Biochem.*, 1991, **198**, 635–639.
27 L. Prodanov, *et al.*, Long-term maintenance of a microfluidic 3D human liver sinusoid, *Biotechnol. Bioeng.*, 2016, **113**(1), 241–246.
28 Y. B. Kang, *et al.*, Liver sinusoid on a chip: Long-term layered co-culture of primary rat hepatocytes and endothelial cells in microfluidic platforms, *Biotechnol. Bioeng.*, 2015, **112**(12), 2571–2582.
29 M. Yamada, *et al.*, Controlled formation of heterotypic hepatic micro-organoids in anisotropic hydrogel microfibers for long-term preservation of liver-specific functions, *Biomaterials*, 2012, **33**(33), 8304–8315.
30 L. Vernetti, *et al.*, Functional Coupling of Human Microphysiology Systems: Intestine, Liver, Kidney Proximal Tubule, Blood-Brain Barrier and Skeletal Muscle, *Sci. Rep.*, 2017, **7**, 42296.
31 R. Baudoin, *et al.*, Evaluation of a liver microfluidic biochip to predict in vivo clearances of seven drugs in rats, *J. Pharm. Sci.*, 2014, **103**(2), 706–718.
32 J. M. Prot, *et al.*, A cocktail of metabolic probes demonstrates the relevance of primary human hepatocyte cultures in a microfluidic biochip for pharmaceutical drug screening, *Int. J. Pharm.*, 2011, **408**(1–2), 67–75.
33 C. Ma, *et al.*, On-Chip Construction of Liver Lobule-like Microtissue and Its Application for Adverse Drug Reaction Assay, *Anal. Chem.*, 2016, **88**(3), 1719–1727.
34 E. Novik, *et al.*, A microfluidic hepatic coculture platform for cell-based drug metabolism studies, *Biochem. Pharmacol.*, 2010, **79**(7), 1036–1044.
35 K. J. Jang, *et al.*, Redproducing human and cross-species drug toxicities using a Liver-Chip, *Sci. Transl. Med.*, 2019, **11**, eaax5516.
36 R. Gebhardt and D. Mecke, Permissive Effect of Dexamethasone on Glucagon Induction of urea-cycle enzymes in perifused, *Eur. J. Biochem.*, 1978, **97**, 6.
37 P. P. C. Poyck, *et al.*, Expression of Glutamine Synthetase and Carbamoylphosphate Synthetase I in a Bioartificial Liver: Markers for the Development of Zonation in vitro, *Cells Tissues Organs*, 2008, **188**(3), 259–269.
38 W. J. McCarty, O. B. Usta and M. L. Yarmush, A Microfabricated Platform for Generating Physiologically-Relevant Hepatocyte Zonation, *Sci. Rep.*, 2016, **6**, 26868.
39 Y. B. A. Kang, *et al.*, Metabolic Patterning on a Chip: Towards in vitro Liver Zonation of Primary Rat and Human Hepatocytes, *Sci. Rep.*, 2018, **8**(1), 8951.
40 A. Junaid, *et al.*, An end-user perspective on Organ-on-a-Chip: Assays and usability aspects, *Curr. Opin. Biomed. Eng.*, 2017, **1**, 15–22.
41 J. Y. Kim, *et al.*, 96-well format-based microfluidic platform for parallel interconnection of multiple multicellular spheroids, *J. Lab. Autom.*, 2015, **20**(3), 274–282.
42 M. Jang, *et al.*, Differentiation of the human liver progenitor cell line (HepaRG) on a microfluidic-based biochip, *J. Tissue Eng. Regener. Med.*, 2019, **13**(3), 482–494.
43 K. Domansky, *et al.*, Perfused multiwell plate for 3D liver tissue engineering, *Lab Chip*, 2010, **10**(1), 51–58.
44 N. Li, M. Schwartz and C. Ionescu-Zanetti, PDMS compound adsorption in context, *J. Biomol. Screening*, 2009, **14**(2), 9.
45 M. W. Toepke and D. J. Beebe, PDMS absorption of small molecules and consequences in microfluidic applications, *Lab Chip*, 2006, **6**(12), 1484–1486.
46 B. J. van Meer, *et al.*, Small molecule absorption by PDMS in the context of drug response bioassays, *Biochem. Biophys. Res. Commun.*, 2017, **482**(2), 323–328.
47 J. Schütte, *et al.*, A method for patterned in situ biofunctionalization in injection-molded microfluidic devices, *Lab Chip*, 2010, **10**, 2551–2558.
48 F. Holzner, *et al.*, Numerical modelling and measurement of cell trajectories in 3-D under the influence of dielectrophoretic and hydrodynamic forces, *Electrophoresis*, 2011, **32**(17), 2366–2376.
49 B. Hagmeyer, *et al.*, Tailoring microfluidic systems for organ-like cell culture applications using multiphysics simulations, *Proc. SPIE*, 2013, **8615**, DOI: 10.1117/12.2002475.
50 V. Kegel, *et al.*, Protocol for Isolation of Primary Human Hepatocytes and Corresponding Major Populations of Non-parenchymal Liver Cells, *J. Visualized Exp.*, 2016, **109**, e53069.
51 S. J. Fey and K. Wrzesinski, Determination of drug toxicity using 3D spheroids constructed from an immortal human hepatocyte cell line, *Toxicol. Sci.*, 2012, **127**(2), 403–411.
52 H. F. Teutsch, The modular microarchitecture of human liver, *Hepatology*, 2005, **42**(2), 317–325.
53 B. Hagmeyer, F. Zechnall and M. Stelzle, Towards plug and play filling of microfluidic devices by utilizing networks of capillary stop valves, *Biomicrofluidics*, 2014, **8**(5), 056501.
54 C. J. Ochs, *et al.*, Oxygen levels in thermoplastic microfluidic devices during cell culture, *Lab Chip*, 2014, **14**(3), 459–462.
55 A. P. Schmeisch, *et al.*, Zonation of the metabolic action of vasopressin in the bivascularly perfused rat liver, *Regul. Pept.*, 2005, **129**(1), 233–243.
56 R. E. McClelland, J. M. MacDonald and R. N. Coger, Modeling O2 transport within engineered hepatic devices, *Biotechnol. Bioeng.*, 2003, **82**(1), 12–27.
57 R. D. Guarino, *et al.*, Method for determining oxygen consumption rates of static cultures from microplate measurements of pericellular dissolved oxygen concentration, *Biotechnol. Bioeng.*, 2004, **86**(7), 775–787.
58 J. Poisson, *et al.*, Liver sinusoidal endothelial cells: Physiology and role in liver diseases, *J. Hepatol.*, 2017, **66**(1), 212–227.
59 E. Pfeiffer, *et al.*, Featured Article: Isolation, characterization, and cultivation of human hepatocytes and non-parenchymal liver cells, *Exp. Biol. Med.*, 2015, **240**(5), 645–656.
60 I. Maschmeyer, *et al.*, A four-organ-chip for interconnected long-term co-culture of human intestine, liver, skin and kidney equivalents, *Lab Chip*, 2015, **15**(12), 2688–2699.

61 K. M. Olsavsky Goyak, E. M. Laurenzana and C. J. Omiecinski, Hepatocyte differentiation, *Methods Mol. Biol.*, 2010, **640**, 115–138.
62 K. Zeilinger, *et al.*, Three-dimensional Co-culture of primary human liver cells in bioreactors for in vitro drug studies: Effects of the initial cell quality on the long-term maintenance of hepatocyte-specific functions, *Altern. Lab. Anim.*, 2002, **30**, 525–538.
63 K. Zeilinger, *et al.*, Scaling down of a clinical three-dimensional perfusion multicompartment hollow fiber liver bioreactor developed for extracorporeal liver support to an analytical scale device useful for hepatic pharmacological in vitro studies, *Tissue Eng., Part C*, 2011, **17**(5), 549–556.
64 D. G. Nguyen, *et al.*, Bioprinted 3D Primary Liver Tissues Allow Assessment of Organ-Level Response to Clinical Drug Induced Toxicity In Vitro, *PLoS One*, 2016, **11**(7), e0158674.
65 T. V. Nguyen, *et al.*, Establishment of a hepatocyte-kupffer cell coculture model for assessment of proinflammatory cytokine effects on metabolizing enzymes and drug transporters, *Drug Metab. Dispos.*, 2015, **43**(5), 774–785.
66 A. J. Foster, *et al.*, Integrated in vitro models for hepatic safety and metabolism: evaluation of a human Liver-Chip and liver spheroid, *Arch. Toxicol.*, 2019, **93**(4), 1021–1037.
67 B. Vinci, *et al.*, Modular bioreactor for primary human hepatocyte culture: medium flow stimulates expression and activity of detoxification genes, *Biotechnol. J.*, 2011, **6**(5), 554–564.
68 C. Haritha, *et al.*, Oxidative Stress Induced by Diclofenac Alone and under the Influence of Certain Variables in Broilers, *Toxicol. Int.*, 2010, **17**(1), 27–29.
69 H. Li, *et al.*, Cyclooxygenase 2-selective and nonselective nonsteroidal anti-inflammatory drugs induce oxidative stress by up-regulating vascular NADPH oxidases, *J. Pharmacol. Exp. Ther.*, 2008, **326**(3), 745–753.
70 J. Pizzorno, Glutathione!, *Integr. Med.*, 2014, **13**(1), 8–12.

Appendix III: Busche M, et al., Continous, non-invasive monitoring of oxygen consumption in a parallelized microfluidic in vitro system provides novel insight into the response to nutrients and drugs of primary human hepatocytes. EXCLI J, 2022; 21: 144–161. doi: 10.17179/excli2021-4351

EXCLI Journal 2022;21:144-161 – ISSN 1611-2156
Received: September 29, 2021, accepted: November 29, 2021, published: January 07, 2022

Original article:

CONTINUOUS, NON-INVASIVE MONITORING OF OXYGEN CONSUMPTION IN A PARALLELIZED MICROFLUIDIC *IN VITRO* SYSTEM PROVIDES NOVEL INSIGHT INTO THE RESPONSE TO NUTRIENTS AND DRUGS OF PRIMARY HUMAN HEPATOCYTES

Marius Busche[1,*], Dominik Rabl[2], Jan Fischer[3], Christian Schmees[1], Torsten Mayr[2,3], Rolf Gebhardt[4,5], Martin Stelzle[1,*]

[1] NMI Natural and Medical Sciences Institute at the University of Tübingen, Reutlingen, Germany
[2] Institute of Analytical Chemistry and Food Chemistry, Graz University of Technology, Graz, Austria
[3] PyroScience AT GmbH, Aachen, Germany
[4] Rudolf-Schönheimer-Institute of Biochemistry, Leipzig University, Leipzig, Germany
[5] InViSys-Tübingen GbR, Leipzig, Germany

* **Corresponding authors:** Marius Busche and Martin Stelzle, NMI Natural and Medical Sciences Institute at the University of Tübingen, Markwiesenstraße 55, 72770 Reutlingen, Germany, Tel.: +49 7121 51530-0;
E-mails: marius.busche@nmi.de; martin.stelzle@nmi.de

https://dx.doi.org/10.17179/excli2021-4351

ABSTRACT

Oxygen plays a fundamental role in cellular energy metabolism, differentiation and cell biology in general. Consequently, *in vitro* oxygen sensing can be used to assess cell vitality and detect specific mechanisms of toxicity. In 2D *in vitro* models currently used, the oxygen supply provided by diffusion is generally too low, especially for cells having a high oxygen demand. In organ-on-chip systems, a more physiologic oxygen supply can be generated by establishing unidirectional perfusion. We established oxygen sensors *in* an easy-to-use and parallelized organ-on-chip system. We demonstrated the applicability of this system by analyzing the influence of fructose (40 mM, 80 mM), ammonium chloride (100 mM) and Na-diclofenac (50 µM, 150 µM, 450 µM, 1500 µM) on primary human hepatocytes (PHH). Fructose treatment for two hours showed an immediate drop of oxygen consumption (OC) with subsequent increase to nearly initial levels. Treatment with 80 mM glucose, 20 mM lactate or 20 mM glycerol did not result in any changes in OC which demonstrates a specific effect of fructose. Application of ammonium chloride for two hours did not show any immediate effects on OC, but qualitatively changed the cellular response to FCCP treatment. Na-diclofenac treatment for 24 hours led to a decrease of the maximal respiration and reserve capacity. We also demonstrated the stability of our system by repeatedly treating cells with 40 mM fructose, which led to similar cell responses on the same day as well as on subsequent days. In conclusion, our system enables in depth analysis of cellular respiration after substrate treatment in an unidirectional perfused organ-on-chip system.

Keywords: Liver, organ-on-chip, perfusion, oxygen, sensors, *in vitro*, model, toxicity, metabolism

EXCLI Journal 2022;21:144-161 – ISSN 1611-2156
Received: September 29, 2021, accepted: November 29, 2021, published: January 07, 2022

INTRODUCTION

Hepatocytes exhibit a high demand for oxygen despite their prevalent supply by venous blood from the gut. In static cell cultures, however, oxygen supply provided by diffusion is generally too low (Scheidecker et al., 2020; Stevens, 1965) leading to suboptimal metabolic rates. On the other hand, cultivation at low oxygen (5 %) concentration can reduce dedifferentiation of primary mouse hepatocytes in vitro when compared to cultures maintained at 21 % oxygen tension (Guo et al., 2017). Hyperoxia, however, was shown to support the differentiation status of hepatocyte cell lines such as HepaRG and C3A as evident from measurements of CYP activity and protein expression (van Wenum et al., 2018). Ast et al. expect culturing cells at physiological oxygen concentration to yield a more robust cellular model and improve *in vitro in vivo* correlation (Ast and Mootha, 2019).

Thus, the integration of oxygen sensing in microphysiological systems might serve in generating a more physiological microenvironment and provide insight into oxygen-dependent cell function. As cellular respiration also is an important marker for cell viability, oxygen sensing can be used to assess the influence of drugs or toxic agents on mitochondrial function (Hynes et al., 2003; O'Riordan et al., 2000). Drug-induced mitochondrial dysfunction is a major cause for liver pathophysiology (Degli Esposti et al., 2012) and can be determined by measuring respiration (Hynes et al., 2006).

Two commercialized benchmark systems to measure respiration rates in *in vitro* systems are the MitoXpress platform and the seahorse XF analyser (Ferrick et al., 2008; Hynes et al., 2009), both from Agilent (Santa Clara, CA, United States). The MitoXpress platform uses standard 96-wellplates with dispensed oxygen sensitive probes (Hynes et al., 2009). The wells are sealed with oil and can be read out by a fluorescence plate reader. This system does not easily enable consecutive treatments and lipophilic substances in the medium can be lost to the oil phase. However, the seahorse XF platform uses customized 96-wellplates which can be sealed by a plunger and enables up to 4 automated consecutive substance injections during continuous measurement (Ferrick et al., 2008). But still, this system does not implement perfusion and continuous medium exchange. This hinders the building of more *in vivo*-like biochemical microenvironments and gradients.

Oxygen supply to cell cultures can be controlled and monitored by employing microfluidic cell culture devices (for a review, see Low et al., 2020). By using materials that are impermeable to oxygen, its supply to the cells by diffusion through the walls of the device can be prevented (Zirath et al., 2018). Thus, oxygen is provided solely through medium perfusion and can be precisely adjusted by controlling the perfusion rate. Under these conditions, the oxygen concentration inside the cell chamber only depends on the initial oxygen concentration at the inlet of the chamber, the oxygen consumption (OC) of the cells and the flow rate. The medium supplied through medium reservoirs will equilibrate its oxygen concentration with the incubator atmosphere. Thus, by measuring the oxygen concentration at the inlet and the outlet of the cell culture chamber, the OC of the cultured cells can be precisely determined. OC has already been measured in microfluidic cell culture devices demonstrating expected cell responses on e.g. cytochalasin B, chloracetaldehyde (Brischwein et al., 2003), stausporine (Rennert et al., 2015) and FCCP (Müller et al., 2021). These systems mostly require complex tubing which renders handling tedious. To enable a broad adoption of microfluidic systems with integrated oxygen sensing methods, convenient systems are needed. These systems should keep up unidirectional perfusion during the measurement to preserve the equilibrium of the cellular microenvironment.

Currently, the readout systems used for oxygen concentration in microfluidic cell culture devices employ either electrochemical or optical oxygen sensors. Electrochemical sensors benefit from their straightforward inte-

EXCLI Journal 2022;21:144-161 – ISSN 1611-2156
Received: September 29, 2021, accepted: November 29, 2021, published: January 07, 2022

gration of miniaturized electrodes in microfluidic systems by processes established in microelectronics (Brischwein et al., 2003). Newer approaches make use of ink-jet printing techniques (Moya et al., 2018). The sensing element of optical oxygen sensors is composed of a phosphorescent dye embedded in a host polymer (for review see Papkovsky and Dmitriev, 2013). Oxygen quenches the phosphorescence of the dye causing a change in the intensity and lifetime of the excited state. In contrast to electrochemical sensors, optical oxygen sensors do not consume the analyte during the measurement and do not require an additional reference element. Optical sensing elements can be read-out contactless via optical fibers from the outside through the wall of the microfluidic cell culture chamber. For detailed reviews of oxygen sensors and their integration in cell culture devices, the reader is referred to the following authors (Gruber et al., 2017; Kieninger et al., 2018; Oomen et al., 2016; Ungerböck and Mayr, 2018).

Recently, we have developed an easy-to-use organ-on-chip system in the SBS-standard well plate format with 24 independent cell culture chambers for permanent perfusion with culture medium – the HepaChip-MP (Busche et al., 2020). In the present work, we demonstrate the non-invasive, continuous and parallelized measurement of the OC of primary human hepatocytes (PHH) after being challenged by diverse metabolic substrates and drugs. This was enabled by integrating oxygen sensing elements at the inlet and the outlet of each chamber, respectively. Unidirectional perfusion of medium results in constant substance supply in the cellular microenvironment. We demonstrate the applicability of our system by analyzing the response of cellular OC to the application of glucose and fructose as well as ammonium chloride and the drug diclofenac. PHH showed an immediate drop of OC after fructose treatment. This effect was not observed after treatment with glucose. Through in depth analysis of mitochondrial respiration after substance treatment, our system also enables insights into the mode of action of ammonium chloride and diclofenac toxicity.

MATERIAL AND METHODS

Integration of sensors in HepaChip-MP

Phosphorescent sensor spots were prepared by applying a sensor formulation with a microdispenser MDS3200+ from VERMES Microdispensing GmbH, equipped with a 70 µm nozzle and a tungsten tappet with a tip diameter of 0.7 mm onto polymeric substrate. The microdispenser was mounted on a custom-made CNC platform, which was controlled via Linux CNC and allowed exact positioning of the sensor spots. The sensor formulation consists of 1.12 mg of platinum(II)meso-tetra(4-fluorophenyl) tetrabenzoporphyrin (PtTPTBPF) and 100 mg polystyrene (PS, 26000 g/mol) dissolved in 900 mg in toluol.

Priming of chip and seeding of cells

All steps, which are not stated as "manually" were performed with a pipetting robot (CyBio FeliX, Analytik Jena, Jena, Germany) modified by Ionovation (Bissendorf, Germany). The priming and handling of the HepaChip-MP (Microfluidic ChipShop, Jena, Germany) has already been described in detail in Busche et al. (2020). Briefly, the chambers were filled with 1 mg/ml Pluronic solution in HEPES buffer (pH 7.4). Afterwards, the chip was flushed with Collagen-Pluronic solution (100 µg/ml Collagen, 1 mg/ml Pluronic) in HEPES buffer (pH 4). The inlet tanks were filled manually with 500 µl Collagen-Pluronic solution and the chip was incubated overnight at room temperature to ensure coating of the assembly ridges. On the next day, the Collagen-Pluronic solution was manually removed from the inlet and outlet tanks. Dielectrophoresis (DEP) medium was flushed through the chambers and subsequently, the cells were assembled. Cells were manually prepared as described in 'Cell preparation for seeding inside the HepaChip-MP' and assembled by dielectrophoresis (V_{pp} = 80 V, f = 360 kHz). Afterwards, cell culture medium was flushed through the chambers and

the inlet tanks were manually filled with 500 µl cell culture medium. After 6 hours, perfused medium and cells were removed and the inlet tank filled up to approximately 900 µl. Cells were used for experiments on days 2 and 3 of culture.

Cell preparation for seeding inside the HepaChip-MP

Cryopreserved primary human hepatocytes were purchased from Cytes Biotechnologies (Barcelona, Spain) (Donors BHuf16068 and BHuf16029). For thawing, cryopreserved cells were kept in a water bath at 37 °C until only a small frozen area was left. Then, cells were transferred to a 15 ml centrifugation tube filled with 7 ml preheated cell culture medium. Cell culture medium was Williams E with glutamax supplemented with the following: 10 % FBS, 15 mM HEPES, 1 mM sodium pyruvate, 1 % MEM non-essential amino acids, 1 µg/ml dexamethasone, 1 µg/ml insulin, 0.55 g/ml human transferrin, 0.5 ng/ml sodium selene, 53.5 mg/ml linoleic acid, 100 µg/ml Primocin. The transferred cells were centrifuged at 50 x g at room temperature for 5 minutes and the supernatant was removed. Afterwards, the cell pellet was resuspended in cell culture medium. Cell number and viability were determined by trypan blue exclusion test. 4 Mio hepatocytes were transferred to another 15 ml centrifugation tube and DEP medium was added to a final volume of 10 ml. Afterwards, cells were centrifuged at 50 x g at room temperature for 5 minutes. The supernatant was removed and the cell pellet resuspended in 2 ml DEP medium. This cell suspension was used to assemble the cells in the HepaChip-MP.

Routine culture

The perfusion in the HepaChip-MP is initiated by gravity. By filling the inlet tank to a higher level than the outlet tank, the medium perfuses from the inlet tank through the cell culture chamber to the outlet tank (Supplementary Figure 1). Consequently, the height difference between medium level in inlet and outlet had to be periodically readjusted during routine culture. Between readjustments, the flow velocity constantly decreases (Supplementary Figure 1). We readjusted the height difference between medium levels in the inlet and outlet tanks at least every 14 hours to ensure flow velocities higher than ~10 µl/h. Medium that is used with the HepaChip-MP in the incubator should always be equilibrated to the temperature and the atmosphere of the incubator to prevent formation of gas bubbles in the microfluidic device.

Oxygen measurements

Calibration

Calibration data for the oxygen sensor spot were similar to those reported in Ehgarnter et al. (2016). The oxygen sensors were calibrated by a two-point calibration. The microfluidic chamber was flushed with gasous N_2 to determine the phase shift (dphi) at deoxygenated conditions. To define the phase shift (dphi) at air saturation, the last value after treatment with rotenone+antimycin A was employed.

Measurement

Experiments were carried out on day two and three after cell assembly. At the beginning of the experiment, the culture medium was removed from the inlet and outlet tanks. Then, the inlet tanks were filled with 900 µl of cell culture medium and the chip was placed on the readout platform in the incubator. Afterwards, the measurement was started.

For substance treatments, the chip was incubated until a baseline was reached before the substance of interest was added. To add the substance, the medium from inlet and outlet tanks was removed and 900 µl of medium supplemented with the substance of interest was added. For successive treatments, the medium with the first substance was removed and the medium with the new substance (or medium only) was filled in the inlet tanks. Substances used, their concentration and incubation time are presented in Table 1.

Table 1: Substances used for treating cells cultured in the HepaChip-MP

Substance	Substance end concentration	Solvent / end concentration	Incubation time	Concentration justification (generally < 200-fold the plasma concentration (Cp) was used (Hengstler et al., 2020))
Fructose	40 mM / 80 mM	none / -	2 / 24 hours	Cp in human and rodents = 0,01 – 16 mM (Douard and Ferraris, 2013)
Glucose	80 mM	none / -	2 hours	Cp = approx. 5.6 mM
Lactate	20 mM	none / -	2 hours	Cp = 1.26 mM (Aduen et al., 1994)
Glycerol	20 mM	none / -	2 hours	Cp = approx. 0.327 mM (Nelson et al., 2011)
Oligomycin A	6 µg/ml	DMSO / 0.3 %	20 – 40 min	Titration carried out based on (Divakaruni et al., 2014)
Carbonyl cyanide-*4*-(trifluoromethoxy)-phenylhydrazone (FCCP)	2400 nM	DMSO / 0.3 %	90 – 100 min	Titration carried out based on (Divakaruni et al., 2014)
Rotenone + Antimycin A (R/A)	3 µM + 6 µM	DMSO / 0.3 %	> 40 min	Titration carried out based on (Divakaruni et al., 2014)
Ammonium chloride	100 mM	none / -	2 hours	Portal vein concentration in vivo 0.5-1.0 mM (Cooper et al., 1989)
Na-Diclofenac	50 µM / 150 µM / 450 µM / 1500 µM	none / -	24 hours	Cp = 1.8 µM – 24.2 µM (Davies and Anderson, 1997); hepatic concentrations expected to be higher (first organ after absorption, metabolism in liver)

The oxygen measurements were performed with a customized multi-channel device obtained from PyroScience GmbH (Aachen, Germany). The miniaturized instrument provides 48 optical oxygen channels in a robust aluminium housing with a dimension of ca. 155 x 124 x 30 mm. The device features fiber-optic ST-receptacles that accept 1 mm-core diameter polymer optical fibers for readout of the luminescent sensor spots. The technology is based on the proprietary "red-flash"-Technology used in other PyroScience devices. Each channel consists of a red excitation LED (λ_{peak}=624 nm), a short-pass excitation filter (λ_{cut} = 690 nm), and focusing optics to couple the excitation light into the optical fiber. The luminescent light from the sensor spot travels through the same fiber back to the instrument. A long-pass emission filter (λ_{cut} = 720 nm) blocks all reflected or back-scattered excitation light that reaches the detector directly from the LED. A photodiode captures the luminescence of the sensor spot. The photodiode current is amplified, digitized by an A/D converter, and analyzed by the microcontroller of the device. The LED current is modulated with sinusoidal light, and therefore the emitted light is modulated likewise. Due to the luminescence lifetime of the sensor material, there is a phase shift between excitation and emission light. The luminescence lifetime and therefore the phase shift is quantitatively coupled to the oxygen partial pressure of the sensor by a proprietary, modified version of the Stern-Volmer equation. The instrument reads out the 48 channels sequentially. Depending on the measurement time for each channel, all channels can be measured within an interval < 1 s. A custom LabView-based software is used to control

the instrument, perform calibrations of the sensor spots, and log the measurement data.

Calculations

By calculating the difference between the oxygen concentration between the inlet and outlet sensor and multiplying this value by the perfusion velocity, the oxygen consumption of the cells in this chamber can be determined. The oxygen consumption was then normalized to the equilibrium value before adding the substance of interest (baseline).

Oligomycin A, FCCP and rotenone+antimycin A (R/A) were added to obtain insights into mitochondrial respiration. Calculations were performed as described in Divakaruni et al. (2014). Briefly, the following values were determined:

Basal respiration = (last value prior to application of oligomycin A) – (last value after adding R/A)

Proton leak-linked respiration = (last value prior to treatment with FCCP) – (last value after adding R/A)

ATP-linked respiration = (basal respiration) – (proton leak-linked respiration)

Maximal respiration = (last value prior to treatment with R/A) - (last value after adding R/A)

Reserve capacity = (maximal respiration) – (basal respiration).

For the statistical analyses and graphs, Prism 8.4.2 (GraphPad Software Inc., San Diego, CA, United States) was used. Where significance is depicted, a one-way ANOVA with post hoc Tukey test was performed. Substance treatments were performed at least in triplicates (n=3) if not depicted otherwise in the figure caption.

ATP assay

To analyze the ATP content of cells treated with fructose, an ATP assay was performed (CellTiter-Glo 3D Cell Viability Assay, Promega, Madison, Wisconsin, United States). Non-treated cells were used as negative controls. For treatment and controls, the medium was removed from the inlet and outlet tanks and the inlet tank was filled with 850 µl of either medium supplemented with 40 mM fructose or medium only. After the respective incubation times, the ATP assay was performed using the CyBio FeliX. Briefly, 10 µl of assay reagent was pipetted into the inlet of all cell culture chambers by pressure driven flow. Then, cell lysis was carried out for one hour at room temperature. Afterwards, 99 µl of cell culture medium was pipetted into the outlets by pressure driven flow. Perfused lysate and cell culture medium in the inlet was transferred to a white 96-well plate. The readout was carried out with a Spark multimode reader from Tecan (Männedorf, Switzerland) with 1000 ms integration time.

RESULTS

The optical sensor spots located at the inlet and the outlet of the cell culture chamber, respectively, were deposited into the HepaChip-MP using a microdispenser prior to bonding (Figure 1A-C). The resulting sensor coating is shown in Figure 1C. To align an array of optical fibers with the microplate, an aluminum plate was fabricated with an array of holes to mount optical fibers and tracks to precisely position the HepaChip-MP (Figure 1D, E). The HepaChip-MP can be moved on the platform to enable monitoring of the chambers of interest in a parallel fashion. Up to 24 chambers can be measured simultaneously. The platform is compatible with use in common incubators. The HepaChip-MP can easily be retrieved from the platform and handled like common multiwell plates (Figure 1F).

EXCLI Journal 2022;21:144-161 – ISSN 1611-2156
Received: September 29, 2021, accepted: November 29, 2021, published: January 07, 2022

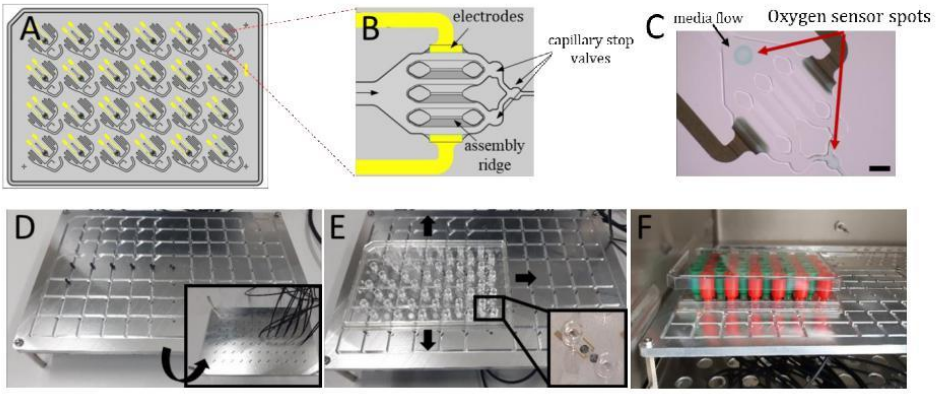

Figure 1: HepaChip-MP with oxygen sensor spots and readout system. **A**) Schematic overview of the HepaChip-MP with 24 independent cell culture chambers in wellplate format. **B**) Individual cell culture chamber of the HepaChip-MP showing electrodes (yellow), capillary stop valves to control bubble free filling and three assembly ridges to culture sinusoid-like micro-tissues. Prior to cell assembly the assembly ridges are functionalized by collagen I. **C**) Microscopic image of cell culture chamber showing the location of the oxygen sensor spots. By measuring oxygen concentration at both the inlet and outlet of the chamber, the oxygen consumption of the microtissue can be determined. **D**) Photo of the readout system: optical fibers illuminating and probing the oxygen sensors are positioned in holes in the bottom plate to address sensor spots in the HepaChip-MP. **E**) The HepaChip-MP is positioned by milled guiding lines to precisely align the oxygen sensor spots with the optical fibers. **F**) The oxygen readout plate is compatible to use in a common incubator. Tanks mounted on the fluidic ports (Luer connectors) of the HepaChip-MP enable continuous perfusion of the cell culture chambers by gravitational driven flow (green: inlet tank; red: outlet tank) (**A** and **B** adapted from Busche et al., 2020).

The OC of PHH was measured for 24 hours in the HepaChip-MP during routine culture. Between medium level adjustments, the OC constantly drops (Figure 2A) as the flow rate decreases. After readjustment of medium levels, the OC immediately rises to higher values again. However, OC does not reach the initial level (Figure 2A). Microscopy images taken at the start and the end of the experiment showed that the cell number during culture time may slightly decrease during cultivation due to occasional detachment of hepatocytes on the ridges of the culture chambers (Figure 2B). Detached hepatocytes may then be flushed out of the chamber. This might explain why the oxygen consumption does not reach the initial levels after readjusting the medium levels. Figure 2C) demonstrates that from day 2 to 3 of the culture, the morphology of assembled cell structures does not change much and cell structures seem to be stable. The following experiments to measure oxygen consumption after substance treatment were carried out at day 2 or 3 of culture. Chambers without cells also were analyzed for comparison to rule out oxygen loss through the culture-ware plastic or other non-cellular effects. These chambers show negligible OC (Supplementary Figure 2).

Since fructose is well known to interfere with ATP metabolism (Latta et al., 2007), we analyzed the impact of fructose on the OC of PHH. The addition of 80 mM fructose to the medium caused a rapid drop of OC to < 50% of the initial value (Figure 3A). Approximately 65 minutes after the onset of fructose treatment, the OC increased again and reached the initial level at 110 minutes. In contrast, incubation with glucose did not cause any change in OC during the 150 minutes of the experiment (Figure 3A). Likewise, lactate and glycerol did not show any effect on OC (Figure 3B).

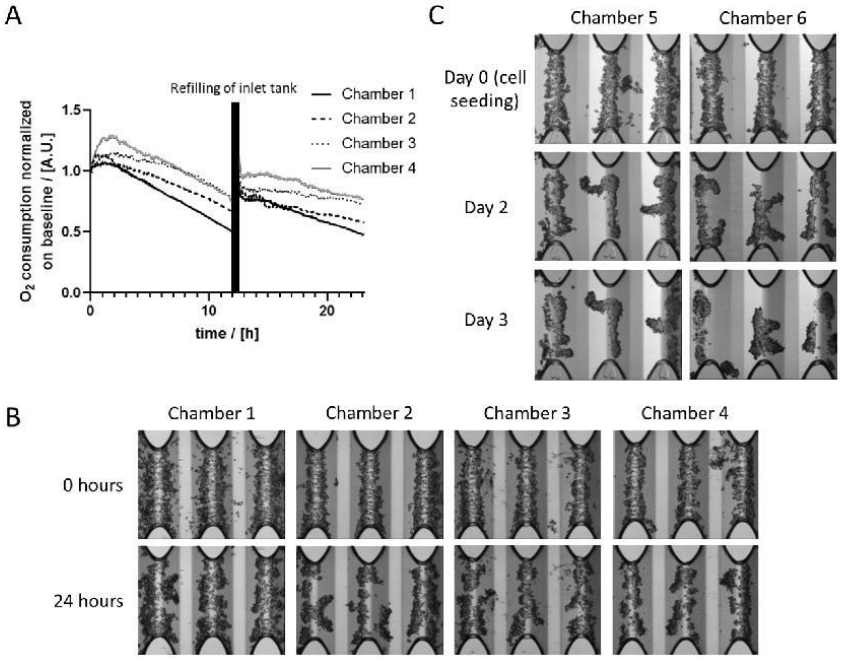

Figure 2: OC of PHH cultured in the HepaChip-MP. **A**) In cell culture chambers containing microtissues, the OC drops over time. After re-adjusting the medium level difference between inlet and outlet after 12 hours, flow rate increases and the OC immediately rises to a higher level. **B**) Microscopic images of the cell culture chambers analyzed in **A**) at the start and the end of the measurement exhibit a slight decrease of cell number. **C**) Representative images of cells cultured in the HepaChip-MP from the day of seeding (day 0) and day 2 and day 3 of culture. Oxygen measurements after substance treatment were carried out at day 2 and day 3 of the culture in this study.

Fructose is known to be taken up and phosphorylated by hepatocytes very fast. We tested the ATP concentration of lysed cells after fructose treatment and compared it to cells cultured in standard culture medium. As expected, the ATP concentration after 20 min of fructose treatment was approx. 30 % of the ATP concentration in control cells (Figure 3C). Even after apparent equilibration of OC close to the initial level, the ATP concentration of fructose-treated PHH remained low. To test the influence of fructose on mitochondrial respiration of PHH, we analyzed PHH pretreated with 40 mM fructose for 2 and 24 hours. We did not detect any significant differences in cell responses to oligomycin A, FCCP and rotenone+antimycin A compared to cells cultivated in medium only after two hours (data not shown) and 24 hours (Supplementary Figure 3) of fructose treatment. Thus, fructose shows a specific effect on OC right after administration, but does not change mitochondrial respiration after longer treatment.

Next, we tested the stability of our system and the cellular regeneration with regard to OC by repeatedly treating PHH cultured in the HepaChip-MP with 40 mM Fructose on DIV (days *in vitro*) 2 and 3, respectively. The response of OC observed was recapitulated after 2 hours of cultivation in medium in between two fructose treatments on DIV 2 as well as on DIV 3 (Figure 4A-B). Furthermore, the relative strength of the response to fructose treatment was on similar levels on DIV 2 and DIV 3.

EXCLI Journal 2022;21:144-161 – ISSN 1611-2156
Received: September 29, 2021, accepted: November 29, 2021, published: January 07, 2022

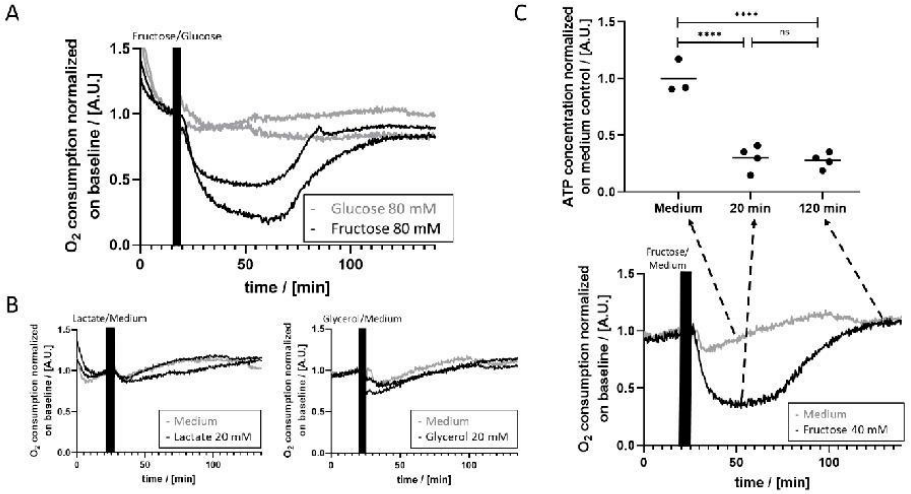

Figure 3: OC and ATP-levels after fructose treatment of PHH. **A**) While OC rapidly decreases to < 50 % of the basal OC in response to fructose treatment and reaches initial levels again after approximately 110 minutes (black graphs), glucose treatment did not substantially affect OC (grey graphs). **B**) Cells were treated with 20 mM lactate (left) and 20 mM glycerol (right). Neither lactate nor glycerol affected OC in comparison to control cells treated with medium only. **C**) The ATP level determined 20 min after the start of the fructose treatment decreased to approximately 30 % of the level of non-treated control cells. Even after reaching close-to-initial levels of cellular OC (illustrated in panel below), the ATP levels did not increase but remained at 30 % of the control cells two hours after the start of the fructose treatment (n = 3 for medium, n = 4 for 20 min and 120 min fructose; significance: **** equals p-values < 0.0001).

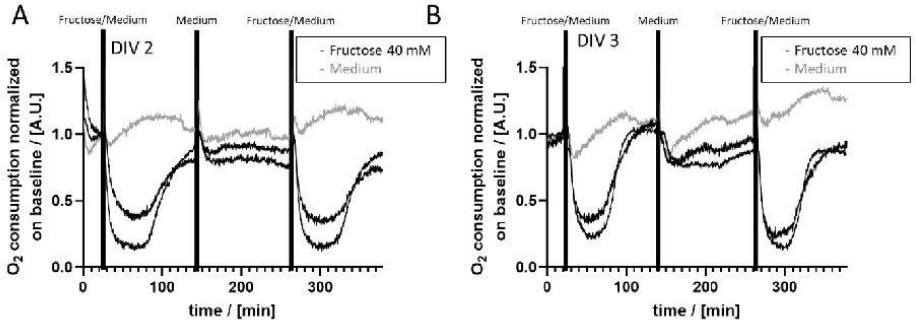

Figure 4: Repeated treatment of hepatocyte cultures by fructose on two consecutive days demonstrates the reproducibility of the effect of fructose on OC. The same cell culture chambers containing PHH were repeatedly treated for 2 hours with 40 mM fructose on DIV (days *in vitro*) 2 (**A**) and DIV 3 (**B**). Fructose treatment reproducibly induced the initial decrease in OC followed by an increase to almost initial levels (black graphs). In addition, the intensity of the relative fructose effect on OC is comparable intra-day as well as inter-day. In order to allow the cells to equilibrate to normal metabolic conditions, cells were cultured in standard culture medium for 2 hours in between fructose treatments. Cells cultured in standard medium, did not show substantial changes in OC (grey graphs).

EXCLI Journal 2022;21:144-161 – ISSN 1611-2156
Received: September 29, 2021, accepted: November 29, 2021, published: January 07, 2022

Further, we went on to modulate different mechanisms contributing to cellular respiration by adding different substances and recording their impact on OC. First, the addition of oligomycin A resulted in a decrease of OC (Figure 5A). Subsequently, incubation with FCCP lead to a rapid increase of OC until reaching a plateau. Finally, after the addition of rotenone+antimycin A (R/A), the OC decreased, reaching a level below the one observed after the addition of oligomycin A. Cells treated with vehicle control (DMSO) did not show any changes in OC (Supplementary Figure 4). Thus, our system shows the expected results on the mentioned substances and can be used to get deeper insights into mitochondrial respiration after substance treatment. As mentioned earlier, fructose for example does initially effect oxygen consumption, but does not induce differences in cell response to oligomycin A, FCCP or R/A treatment (Figure 3, Supplementary Figure 3).

We tested the influence of ammonium chloride on cellular respiration of PHH. Cells either were pretreated for 2 hours with 100 mM ammonium chloride or medium only (negative control). Oligomycin A treatment did not induce any differences between non-treated and pre-treated cells (Figure 5B). Also, the treatment with R/A led to a very similar drop in OC. In contrast, the addition of FCCP yielded differing responses. Pretreated cells showed a sigmoidal-shaped increase of OC while the OC of non-pretreated cells rapidly increased to reach a plateau (Figure 5B).

Finally, we tested the influence of diclofenac as a known hepatotoxic drug on the OC of PHH. Cells pretreated with 50 µM, 150 µM and 450 µM of diclofenac showed the expected trend of OC after treatment with oligomycin A, FCCP and R/A (Figure 6A). However, the cells pretreated with 450 µM diclofenac reached substantially lower levels of OC after FCCP treatment as compared to cells pretreated with lower diclofenac concentrations (Figure 6A, solid line). This observation was confirmed by quantification of the maximal respiration and reserve capacity of diclofenac-treated and control cells. PHH pretreated with 450 µM diclofenac show significant lower values for maximal respiration and reserve capacity (Figure 6B). For basal respiration, proton-leaked respiration and ATP-linked respiration, no significant differences were observed. PHH pretreated with 1500 µM diclofenac do not show any response in OC on treatment which implicates that they are dead (Supplementary Figure 5) as observed previously (Busche et al., 2020).

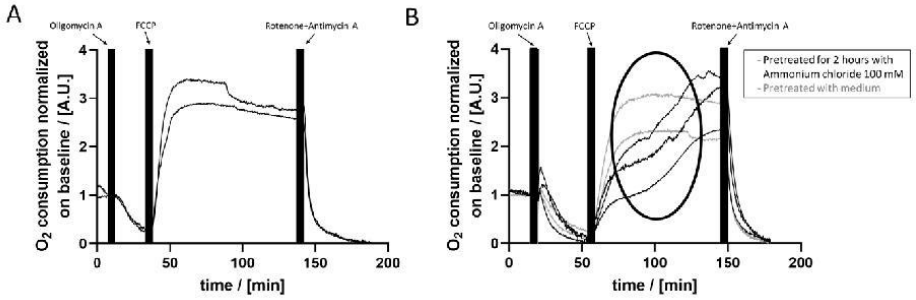

Figure 5: OC of PHH after subsequent application of oligomycin A, FCCP and rotenone+antimycin A (R/A). **A**) Oligomycin A causes a drop to approximately 25 % of the initial OC. FCCP leads to a rapid increase to > 200 % of the OC, while R/A treatment results in a rapid decrease to negligible OC values. **B**) Cells were pretreated for 2 hours with 100 mM ammonium chloride (black graphs) or culture medium (grey graphs). Oligomycin A and R/A caused a similar decrease of the OC for pretreated as well as non-pretreated cells as observed in **A)**. However, while the FCCP treatment caused the expected rapid increase until reaching a plateau for non-pretreated cells, cells pretreated with 100 mM ammonium chloride showed a sigmoidal-like increase of the OC thereafter (pointed out by the black ellipse).

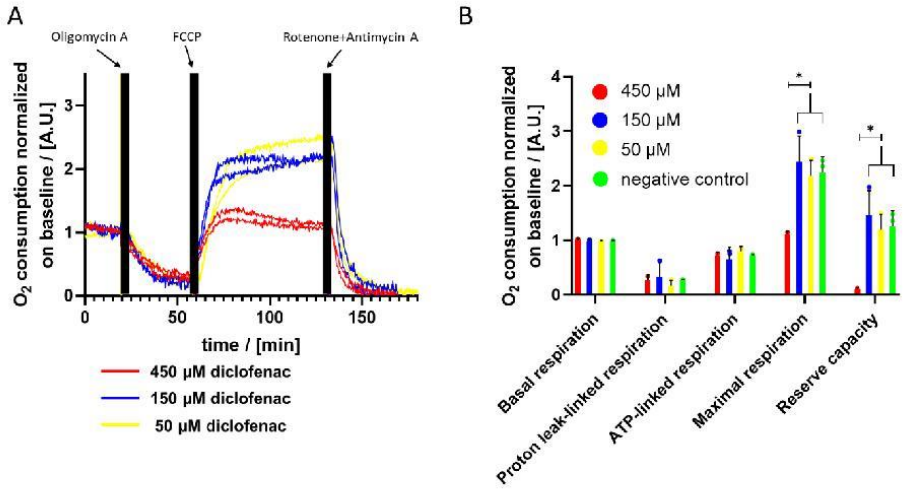

Figure 6: Analysis of the influence of the treatment with different concentrations of diclofenac for 24 hours. **A**) OC after subsequent application of oligomycin A, FCCP and R/A of PHH pretreated with diclofenac. **B**) Detailed analysis of cellular respiration of PHH treated with different concentrations of diclofenac (n=2 for 450 µM diclofenac; n=3 for 150 µM and 50 µM diclofenac; significance: * equals p-values < 0.05).

DISCUSSION

Novel, parallelized readout system for continuous measurement of OC in an organ-on-chip model

Nutrition plays an important role in liver metabolism and influences the metabolic status of hepatocytes (Jorquera et al., 1996; Walter-Sack and Klotz, 1996). Different diets can also influence drug metabolism (Walter-Sack and Klotz, 1996). Altered drug metabolism on the other hand may lead to drug-induced liver injury (DILI), which is accompanied by mitochondrial disfunction (Corsini and Bortolini, 2013; Pessayre et al., 2010). By measuring the cellular oxygen consumption after substance-challenge, conclusions can be drawn concerning the metabolic status of the cell and the function of mitochondria. Hence, measurement of oxygen consumption is very useful to gain deeper insights into effects of various nutrients and drugs on the liver.

In this work, we introduce a novel platform to analyze the effect of substances on OC and respiration. Optical oxygen sensors were integrated in the previously described HepaChip-MP enabling parallelized readouts (Busche et al., 2020). The sensor platform is compatible for use in common incubators thus enabling continuous monitoring of OC without interference with the cell culture. The HepaChip-MP is developed in the SBS-standard 96-well plate format and can be easily integrated into common cell culture workflows. Unidirectional perfusion results in continuous substance supply at the cells representing a more realistic substance exposure than observed in static cell culture systems for most applications. Cell response to fructose treatment demonstrated stability and robustness as well as intraday and interday reproducibility of OC measurements (Figure 4). When compared to the benchmark systems MitoXpress and the seahorse XF analyser (Ferrick et al., 2008; Hynes et al., 2009) the system presented here adds perfusion and thus, a more *in vivo*-like supply of oxygen. In addition, medium and test substances can easily be exchanged during the continuous measurement,

EXCLI Journal 2022;21:144-161 – ISSN 1611-2156
Received: September 29, 2021, accepted: November 29, 2021, published: January 07, 2022

which enables numerous consecutive treatments and versatile treatment schemes (see Table 2). In contrast to electrochemical oxygen sensors (used by e.g. Moya et al., 2018; Weltin et al., 2017), optical sensors do not consume oxygen. The consumption of oxygen by the sensors would lead to erroneous results in static cultures, in case of very low perfusion rates, low medium volume or under hypoxic conditions. In these conditions, the amount of oxygen is initially already low and by consuming oxygen, the sensors might influence cellular function. Organ-on-chip systems often have low medium volumes and oxygen exchange with the atmosphere may be difficult due to the closed chamber. Hence, optical sensors are preferred in these systems. Optical sensors have already been introduced in organ-on-chip systems (Matsumoto et al., 2018; Prill et al., 2016; Rennert et al., 2015). These

Table 2: Comparison of features of the HepaChip-MP to other available systems to measure oxygen consumption in cell culture systems

System	Perfusion	Dimensionality of cell aggregates	Principle	Influence on culture conditions	Consecutive treatment possible	Easy substance exchange	Concentration of substance of interest	Source
HepaChip-MP	yes	Sinusoid	Optical	no	yes	yes	Constant due to perfusion	This paper
Seahorse XF analyzer	no	2D	Optical	Yes (declining of oxygen concentration [closed chamber])	yes	no	Declines over time due to consumption	Ferrick et al., 2008
MitoXpress platform	no	2D	optical	Yes (declining of oxygen concentration [closed chamber])	no	no	Decreases over time due to consumption	Hynes et al., 2009
Moya, 2018	yes	2D	electrochemical	Yes (sensors using up oxygen)	yes	yes	Constant due to perfusion	Moya et al., 2018
Weltin, 2017	no	3D spheroids	electrochemical	Yes (declining of oxygen concentration [closed chamber] + sensors using up oxygen)	yes	No (medium has to be left in the well to ensure spheroids stay in well)	Declines over time due to consumption	Weltin et al., 2017
Prill, 2016	yes	3D	optical	Yes (sensor probes in contact to cells)	yes	yes	Constant due to perfusion	Prill et al., 2016
Rennert, 2015	yes	2D on membrane	optical	no	yes	yes	Constant due to perfusion	Rennert et al., 2015
Matsumoto, 2019	yes	2D	optical	Yes (cells grow on sensor film)	yes	yes	Constant due to perfusion	Matsumoto et al., 2018

systems enable exciting insights in e.g. the establishment of an oxygen gradient (Matsumoto et al., 2018), mechanisms of action of amiodarone (Prill et al., 2016) and the influence of the flow rate on oxygen consumption (Rennert et al., 2015). However, cells are cultured in a 2D configuration which does not resemble the hepatic sinusoid (Matsumoto et al., 2018; Rennert et al., 2015). Or sensor probes are in direct contact to the cells which may influence cell function (Matsumoto et al., 2018; Prill et al., 2016). The HepaChip-MP combines culturing cells in an elongated sinusoid-like pattern under perfusion with non-invasively and continuously measuring the oxygen consumption (Table 2).

Relation of OC and flow rate

We found that the OC of the cultured PHH decreased over time between readjustments of the difference of medium levels between inlet and outlet reservoirs (Figure 2). After readjusting the height difference, the OC is elevated again and starts to decrease until the following refillment. Most probably, this is due to decreasing flow velocities (see Supplementary Figure 1). Supporting this hypothesis, Felder et al. showed that the OC of mesenchymal stem cells decreases with lower flow rates (Felder et al., 2020). Rennert et al. demonstrated that higher perfusion rates lead to a higher total OC in a liver-on-a-chip platform (Rennert et al., 2015). Wei et al. showed that in brains of aged mice both flow rate and OC increase (Wei et al., 2020) suggesting that the relationship between flow rate and OC might also have relevance *in vivo*. It would certainly be interesting to analyze the correlation of flow rate and OC in pathological contexts, e.g. high and low blood pressure or aging.

We also observed that after readjusting the level difference between the inlet and outlet reservoirs, the OC does not reach initial levels anymore but only slightly lower values (Figure 2). We attribute this to a small number of cells being flushed out of the culture chamber over time. As a result, fewer cells are present consuming less oxygen.

Other effects observed upon treatment (e.g. the fructose-effects), however, cannot be attributed to a decrease of cell number. As Figure 4 shows, the relative intensity of the fructose-induced effect is reproduced well over different days and different chambers while the oxygen consumption of the reference is reproduced over 5-6 hours within a few percent.

Normalizing OC to cell number would be highly desirable to account adequately for the possible loss of cells. However, chip dimensions, 3-dimensional structure of cell aggregates and perfusion hamper precise cell count in organ-on-chip systems. Therefore, data was normalized to the initial oxygen consumption to determine relative changes in oxygen consumption over the course of an experiment.

Fructose effect

Fructose is used extensively as a sweetener for food and especially drinks. Conducted studies have correlated long-term fructose intake with an increased risk of developing liver diseases and diabetes mellitus (for reviews see (Alwahsh and Gebhardt, 2017; Bidwell, 2017)). Fructose is also known to be quickly phosphorylated by hepatocytes and thus using a large amount of energy (van den Berghe et al., 1977). Hence, we applied fructose as a model substance in our system to analyze treatment-induced changes of cellular OC. Fructose treatment resulted in an initial drop of OC and a subsequent increase to similar to initial levels within approximately 2 hours after treatment start (Figure 3). We used glucose as a control since it consists of the same atoms but has a slightly different structure than fructose. Lactate and glycerol are used as controls because they are products of the fructose metabolism. None of the control substances caused a change in OC of PHH after treatment (Figure 3). Therefore, the demonstrated effect of fructose seems to be fructose-specific. Pyruvate also did not show the biphasic effect of fructose on OC after treatment of PHH in preliminary experiments (data not shown). Hence, the availability of

NADH does not seem to play an important role in the fructose effect. The biphasic effect of fructose has already been described by Ylikhari et al. in perfused rat livers in 1971 (Ylikahri et al., 1971). To our knowledge, there are not any more recent experiments giving insights into the immediate effect on OC after fructose-treatment of hepatocytes. Ylikhari et al. propose that the initial drop in oxygen consumption is due to depletion of P_i and thus inhibition of oxidative phosphorylation (Ylikahri et al., 1971). With increasing concentrations of P_i, the oxidative phosphorylation is induced again and thus cellular respiration also increases. This would imply that the ATP is regenerated through oxidative phosphorylation. In our experiments however, the ATP concentration stayed low even though the cellular OC increased to the initial level after two hours of fructose incubation (Figure 3). This finding suggests that a mechanism different from ATP and P_i depletion might be responsible for the change of oxygen usage of PHH after fructose treatment. One might then expect that glycolysis instead of oxidative phosphorylation would fuel ATP recovery in order to regenerate the metabolic equilibrium. However, after fructose treatment ATP level remained low even as oxygen consumption reaches initial levels again. In case of enhanced glycolytic activity, ATP level would be expected to rise independently of oxygen consumption rather than remaining at a low level. Short-term application of fructose is known to protect cells from hypoxia-induced injury and oxidative stress (Lefebvre et al., 1994; Semchyshyn, 2013). Our experiments implicate that 2 hours of fructose-treatment might result in a new equilibrium between cellular OC and ATP concentration (Figure 3). The mechanisms behind this equilibrium are still unclear but may give more insight into the protective effect of short-term treatment with fructose.

Cellular respiration and toxicity measurements

Measuring the uptake of oxygen by cell cultures is an important marker of cell viability and status of cellular metabolism. In general, a higher energy demand of cells leads to higher oxygen uptake while a low energy demand results in lower OC. The consecutive treatment with oligomycin A, FCCP and rotenone+antimycin A (R/A) in combination with a measurement of OC gives insights into cellular respiration and mitochondrial (dis-)function (Divakaruni et al., 2014). Oligomycin A inhibits the ATP synthase and thus the OC decreases after treatment. FCCP functions as an uncoupling agent and rapidly increases OC. Rotenone and antimycin A inhibit the electron transport chain, which leads to the inhibition of OC of mitochondria. Here, we demonstrated that these effects can be reproduced in our system as expected (Figure 5). This enables the possibility to analyze the influence of substances on cellular respiration and its mechanisms.

As an example, we treated PHH cultured in the HepaChip-MP with ammonium chloride. Ammonium is known to have toxic effects on different tissues, cells and mitochondria, but the detailed mechanism of action is still unclear (Dasarathy et al., 2017). Niknahad et al. demonstrated mitochondrial toxicity in hepatocytes treating isolated liver mitochondria of mice with ammonia (Niknahad et al., 2017). Mechanisms of action possibly include activation of NMDA receptors, intracellular Ca^{2+} accumulation, opening of mitochondrial permeability transition pores and thus a disturbance of the mitochondrial membrane potential (Bai et al., 2001; Monfort et al., 2002; Rama Rao et al., 2003). We found that PHH treatment with FCCP did not lead to the expected rise in cellular OC if cells are pretreated with ammonium (Figure 5). Instead, the OC of pretreated cells rose in a sigmoidal curve in contrast to the fast increase of OC in untreated PHH. This finding was specific for ammonium chloride in our experiments (compare to Figure 6, Sup-

plementary Figure 3) and might act as a starting point to obtain deeper insights into its toxicity.

Diclofenac is known to be connected with drug-induced liver injury (DILI) and mitochondrial damage (Boelsterli, 2003). Van Leeuwen et al. reported that diclofenac inhibits cellular respiration by inhibiting subunits of the respiratory chain in *Saccharomyces cerevisiae* (van Leeuwen et al., 2011). We also demonstrated disturbed mitochondrial respiration after treatment with 450 µM diclofenac for 24 hours (Figure 6). Syed et al. reported IC_{50} values as low as 19.5 µM for diclofenac in isolated rat mitochondria (Syed et al., 2016). They also demonstrated the protective effect of GSH. Thus, the GSH contained in whole hepatocytes could explain the higher concentration needed to induce toxic effects in our study. In a previous study, we presented diminished viability after diclofenac treatment for 24 hours only at a concentration as high as 1500 µM (Busche et al., 2020). Hence, analyzing the cellular respiration with on-chip oxygen sensors seems to be more sensitive than the resazurine assay, we used in our earlier study to detect diclofenac-induced toxicity. The main differences between cells treated with ammonium chloride or diclofenac and control cells were in the response to FCCP treatment. Zhdanov et al. showed that cell response on FCCP treatment may depend on the nutrient supply and the metabolic status of the cell (Zhdanov et al., 2014). Thus, modulating the cellular microenvironment in combination with FCCP treatment supports in depth analysis of metabolic changes in cells treated with various physiologic and toxic compounds. In summary, the microfluidic system presented here allows extensive investigations of metabolic interactions and DILI by measuring cellular respiration and mitochondrial function.

CONCLUSION

We presented an innovative organ-on-chip system to measure oxygen concentration online and non-invasively after substance treatment. This enables the analysis of detailed mitochondrial (dis-)function in pathophysiological situations. The system is parallelized, easy-to-use and integrates well into common cell culture workflows. The demonstration of different effects of fructose, ammonium chloride and diclofenac shows potential to enable analysis of mechanisms of action of diverse substances under continuous and unidirectional perfusion in an advanced *in vitro* model.

Acknowledgments

We thank Clara Daab, Matthew McDonald and Martin Gaier of the biomedical micro and nano engineering group of the NMI for fabricating the aluminium plate to align the optical fibers with HepaChip-MP.

Funding

Funding for this research provided by the German ministry for education and research (BMBF) through grant no. 031B0481D is gratefully acknowledged.

This work received financial support from the State Ministry of Baden-Wuerttemberg for Economic Affairs, Labour and Housing Construction.

Conflict of interest

M.S. is inventor in patents covering HepaChip-MP technology. J.F. and T.M. are working with PyroScience AT GmbH.

REFERENCES

Aduen J, Bernstein WK, Khastgir T, Miller J, Kerzner R, Bhatiani A, et al. The use and clinical importance of a substrate-specific electrode for rapid determination of blood lactate concentrations. JAMA. 1994;272:1678-85.

Alwahsh SM, Gebhardt R. Dietary fructose as a risk factor for non-alcoholic fatty liver disease (NAFLD). Arch Toxicol. 2017;91:1545-63. doi: 10.1007/s00204-016-1892-7.

Ast T, Mootha VK. Oxygen and mammalian cell culture: are we repeating the experiment of Dr. Ox? Nat Metab. 2019;1(9):858-60. doi: 10.1038/s42255-019-0105-0.

Bai G, Rama Rao KV, Murthy CR, Panickar KS, Jayakumar AR, Norenberg MD. Ammonia induces the mitochondrial permeability transition in primary cultures of rat astrocytes. J Neurosci Res. 2001;66:981-91. doi: 10.1002/jnr.10056.

Bidwell AJ. Chronic fructose ingestion as a major health concern: is a sedentary lifestyle making it worse? A review. Nutrients. 2017;9(6):549. doi: 10.3390/nu9060549.

Boelsterli U. Diclofenac-induced liver injury: a paradigm of idiosyncratic drug toxicity. Toxicol Appl Pharmacology. 2003;192:307-22. doi: 10.1016/s0041-008x(03)00368-5.

Brischwein M, Motrescu ER, Cabala E, Otto AM, Grothe H, Wolf B. Functional cellular assays with multiparametric silicon sensor chips. Lab Chip. 2003;3: 234-40. doi: 10.1039/b308888j.

Busche M, Tomilova O, Schutte J, Werner S, Beer M, Groll N, et al. HepaChip-MP - a twenty-four chamber microplate for a continuously perfused liver coculture model. Lab Chip. 2020;20:2911-26. doi: 10.1039/d0lc00357c.

Cooper AJL, Lai JCK, Gelbard AS. Ammonia in liver and extrahepatic tissues: an overview of metabolism and toxicity in mammals. In: Butterworth RF, Layrargues GP (eds): Hepatic encephalopathy: pathophysiology and treatment (pp 27-48). Totowa, NJ: Humana Press, 1989.

Corsini A, Bortolini M. Drug-induced liver injury: the role of drug metabolism and transport. J Clin Pharmacol. 2013;53:463-74. doi: https://doi.org/10.1002/jcph.23.

Dasarathy S, Mookerjee RP, Rackayova V, Rangroo Thrane V, Vairappan B, Ott P, et al. Ammonia toxicity: from head to toe? Metab Brain Dis. 2017;32:529-38. doi: 10.1007/s11011-016-9938-3.

Davies NM, Anderson KE. Clinical pharmacokinetics of diclofenac. Clin Pharmacokinet. 1997;33:184-213. doi: 10.2165/00003088-199733030-00003.

Degli Esposti D, Hamelin J, Bosselut N, Saffroy R, Sebagh M, Pommier A, et al. Mitochondrial roles and cytoprotection in chronic liver injury. Biochem Res Int. 2012;2012:387626. doi: 10.1155/2012/387626.

Divakaruni AS, Paradyse A, Ferrick DA, Murphy AN, Jastroch M. Analysis and interpretation of microplate-based oxygen consumption and pH data. Methods Enzymol. 2014;547:309-54.

Douard V, Ferraris RP. The role of fructose transporters in diseases linked to excessive fructose intake. J Physiol. 2013;591:401-14. doi: 10.1113/jphysiol.2011.215731.

Ehgartner J, Sulzer P, Burger T, Kasjanow A, Bouwes D, Krühne U, et al. Online analysis of oxygen inside silicon-glass microreactors with integrated optical sensors. Sensors Actuators B: Chemical. 2016;228:748-57. doi: 10.1016/j.snb.2016.01.050.

Felder ML, Simmons AD, Shambaugh RL, Sikavitsas VI. Effects of flow rate on mesenchymal stem cell oxygen consumption rates in 3d bone-tissue-engineered constructs cultured in perfusion bioreactor systems. Fluids. 2020;5(1):30. doi: 10.3390/fluids5010030.

Ferrick DA, Neilson A, Beeson C. Advances in measuring cellular bioenergetics using extracellular flux. Drug Discov Today. 2008;13:268-74. doi: 10.1016/j.drudis.2007.12.008.

Gruber P, Marques MPC, Szita N, Mayr T. Integration and application of optical chemical sensors in microbioreactors. Lab Chip. 2017;17:2693-712. doi: 10.1039/c7lc00538e.

Guo R, Xu X, Lu Y, Xie X. Physiological oxygen tension reduces hepatocyte dedifferentiation in in vitro culture. Sci Rep. 2017;7(1):5923. doi: 10.1038/s41598-017-06433-3.

Hengstler JG, Sjogren AK, Zink D, Hornberg JJ. In vitro prediction of organ toxicity: the challenges of scaling and secondary mechanisms of toxicity. Arch Toxicol. 2020;94:353-6. doi: 10.1007/s00204-020-02669-7.

Hynes J, Floyd S, Soini AE, O'Connor R, Papkovsky DB. Fluorescence-based cell viability screening assays using oxygen probes. J Biomol Screen. 2003;8:264-72. doi: 10.1177/1087057103253567.

Hynes J, Marroquin LD, Ogurtsov VI, Christiansen KN, Stevens GJ, Papkovsky DB, et al. Investigation of drug-induced mitochondrial toxicity using fluorescence-based oxygen-sensitive probes. Toxicol Sci. 2006;92:186-200. doi: 10.1093/toxsci/kfj208.

Hynes J, O'Riordan TC, Zhdanov AV, Uray G, Will Y, Papkovsky DB. In vitro analysis of cell metabolism using a long-decay pH-sensitive lanthanide probe and extracellular acidification assay. Anal Biochem. 2009; 390:21-8. doi: 10.1016/j.ab.2009.04.016.

Jorquera F, Culebras JM, González-Gallego J. Influence of nutrition on liver oxidative metabolism. Nutrition. 1996;12:442-7. doi: https://doi.org/10.1016/S0899-9007(96)00101-3.

Kieninger J, Weltin A, Flamm H, Urban GA. Microsensor systems for cell metabolism - from 2D culture to organ-on-chip. Lab Chip. 2018;18:1274-91. doi: 10.1039/c7lc00942a.

Latta M, Kunstle G, Lucas R, Hentze H, Wendel A. ATP-depleting carbohydrates prevent tumor necrosis factor receptor 1-dependent apoptotic and necrotic liver injury in mice. J Pharmacol Exp Ther. 2007;321: 875-83. doi: 10.1124/jpet.107.119958.

Lefebvre V, Goffin I, Buc-Calderon P. Fructose metabolism and cell survival in freshly isolated rat hepatocytes incubated under hypoxic conditions: Proposals for potential clinical use. Hepatology. 1994;20:1567-76. doi: https://doi.org/10.1002/hep.1840200628.

Low LA, Mummery C, Berridge BR, Austin CP, Tagle DA. Organs-on-chips: into the next decade. Nat Rev Drug Discov. 2020;21:345-61. doi: 10.1038/s41573-020-0079-3.

Matsumoto S, Leclerc E, Maekawa T, Kinoshita H, Shinohara M, Komori K, et al. Integration of an oxygen sensor into a polydymethylsiloxane hepatic culture device for two-dimensional gradient characterization. Sensors and Actuators B: Chemical. 2018;273:1062-9. doi: https://doi.org/10.1016/j.snb.2018.05.053.

Monfort P, Kosenko E, Erceg S, Canales JJ, Felipo V. Molecular mechanism of acute ammonia toxicity: role of NMDA receptors. Neurochem Int.. 2002;41:95-102. doi: 10.1016/s0197-0186(02)00029-3.

Moya A, Ortega-Ribera M, Guimerà X, Sowade E, Zea M, Illa X, et al. Online oxygen monitoring using integrated inkjet-printed sensors in a liver-on-a-chip system. Lab on a Chip. 2018;18:2023-35. doi: 10.1039/C8LC00456K.

Müller B, Sulzer P, Walch M, Zirath H, Buryška T, Rothbauer M, et al. Measurement of respiration and acidification rates of mammalian cells in thermoplastic microfluidic devices. Sensors and Actuators B: Chemical. 2021;334:129664. doi: 10.1016/j.snb.2021.129664.

Nelson JL, Harmon ME, Robergs RA. Identifying plasma glycerol concentration associated with urinary glycerol excretion in trained humans. J Anal Toxicol. 2011;35:617-23. doi: 10.1093/anatox/35.9.617.

Niknahad H, Jamshidzadeh A, Heidari R, Zarei M, Ommati MM. Ammonia-induced mitochondrial dysfunction and energy metabolism disturbances in isolated brain and liver mitochondria, and the effect of taurine administration: relevance to hepatic encephalopathy treatment. Clin Exp Hepatol. 2017;3:141-51. doi: 10.5114/ceh.2017.68833.

O'Riordan TC, Buckley D, Ogurtsov V, O'Connor R, Papkovsky DB. A cell viability assay based on monitoring respiration by optical oxygen sensing. Anal Biochem. 2000;278:221-7. doi: 10.1006/abio.1999.4431.

Oomen PE, Skolimowski MD, Verpoorte E. Implementing oxygen control in chip-based cell and tissue culture systems. Lab Chip. 2016;16:3394-414. doi: 10.1039/c6lc00772d.

Papkovsky DB, Dmitriev RI. Biological detection by optical oxygen sensing. Chem Soc Rev. 2013;42:8700-32. doi: 10.1039/c3cs60131e.

Pessayre D, Mansouri A, Berson A, Fromenty B. Mitochondrial involvement in drug-induced liver injury. In: Uetrecht J (ed): Adverse drug reactions (pp 311-65). Berlin: Springer, 2010.

Prill S, Bavli D, Levy G, Ezra E, Schmalzlin E, Jaeger MS, et al. Real-time monitoring of oxygen uptake in hepatic bioreactor shows CYP450-independent mitochondrial toxicity of acetaminophen and amiodarone. Arch Toxicol. 2016;90:1181-91. doi: 10.1007/s00204-015-1537-2.

Rama Rao KV, Jayakumar AR, Norenberg MD. Ammonia neurotoxicity: role of the mitochondrial permeability transition. Metab Brain Dis. 2003;18:113-27. doi: 10.1023/A:1023858902184.

Rennert K, Steinborn S, Groger M, Ungerbock B, Jank AM, Ehgartner J, et al. A microfluidically perfused three dimensional human liver model. Biomaterials. 2015;71:119-31. doi: 10.1016/j.biomaterials.2015.08.043.

Scheidecker B, Shinohara M, Sugimoto M, Danoy M, Nishikawa M, Sakai Y. Induction of in vitro metabolic zonation in primary hepatocytes requires both near-physiological oxygen concentration and flux. Front Bioeng Biotechnol. 2020;8:524. doi: 10.3389/fbioe.2020.00524.

Semchyshyn HM. Fructation in vivo: detrimental and protective effects of fructose. Biomed Res Int. 2013; 2013:343914. doi: 10.1155/2013/343914.

Stevens KM. Oxygen requirements for liver cells in vitro. Nature. 1965;206:199.

Syed M, Skonberg C, Hansen SH. Mitochondrial toxicity of diclofenac and its metabolites via inhibition of oxidative phosphorylation (ATP synthesis) in rat liver mitochondria: Possible role in drug induced liver injury (DILI). Toxicol In Vitro. 2016;31:93-102. doi: 10.1016/j.tiv.2015.11.020.

Ungerböck B, Mayr T. Microfluidic systems and optical oxygen sensors: a perfect match for advancing bioprocessing and microbiology. In: Papkovsky DB, Dmitriev RI (eds): Quenched-phosphorescence detection of molecular oxygen: applications in life sciences (pp 278-97). London: The Royal Society of Chemistry, 2018.

van den Berghe G, Bronfman M, Vanneste R, Hers HG. The mechanism of adenosine triphosphate depletion in the liver after a load of fructose. A kinetic study of liver adenylate deaminase. Biochem J. 1977;162:601-9. doi: 10.1042/bj1620601.

van Leeuwen JS, Orij R, Luttik MAH, Smits GJ, Vermeulen NPE, Vos JC. Subunits Rip1p and Cox9p of the respiratory chain contribute to diclofenac-induced mitochondrial dysfunction. Microbiology (Reading). 2011;157:685-94. doi: 10.1099/mic.0.044578-0.

van Wenum M, Adam AAA, van der Mark VA, Chang JC, Wildenberg ME, Hendriks EJ, et al. Oxygen drives hepatocyte differentiation and phenotype stability in liver cell lines. J Cell Commun Signal. 2018;12:575-88. doi: 10.1007/s12079-018-0456-4.

Walter-Sack I, Klotz U. Influence of diet and nutritional status on drug metabolism. Clin Pharmacokinet. 1996;31:47-64. doi: 10.2165/00003088-199631010-00004.

Wei Z, Chen L, Hou X, van Zijl PCM, Xu J, Lu H. Age-related alterations in brain perfusion, venous oxygenation, and oxygen metabolic rate of mice: a 17-month longitudinal MRI study. Front Neurol. 2020;11:559. doi: 10.3389/fneur.2020.00559.

Weltin A, Hammer S, Noor F, Kaminski Y, Kieninger J, Urban GA. Accessing 3D microtissue metabolism: Lactate and oxygen monitoring in hepatocyte spheroids. Biosens Bioelectron. 2017;87:941-8. doi: 10.1016/j.bios.2016.07.094.

Ylikahri RH, Hassinen IE, Kähönen MT. Metabolic interactions of fructose and ethanol in perfused liver of normal and thyroxine-treated rats. Metabolism. 1971;20:555-67. doi: https://doi.org/10.1016/0026-0495(71)90004-7.

Zhdanov AV, Waters AH, Golubeva AV, Dmitriev RI, Papkovsky DB. Availability of the key metabolic substrates dictates the respiratory response of cancer cells to the mitochondrial uncoupling. Biochim Biophys Acta. 2014;1837:51-62. doi: 10.1016/j.bbabio.2013.07.008.

Zirath H, Rothbauer M, Spitz S, Bachmann B, Jordan C, Muller B, et al. Every breath you take: non-invasive real-time oxygen biosensing in two- and three-dimensional microfluidic cell models. Front Physiol. 2018;9:815. doi: 10.3389/fphys.2018.00815.